DR-156

SAN/1109–76/T1

SOLAR PILOT PLANT

Phase I, Quarterly Report No. 1, July–December 1975

February 20, 1976

Work performed under contract No. E(04-3)-1109

Systems and Research Center
Honeywell, Incorporated
Minneapolis, Minnesota

ENERGY RESEARCH AND DEVELOPMENT ADMINISTRATION
Division of Solar Energy

DISCLAIMER

NOTICE

Available from the National Technical Information Service, U. S. Department of Commerce, Springfield, Virginia 22161

Price: Paper Copy $5.50 (domestic)
$8.00 (foreign)
Microfiche $2.25 (domestic)
$3.75 (foreign)

Printed in the United States of America
USERDA Technical Information Center, Oak Ridge, Tennessee

SAN/1109-76/T1
Distribution Category UC-62

SOLAR PILOT PLANT
PHASE I

QUARTERLY REPORT NO. 1
(July - December 1975)
(Approved)

CDRL Item No. 10

20 February 1976

Contract No. E(04-3)-1109

Honeywell, Incorporated
Systems & Research Center
2600 RIDGWAY PARKWAY,
MINNEAPOLIS, MINNESOTA 55413

FOREWORD

This is the final submittal of Solar Pilot Plant Quarterly Technical Report No. 1 per CDRL Item 10 of Contract E(04-3) 1109. The report has been reviewed and approved by ERDA.

ABSTRACT

Honeywell Inc. is investigating the technical and economic feasibility of generating electricity from solar energy under Energy Research and Development Administration contract E(04-3)-1109. During the first 6 months of the program (1 July - 31 December 1975), a preliminary design baseline for a 10-MW(e) solar pilot plant was generated and analyzed. Subsequently, several changes were made to improve performance and/or reduce cost. Conceptual designs and research experiments were generated for three key subsystems -- collector, steam generator, and thermal storage. Limited testing was done to study the problem of removing eutectic salts from vaporizer tubes in the thermal storage subsystem. The program was on schedule at the end of 1975. Plans for the first quarter of 1976 include ordering long-leadtime items for the subsystem research experiments, continuing analysis of the conceptual designs preparatory to detailing them, and continuing engineering model experiments.

THIS PAGE

WAS INTENTIONALLY

LEFT BLANK

CONTENTS

ILLUSTRATIONS

TABLES

SECTION I
INTRODUCTION

BACKGROUND

The Energy Research and Development Administration (ERDA) is commissioned to identify and evaluate alternate sources of energy to ensure orderly and timely development of those offering potential for supplementing and/or replacing conventional fuels that will be in increasingly short supply. An alternate source with great potential is solar energy, and one goal of the overall national energy program is to demonstrate the technical and economic feasibility of a central receiver solar power plant for generating electricity. Pursuant to that goal, ERDA, on 1 July 1975, awarded Honeywell Inc. a 2-year contract to develop a preliminary design for a 10-MW(e) proof-of-concept pilot plant.

PROGRAM SCOPE

The program being conducted by Honeywell under ERDA Contract E(04-3)-1109 calls for preparing a solar pilot plant baseline design and carrying out research experiments on three key subsystems to obtain data for evaluating the baseline. Since these subsystems (collector, receiver, and thermal storage) and their integration are critical to the success of this portion of the program and to initiation of the next phase [constructing and operating the 10-MW(e) pilot plant], Honeywell is using a team approach to provide a low-risk, cost-effective preliminary design. The team and individual responsibilities are shown in Figure 1.

PROGRAM STATUS

Figure 2 is the program schedule. It shows work began on 1 July 1975 and proceeded on schedule through December. This report, submitted in compliance with Contract Data Requirements List (CDRL) Item 10, documents the program during that period. Future reports will be on a quarterly basis.

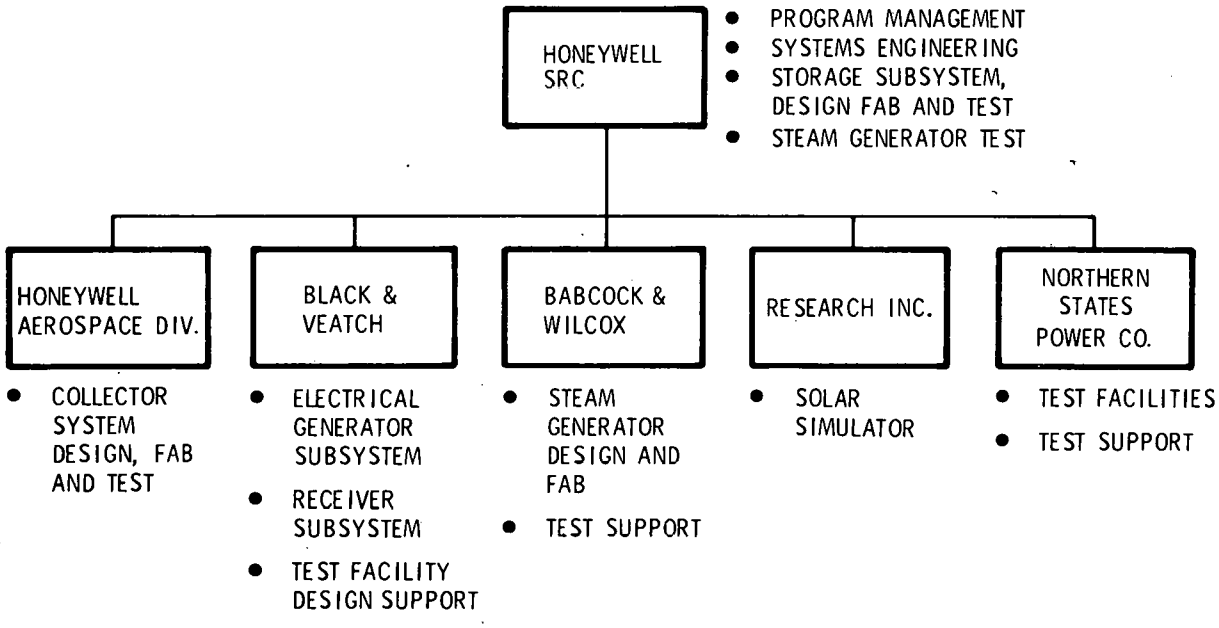

Figure 1. Honeywell Team for Solar Pilot Plant Program

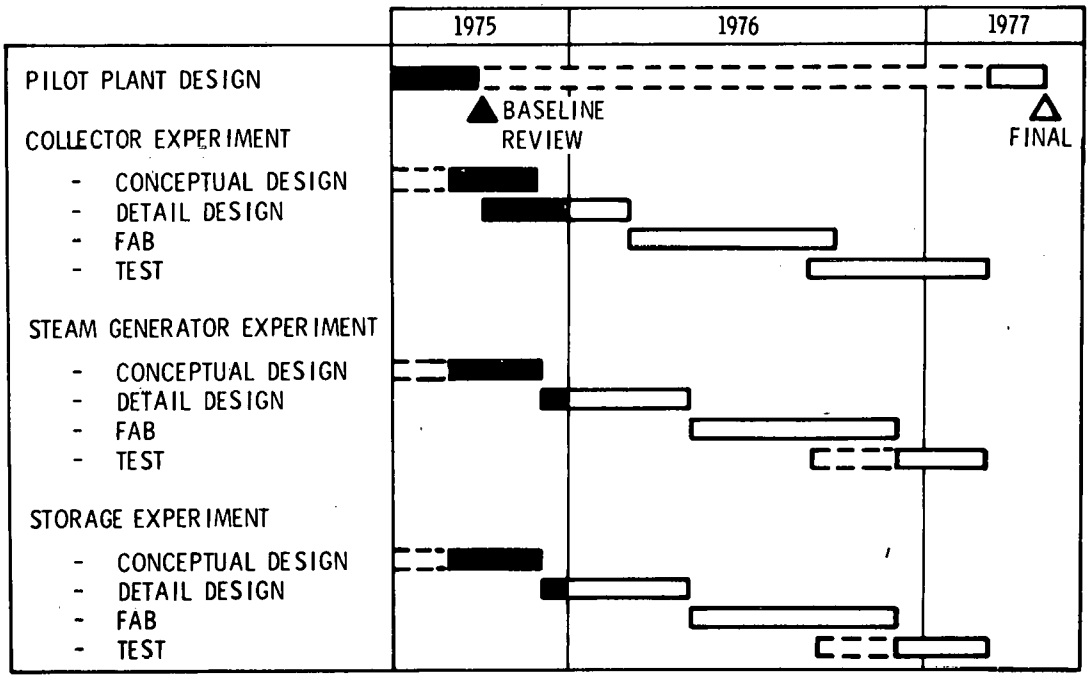

Figure 2. Solar Pilot Plant Phase I Schedule

SECTION II
SOLAR PILOT PLANT CHARACTERISTICS

CONCEPT

Description

The pilot plant concept generated for this program and refined during the first 6 months consists of a circular field of heliostats that concentrate solar energy through the annulus aperture of a central receiver, as illustrated in Figure 3. The concentrated solar energy is converted to thermal energy by an array of boiler and superheater tubes in the cavity to generate electricity from superheated steam produced in the receiver, or from thermal energy stored by melting a eutectic salt (Figure 4).

The 10-MW(e) pilot plant is scaled from a 215-MW(e) nameplate capacity plant, which is considered upper limit commercial size due to the limiting factor of tower height. The scaling ensures that data obtained from the pilot plant will be applicable to commercial-size operations. A comparison is presented in Figure 5.

Changes to Original Baseline

Three major changes were made to the pilot plant baseline after 15 July 1975 to improve performance and/or reduce cost. They are:

1) Heliostat Configuration -- The heliostat azimuth/elevation (Az-El) gimbal order was changed to a tilt-tilt order to reduce the high torque rate induced by rotation of the former, and to realize a cost saving. The two configurations are shown in Figure 6.

2) Turbine Configuration -- The original baseline featured primary turbine admission for both receiver and storage steam. The temperature mismatch between the two (about 230°C) represented a potential flow problem. By injecting storage steam downstream from the receiver steam (dual pressure admission), a better temperature/pressure match is achieved and simultaneous admission from the two sources becomes practical (Figure 4).

3) Receiver Steam-Cycle Selection -- The original baseline characteristic of receiver steam was 59 bar/510°C. This was changed to 100 bar/510°C to obtain greater cyclic efficiency. The storage steam value of 40 bar/280°C was retained.

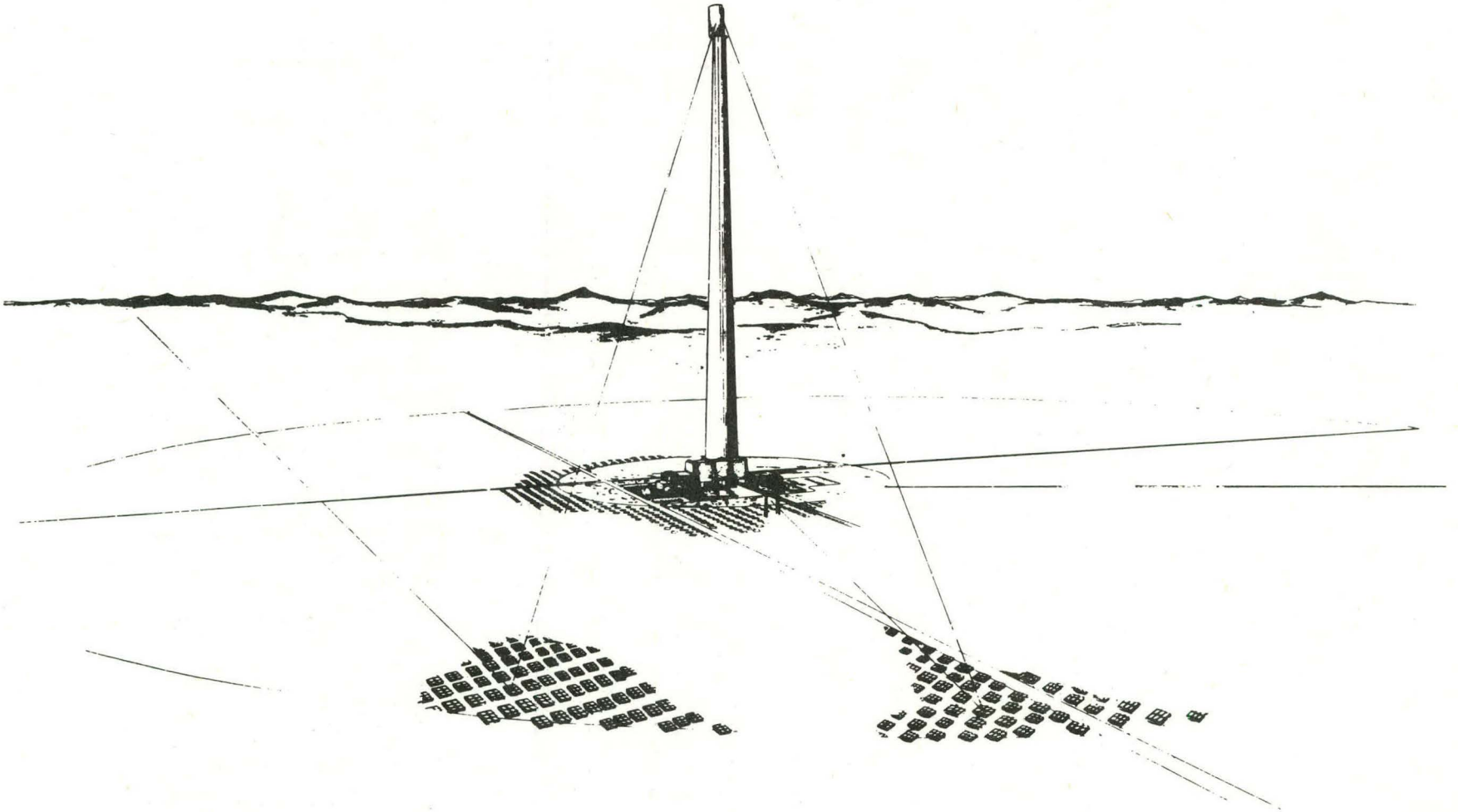

Figure 3. Solar Pilot Plant Concept

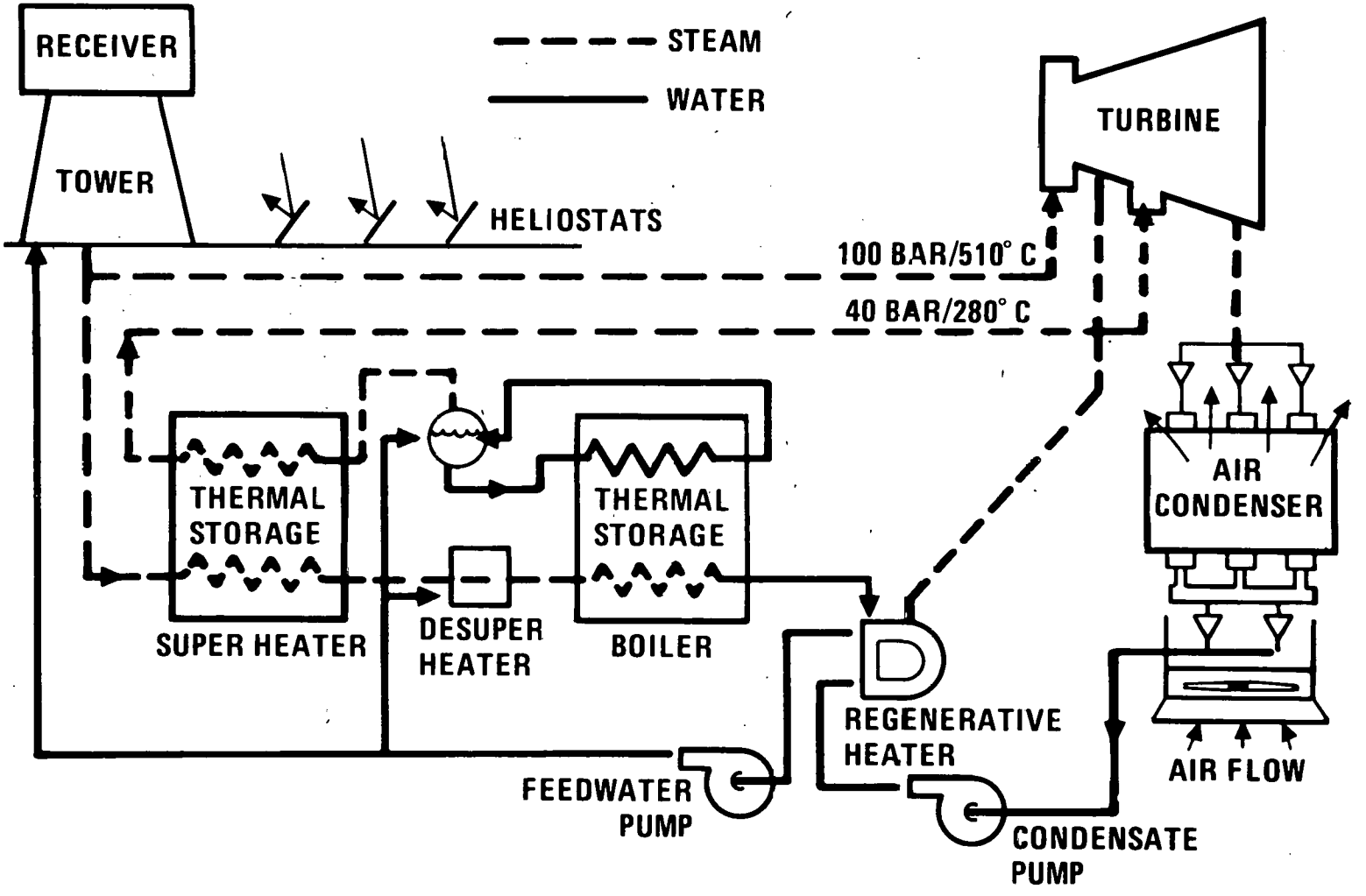

Figure 4. Solar Pilot Plant Baseline Schematic

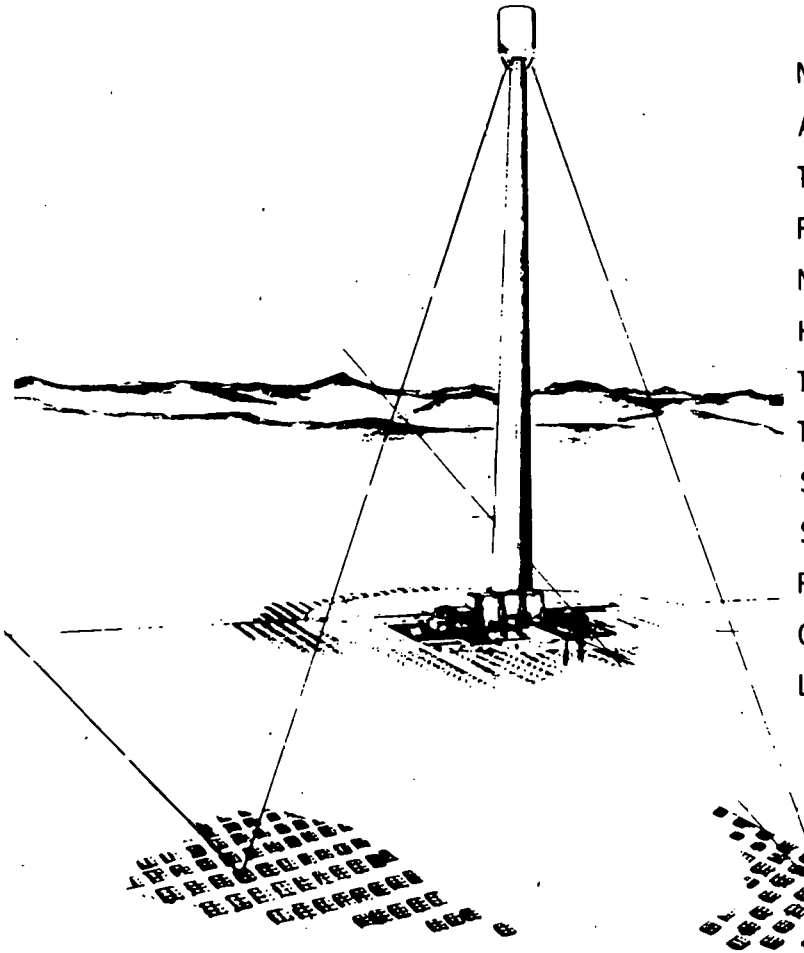

	COMMERCIAL	PILOT PLANT
NAMEPLATE CAPACITY	215 MW(e)	15 MW(e)
AVERAGE POWER (NET ~4000 HOURS)	172 MW(e)	10 MW(e)
TOWER HEIGHT	569 m	137 m
FIELD OD	2402 m	579 m
NUMBER OF HELIOSTATS	32,766	1905
HELIOSTAT SIZE	40 m^2	---
TURBINE CYCLE (FROM RCVR)	100 BAR/510°C	---
TURBINE CYCLE (FROM STORAGE)	40 BAR/280°C	---
STORAGE TYPE	PHASE CHANGE	---
STORAGE CAPACITY	TO BE DETERMINED	200 MWhr(t)
RECEIVER	CAVITY	---
COOLING	DRY	---
LOCATION	INYOKERN	---

Figure 5. Comparison of Commercial and Pilot Plant Parameters

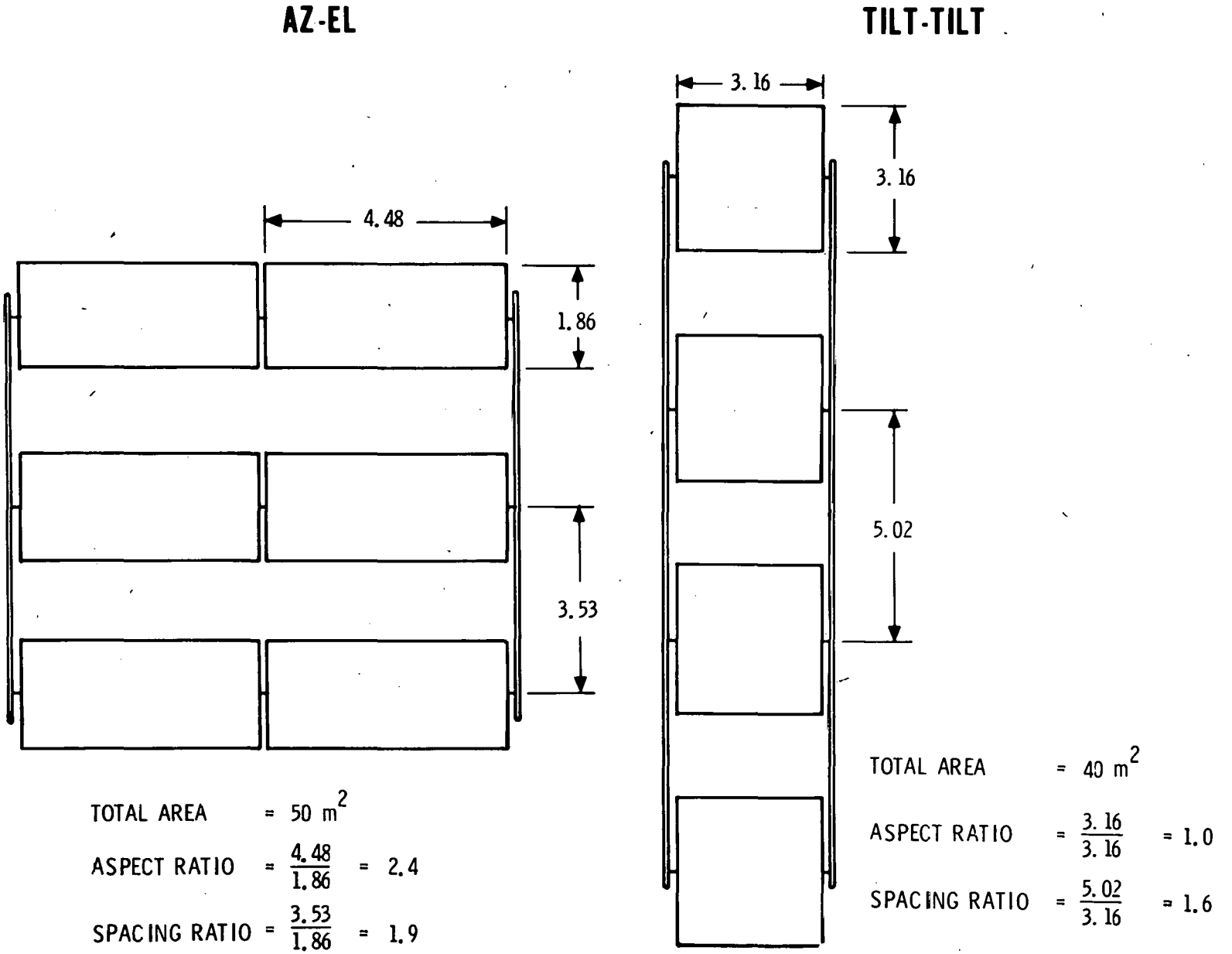

Figure 6. Candidate Heliostat Configurations

The combination of these changes with the other pilot plant baseline features offers the performance/cost benefits listed in Table 1.

MAJOR SUBSYSTEMS

The major subsystems of the pilot plant are identified in Table 2. They are the collector, receiver, thermal storage, and electrical-generation subsystems. The first three are of primary interest in this phase of the program, since the practical generation of electricity is dependent on how well they function.

Collector Subsystem

The collector subsystem is designed to gather and transmit as much solar energy as is economically feasible using prefocused heliostats. It interfaces with the receiver subsystem and the communication/control center as shown in Figure 7, and has the characteristics as listed in Table 3.

The collector field is flat rather than sloped or tiered to reduce cost and the impact on the ecology. The size was selected to optimize the annual thermal energy per unit mirror area within the overall requirements for plant layout. The multifaceted, low-profile focusing heliostats minimize wind loading and offer relatively low cost per unit area.

Receiver Subsystem

The receiver subsystem receives the solar energy directed by the heliostats into the annualr aperture of the tower. Feedwater in the receiver boiler tubes is superheated and piped directly to the electrical-generation subsystem and/or to the thermal storage subsystem. Pertinent characteristics are listed in Table 4. The receiver subsystem interfaces with the other subsystems and the communications/control center as shown in Figure 8.

Thermal Storage Subsystem

Feedwater from the thermal storage subsystem is pumped to the receiver boiler tubes and superheated steam flows from the receiver to the thermal storage subsystem and into the electrical generation subsystem during the charge cycle. Feedwater from the electrical generation subsystem is pumped to the thermal storage subsystem during the discharge cycle. Interfaces with the other subsystems and the communication/control center are shown in Figure 9. Pertinent characteristics are listed in Table 5.

Table 1. Solar Pilot Plant Design Features and Benefits

Feature/Benefit	Feature/Benefit
• 360° Heliostat Field: - Optimizes annual energy - Uniform azimuthal flux distribution • Low-Profile Heliostat: - Wind load performance - Lowest $/stiffness - Night and safety stowage - Lower-cost central control • Cavity Receiver/Drum Control: - High efficiency - Low night losses - Greater turndown ratio - Conventional technology	• 100 Bar/510°C Steam Cycle: - Higher cycle efficiency - Reliability versus efficiency compromise • Dual-Pressure-Admission Turbine: - Receiver/storage steam simultaneously - Smooth transition of steam sources - Turbine capacity match with storage steam • Phase Change Storage: - Lower cost - High energy density - Matches water/steam phase change • Dry Cooling: - Eliminates high water use in arid locations

Table 2. Solar Pilot Plant Major Subsystems

Parameter	Value
Collector Subsystem:	
Field outer radius	290 m
Number of heliostats	1905
Receiver Subsystem:	
Tower height	137 m
Cavity diameter	11 m
Cavity height	13.7 m
Thermal Storage Subsystem:	
Thermal storage capacity	255 MWhr(t)
Total quantity of phase change material ($NaCl$-$NaNO_3$-Na_2SO_4, $NaCl$-$NaOH$)[3]	5.1×10^6 kg
Electrical-Generation Subsystem:	
Turbine name-plate capacity	15,000 kW
High-pressure steam turbine inlet conditions	100 bar/510°C
Low-pressure steam turbine conditions	40 bar/280°C

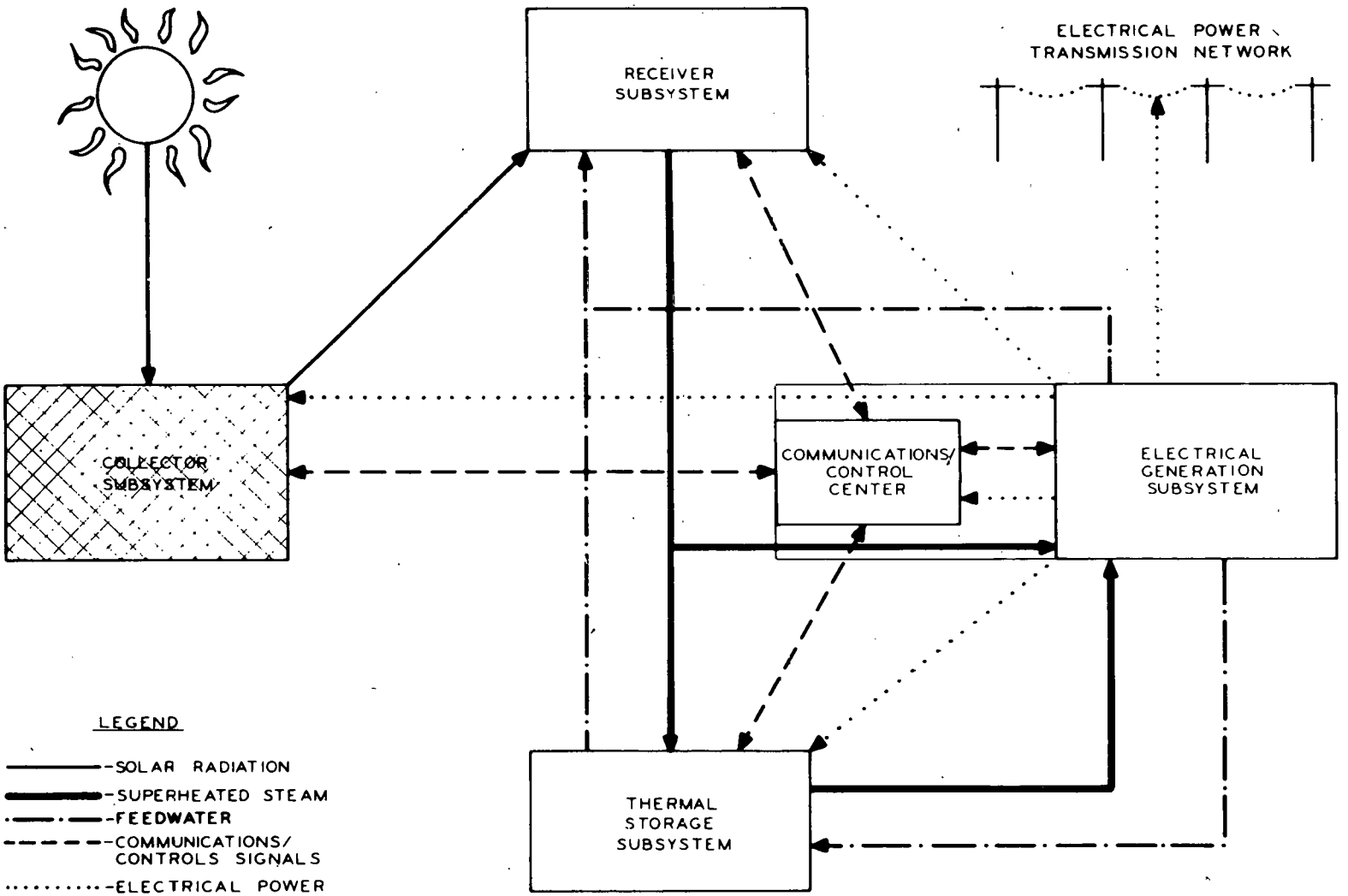

Figure 7. Collector Subsystem Interfaces

Table 3. Collector Subsystem Characteristics

Parameter	Value
Field outer radius	290 m
Field inner radius	55 m
Number of heliostats	1905
Individual heliostat area	40 m^2
Total heliostat area	76,200 m^2
Peak thermal power into aperture	53 MW
Annual thermal energy into cavity aperture	1.58 x 10^5 MWhr
Net annual thermal energy per unit mirror area	1.95 MWhr/m^2
Net peak power per unit mirror area (thermal)	0.66 kW/m^2

Table 4. Receiver Subsystem Characteristics

Parameter	Value
Tower height	137 m
Cavity diameter	11 m
Cavity height	13.7 m
Steam generator housing height	20 m
Steam generator housing diameter	14.6 m
Aperture slant height	4.9 m
Aperture lower diameter	6.1 m
Annulus aperture area	133 m^2
Peak absorbed thermal power	49 MW
Peak wall incident thermal power flux	440 kW/m^2
Annual thermal energy absorbed by cavity working fluid	1.49 x 10^5 MWhr

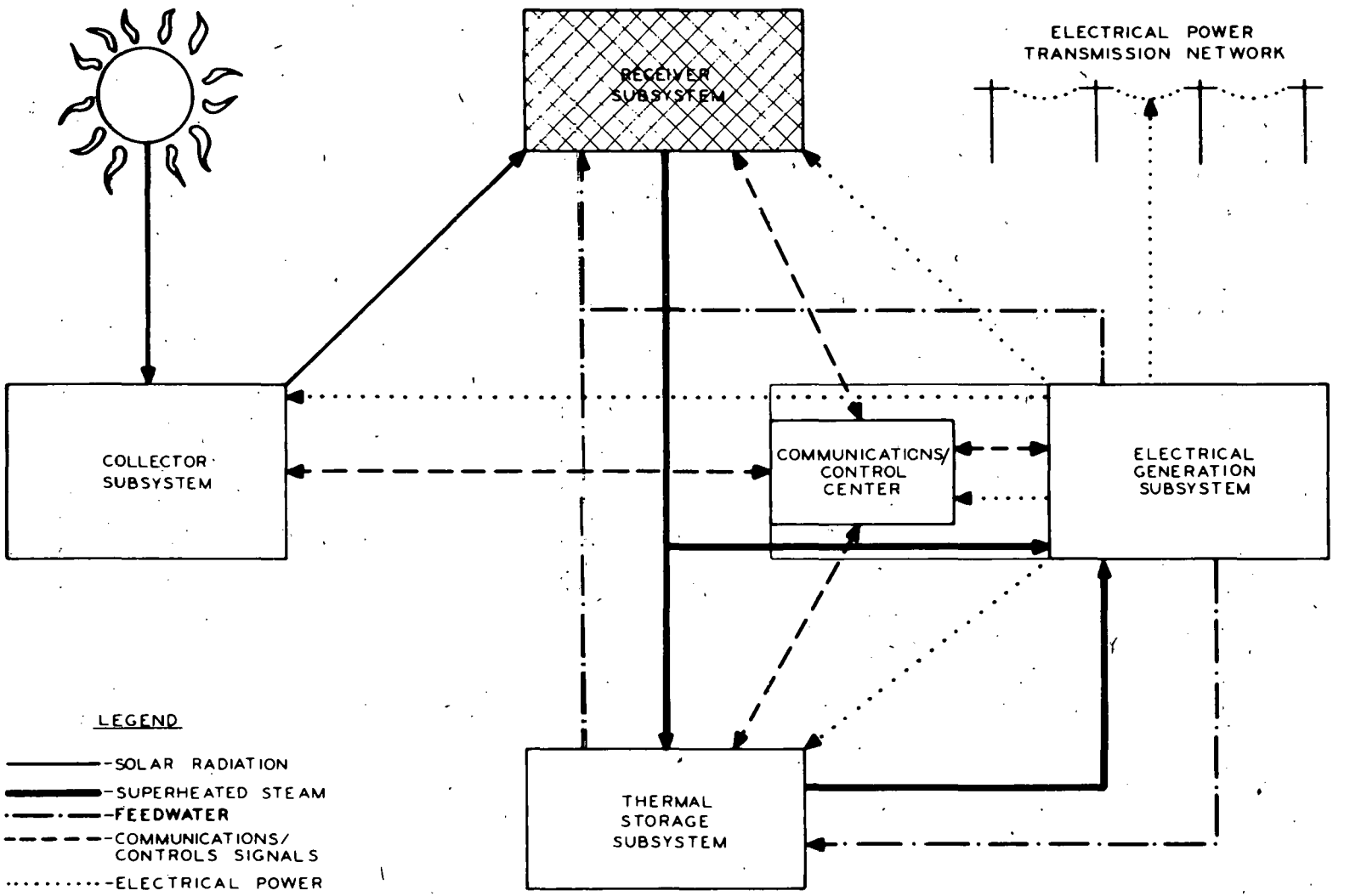

Figure 8. Receiver Subsystem Interfaces

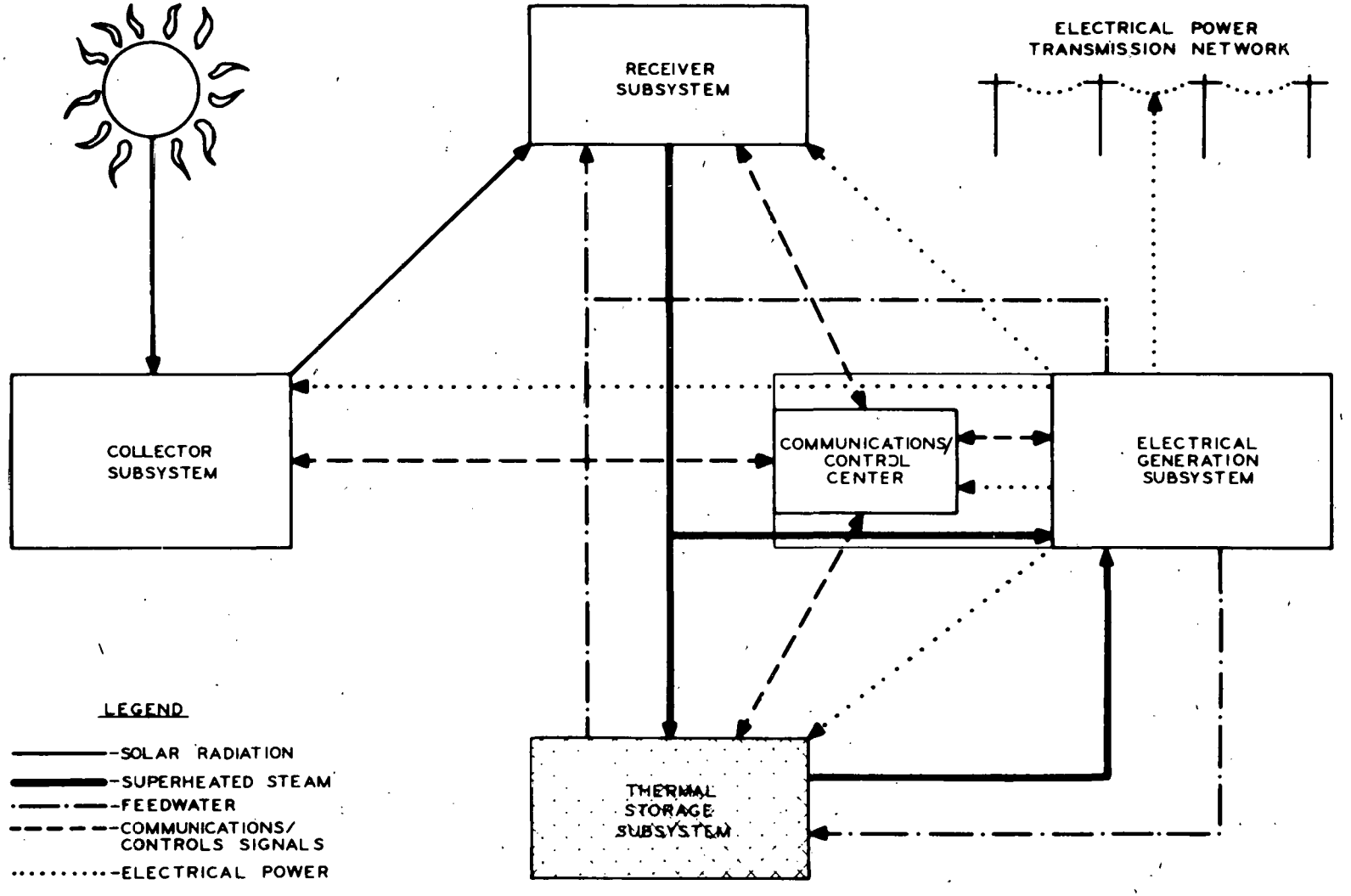

Figure 9. Thermal Storage Subsystem Interfaces

Electrical-Generation Subsystem

The electrical-generation subsystem pumps feedwater to the receiver boiler tubes and/or the thermal storage subsystem and receives steam from either or both of those subsystems. The electrical-generation subsystem also provides electrical power to the other subsystems and the communication/control center. Pertinent subsystems characteristics are listed in Table 6. Interfaces with the other subsystems and the control center are shown in Figure 10.

Subsystems Control

The plant control scheme (Figure 11) is based on providing centralized coordination and control of the subsystems while maximizing utilization of the solar energy collected. Safety is a primary consideration, and adequate protection against dangerous operating conditions is incorporated in the control scheme.

PLANT LAYOUT

The pilot plant site plan (Figure 12) respects the functional relationships between plant systems. The site arrangement was developed by giving priorities to those major facilities whose parameters can be manipulated least.

The collector field location is governed by topographical features accommodating the specified outer radius (i.e., the concept of a flat field is maintained).

The central plant complex (Figure 13) is positioned at the center of the collector field in such a manner as to avoid blocking any of the heliostats on the collector field inner radius. The receiver tower, at the center of the complex, and of the collector field, maximizes the amount of solar energy collected annually.

An access road and rail line into the plant site are located to facilitate plant operation and maintenance while minimizing energy loss in the collector field.

The electrical transmission lines that integrate the plant output with the existing network are located to minimize interference with other facilities or lines.

Table 5. Thermal Storage Subsystem Characteristics

Parameter	Value
Thermal storage capacity	255 MWhr(t)
Total quantity of phase change materials ($NaCl-NaNO_3-Na_2SO_4$, $NaCl-NaOH$)	5.1×10^6 kg
Maximum thermal power input to storage	49 MW
Maximum thermal power output from storage	29.8 MW
Net annual electrical energy produced if storage is charged and discharged daily	4.15×10^4 MWhr
Net annual electrical energy produced if storage is not used	4.4×10^4 MWhr
Outlet stream conditions	42 bar/282°C

Table 6. Electrical-Generation Subsystem Characteristics

Parameter	Value
Turbine nameplate capacity	15,000 kW
Turbine type	Dual-pressure admission
High-pressure steam turbine inlet conditions	100 bar/510°C
Low-pressure steam turbine inlet conditions	40 bar/280°C
Peak steam flow rate to turbine inlet	92,165 kg/hr

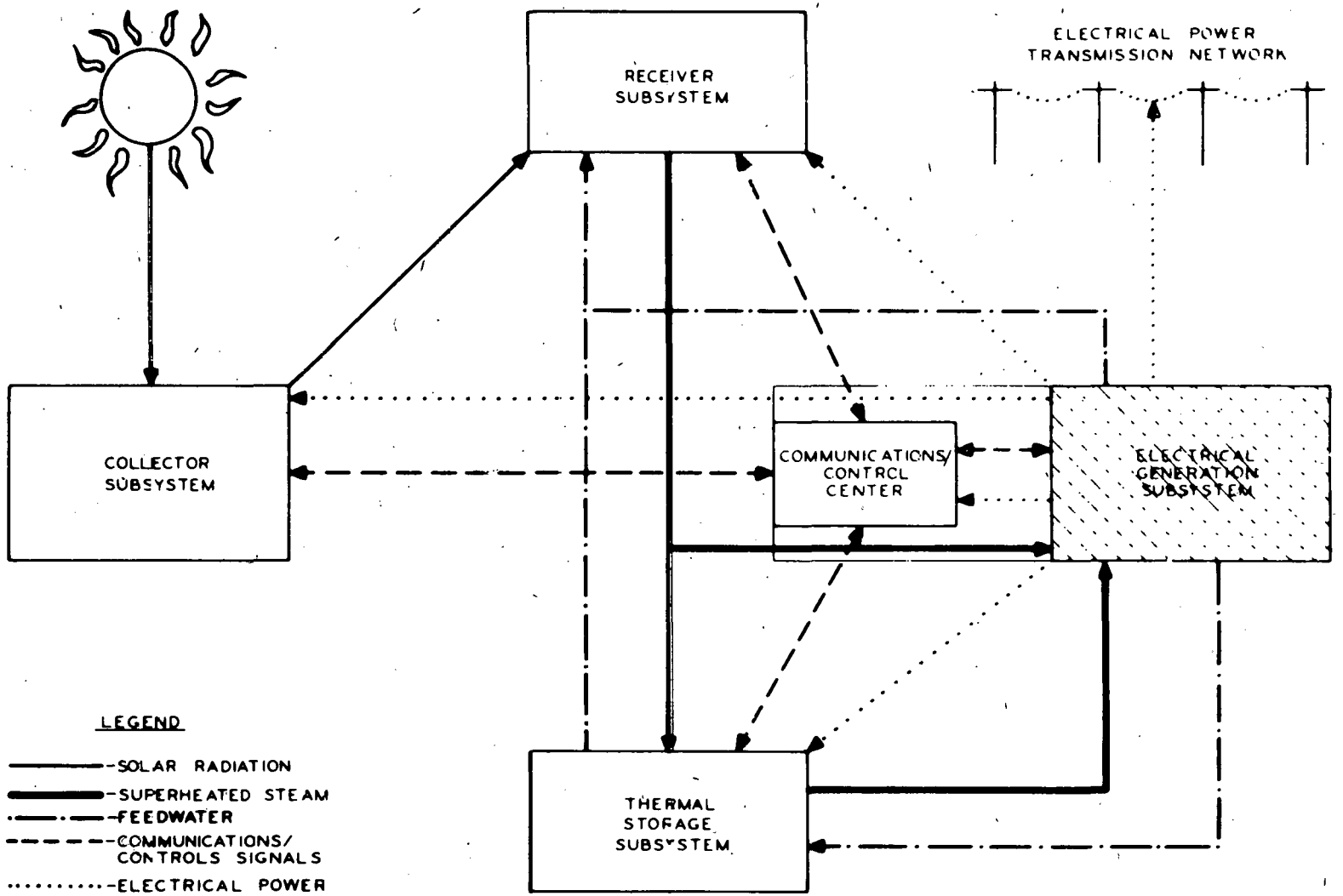

Figure 10. Electrical-Generation Subsystem Interfaces

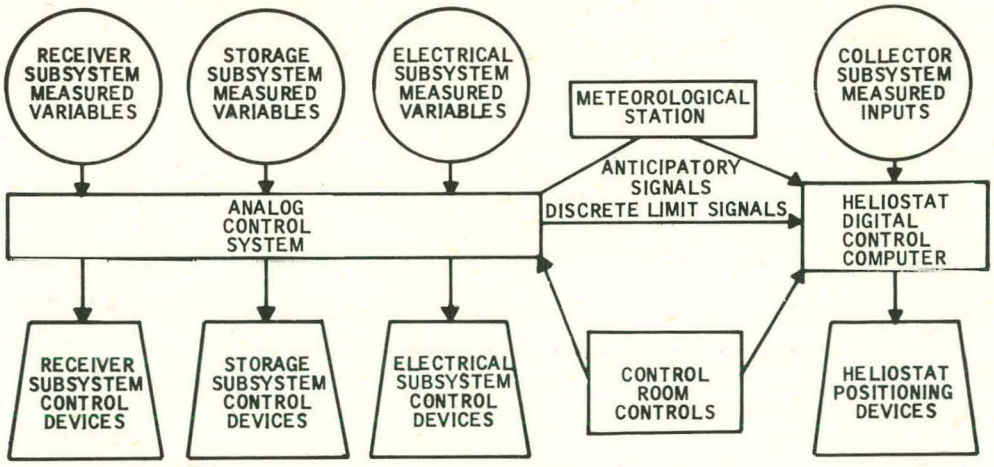

Figure 11. Control Coordination of Plant Subsystems

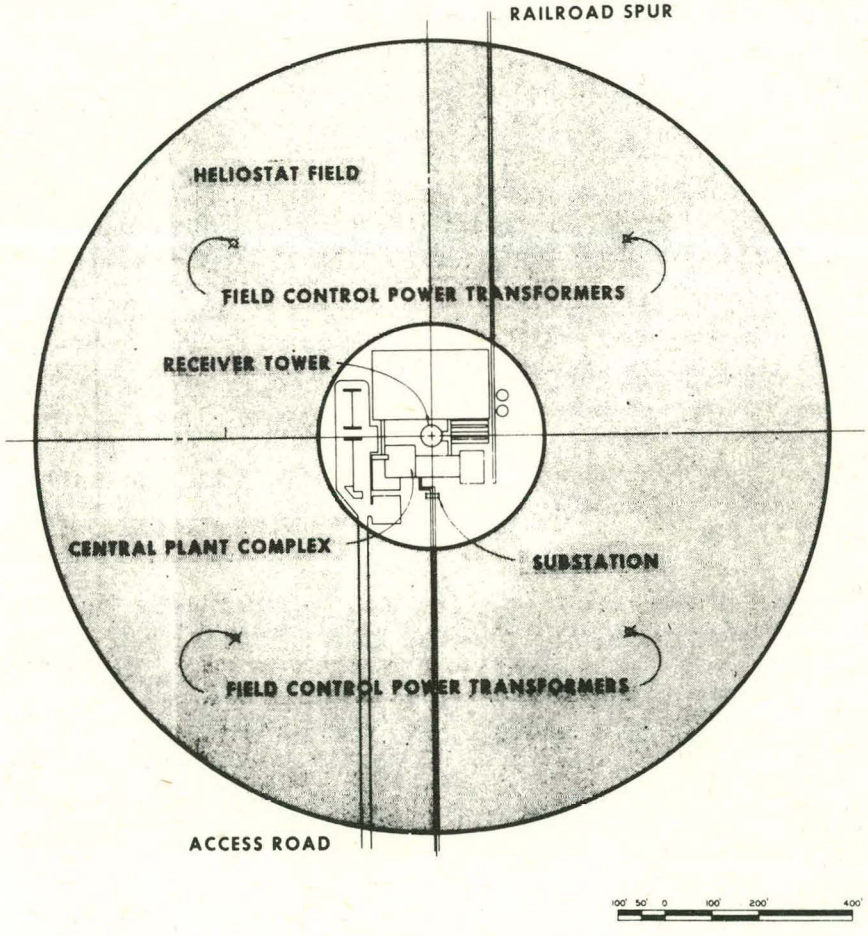

Figure 12. 10-MW Solar Pilot Plant Site Plan

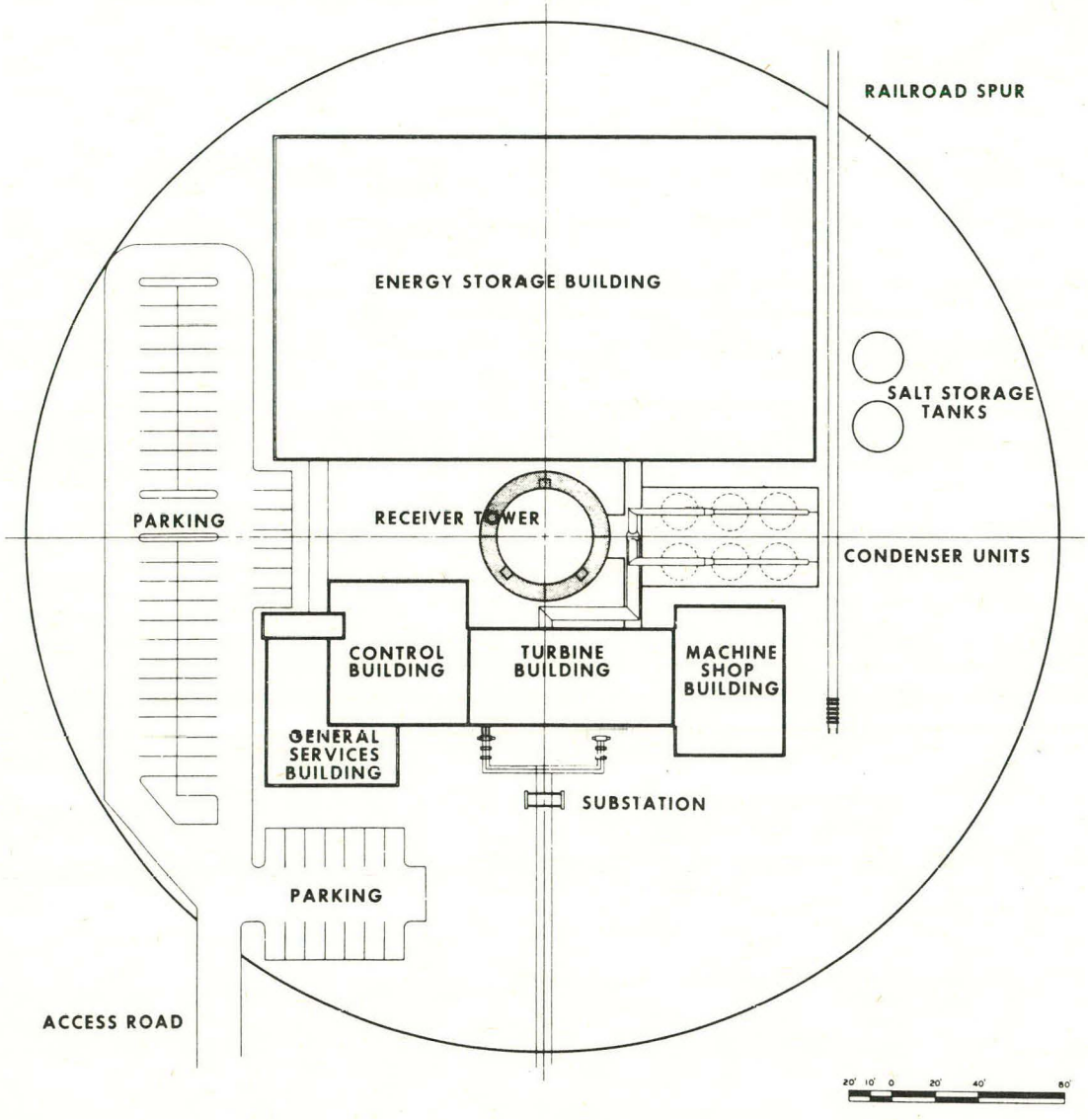

Figure 13. 10-MW Solar Pilot Plant Central Plant Complex

SECTION III
COLLECTOR SUBSYSTEM RESEARCH EXPERIMENT

DESCRIPTION OF SUBSYSTEM

The essential elements of the solar collector subsystem are shown in Figure 14. This baseline features:

- Computed sun tracking and calculation of heliostat commands based on line-of-sight vectors to the sun and the tower
- Low-profile, two-axis gimbaled heliostats
- Commands to two motors at each heliostat from the central controller
- Periodic heliostat calibration on a target array on the tower near the receiver
- Continuous central control of heliostats for flexibility of power plant operation. The subsystem control scheme is shown in Figure 15.

The subsystem baseline is predicated on a tilt-tilt gimbal configuration for the heliostat array. The parametric tradeoff considerations by which this choice was made are presented in Appendix A.

OBJECTIVE OF THE EXPERIMENT

The collector subsystem research experiment (SRE) is designed to evaluate the preliminary baseline by testing:

- Signal distribution to heliostats
- Noise rejection and signal detection at the calibration array
- Tracking and control concepts
- Environmental effects on field operation of the subsystem

The findings of the experiment will be directly applicable to the subsystem design for the pilot plant. Table 7 compares the current elements of the experiment with those of the current conceptual pilot plant.

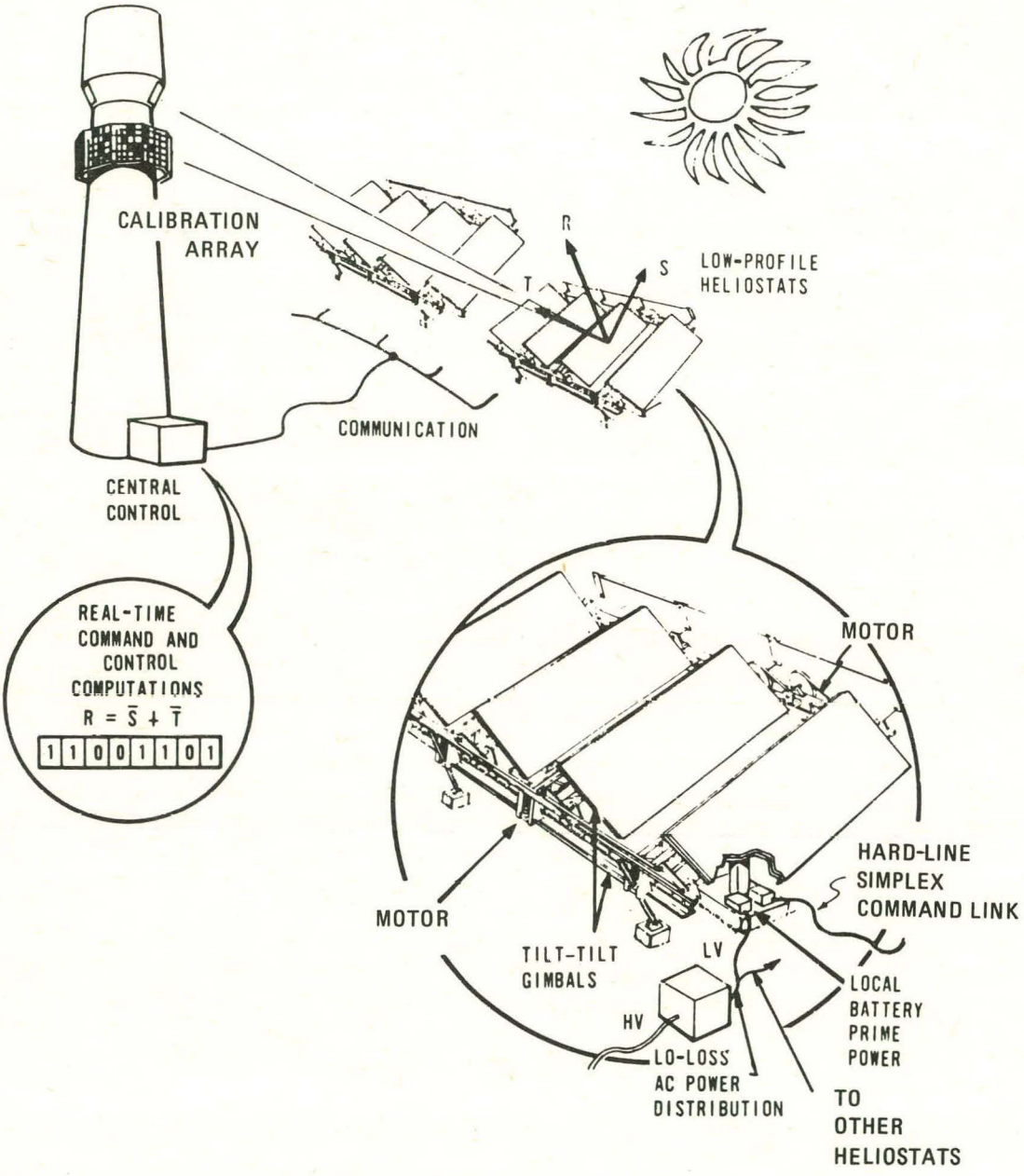

Figure 14. Collector Subsystem Baseline

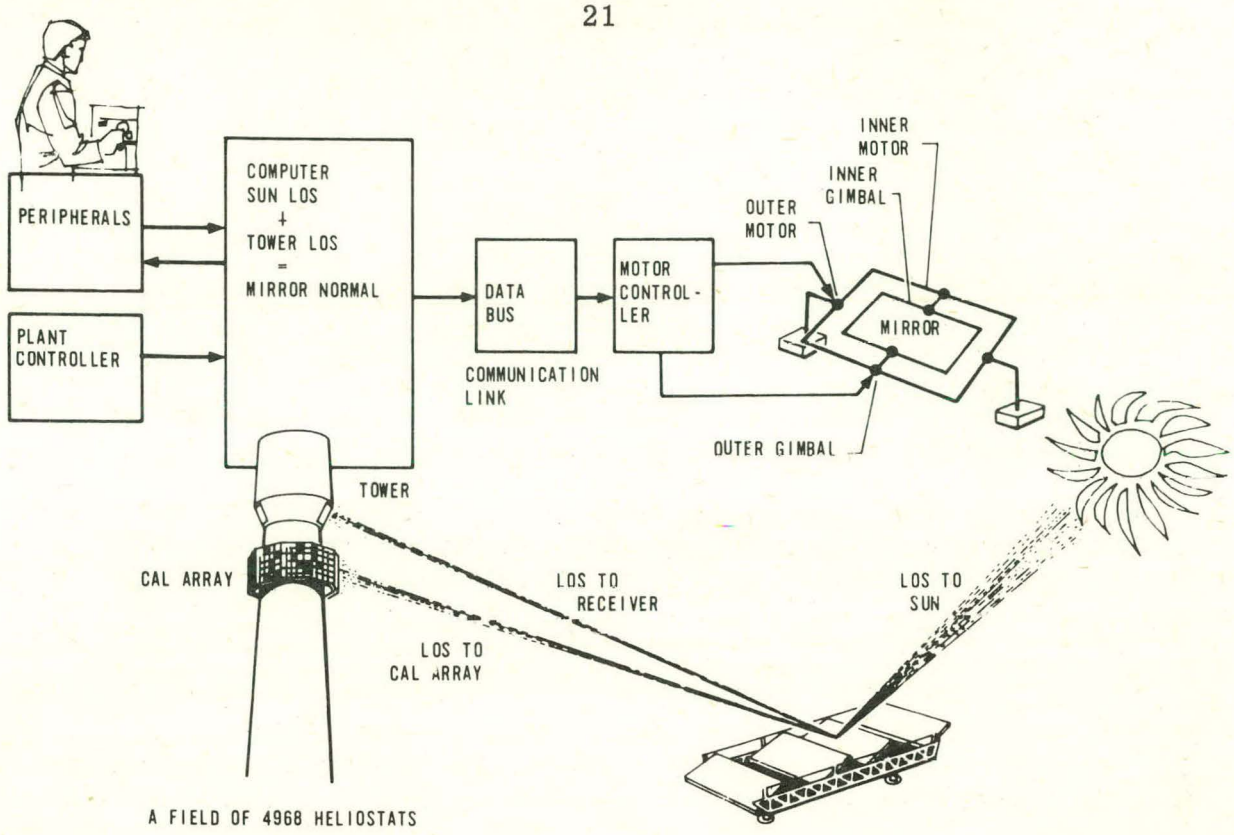

Figure 15. Collector Subsystem Control Scheme

Table 7. Comparison of Research Experiment Elements With Pilot Plant Concepts

Element	Research Experiment	Pilot Plant
Heliostat	40-square-meter tilt-tilt heliostat	Same
Power distribution	110V, 60-Hz, plus battery. No high voltage.	High voltage, 110V, 60-Hz, plus battery
Signal distribution	Serial data bus	Same
Tower	Simulated, scaled	Concrete, about 400 ft high
Calibration array	Light detectors on a matrix grid with electronics	Same
Target	Similar to calibration array	Receiver
Processor	One minicomputer with special I/O	Could be same except increased quantity
Control software	Sized for experiment; simulates operator and central controller I/O	Differs in heliostat quantity, geodetic and field layout constants
Test software	As necessary for data collection and correlation for research experiment	As necessary for initialization and maintenance for pilot plant
Test equipment	Meteorological and other commercial instrumentation for test data collection	No nonstandard instrumentation, meteorological and other commercial instrumentation for station maintenance

DEFINITION OF THE EXPERIMENT

Test Plan

The collector subsystem test plan elements are listed in Table 8. The testing is being done at Honeywell's Aerospace Division, St. Petersburg, Florida, facility. Performance data will be gathered continually by computer. Manual tests will be conducted in areas that do not readily lend themselves to automation. Table 9 is a list of support equipment for the experiment. Provisions will be made to interrupt the power or introduce power transients to test the capability of the heliostat to recover and/or cover up. Emergency conditions will be simulated to test the defocusing of the heliostat.

Environmental testing at the system level will be done in the natural Florida environment, augmented by additional heat and wind. Cold temperature data will be extrapolated from the operational data gathered over the course of the experiment.

Receiver Simulation

A photodetector array will be used to monitor the heliostats for pointing accuracy and image quality. The array will be similar to that used for calibration. The energy centroid will be measured and recorded as a measure of pointing accuracy. Concentration will be determined from image shape, and a map will be made of the image shape. Background light is expected to be 0.2 sun, with average signal strength equal to the ratio of the collected area/concentrated area, or 2.5 suns. This provides a signal-to-background ratio of 12.5 to 1.

Test Tower

The receiver simulation array may be mounted on the test tower above the calibration array, as shown in Figure 16. The tower may be located on the corner near the roof of Environmental Building No. 2. The central location of this building, shown in Figure 17, provides omnidirectional access to the target and calibration arrays. The stairway providing access to the roof and test tower will be fenced to control entry onto the roof when the test heliostats are pointed at the tower.

Collector SRE Schedule

The schedule for the collector SRE is shown in Figure 18. Detailed design work and initial construction of test items, which were preceded by a thorough parametric analysis to select the heliostat configuration, began in the last quarter of 1975 and was completed satisfactorily at the end of that period. Most of the subsystem fabrication, integration, test, analysis, and documentation work will be done in 1976.

Table 8. Collector Subsystem Test Plan Elements

Major Test Area	Parameter	Data Logging
Mirror tests	Reflectivity, cleanliness	Manual/auto
Drive system	Capability, load, smoothness, repeatability	Manual/auto
Drive scale factors	Scale factor and linearity	Manual/auto
Tracking and pointing	Accuracy, repeatability	Manual/auto
Focus stability	Long-term stability, day-to-day	Manual/auto
Emergency conditions	Defocus, shut down, recovery	Manual/auto
Field power consumption	Heliostat consumption, duty cycle	Manual
Environmental:		
Additional heat	Raise temperature to upper limits	Manual/auto
Wind	Pointing accuracy of motor power versus wind	Manual/auto
Natural	Rain, clouds, temperature, wind	Manual/auto
Weather	Record weather profile versus test conditions	Manual/auto

Table 9. Support Equipment for Collector SRE

Capital	Purchased
Honeywell Model 153x17 temperature Recorder	MRI Model 1022 Wind Sensors
Computer, DDP-516	MRI Model 815-1 Temperature Sensor
Wild Autocollimators	MRI Model 751 Pressure Sensor
Kern Model DKM2 Theodolites	MRI Model 817-1 Humidity Sensor
Tektronix Model 7704 Oscilloscope	
Lambda Model LMCC15 Power Supply	
Power Design Model TW5005 Power Supply	
Simpson Model 260 Multimeter	
Fluke Model 8000 DVM	
Weston Model 433 Ammeter	
Weston Model 432 Wattmeter	
EH Model 139B Pulse Generator	
HP Model 5327B Counters	
Cary Model 14 Reflectometer (Mpls)	

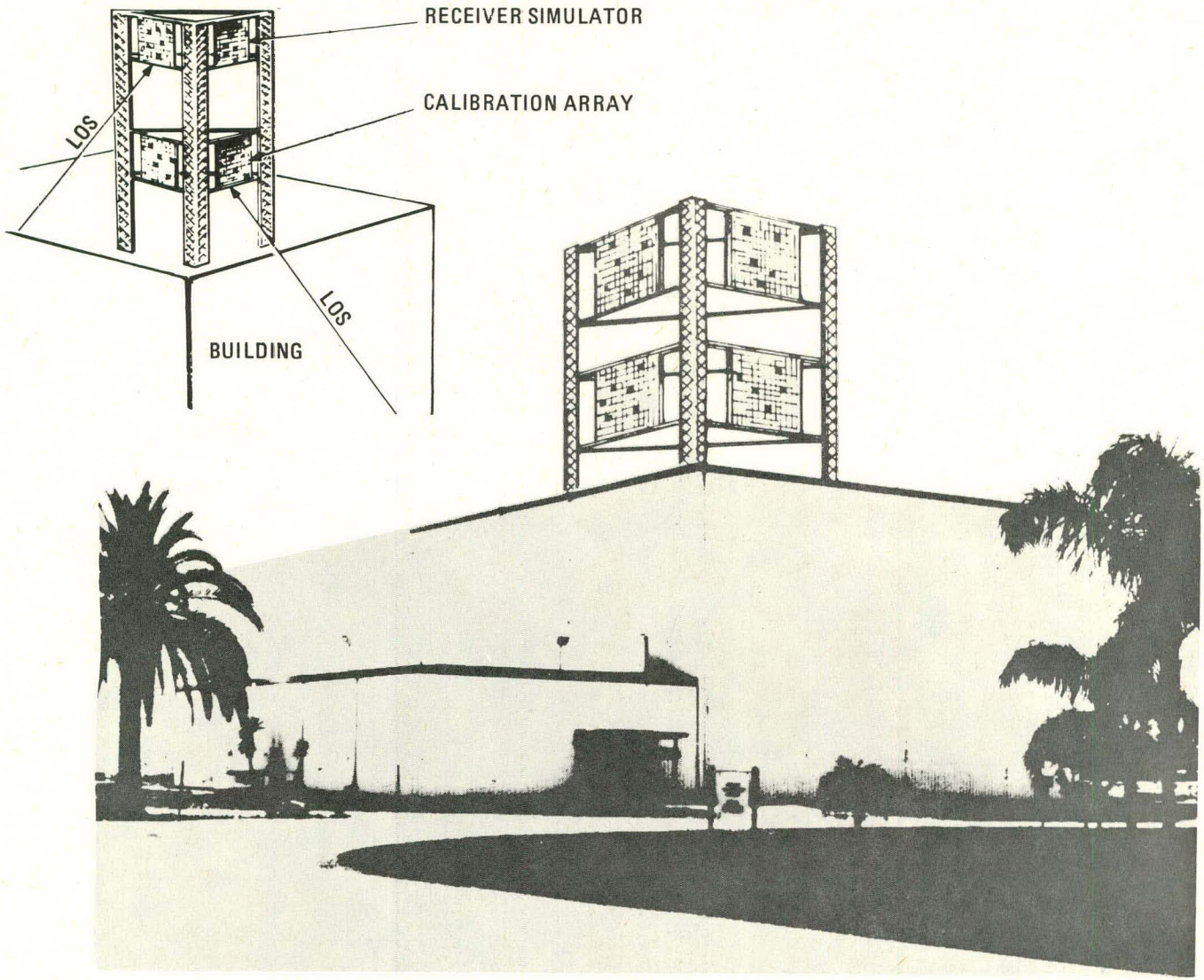

Figure 16. Target and Test Tower for Collector Subsystem Tests

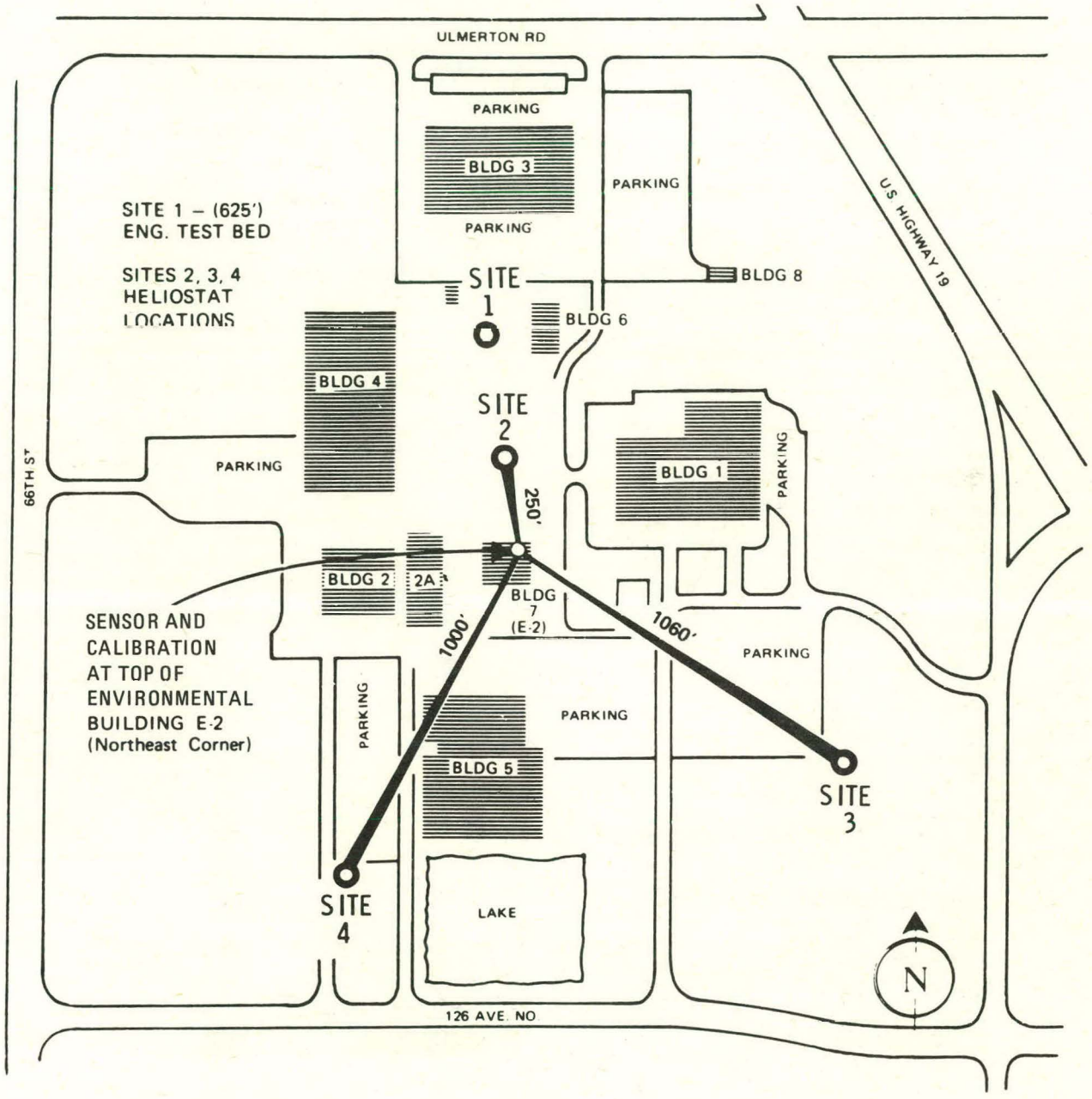

Figure 17. Collector SRE Preliminary Plot Plan

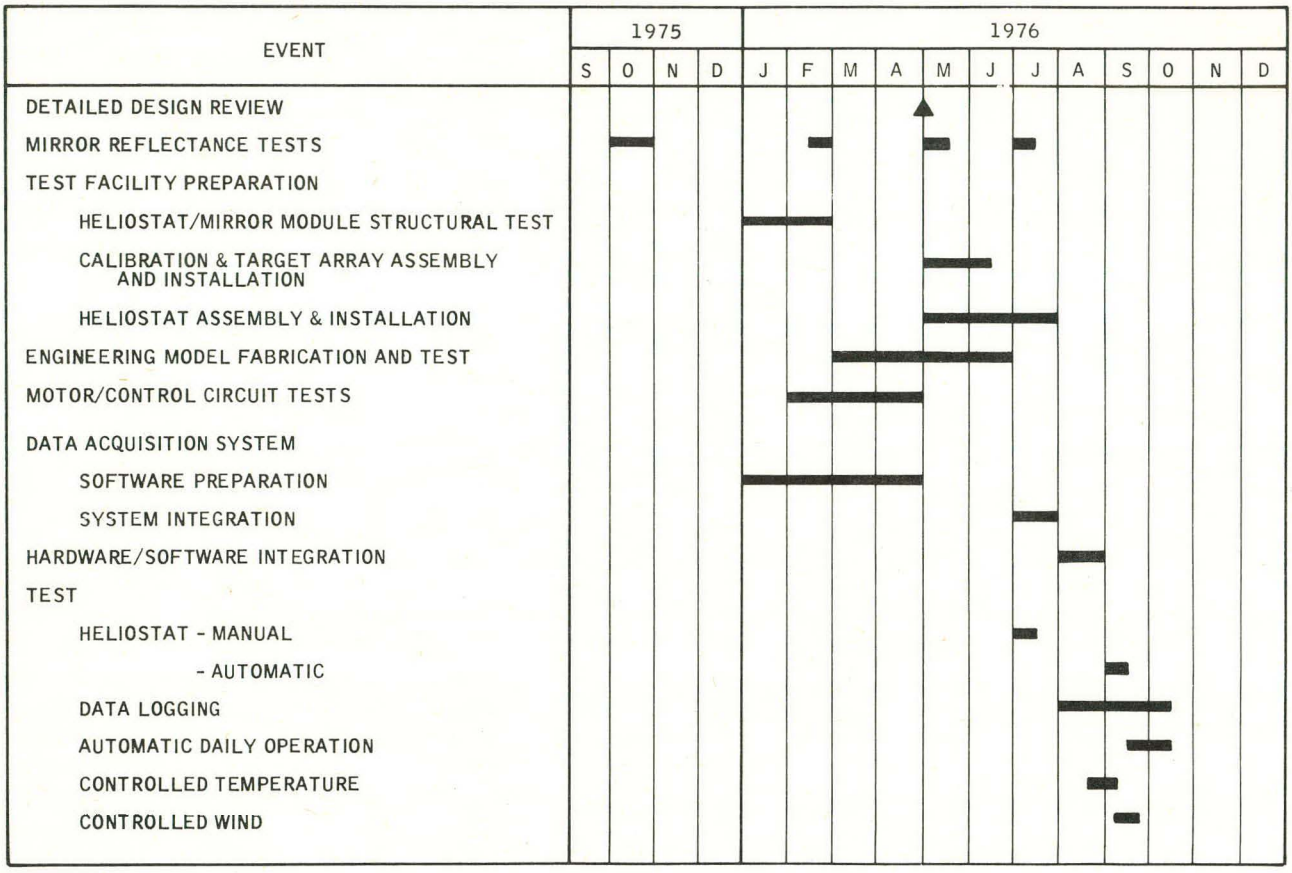

Figure 18. Collector SRE Test Schedule

PLANS FOR NEXT QUARTER

Plans for the first quarter of 1976 include:

- Continue detail design and development
- Assemble and install one target and calibration array
- Conduct mirror module structural and reflectance tests
- Continue motor and motor control circuit development
- Submit pilot plant initial cost data
- Hold coordination meetings with other SRE participants.

SECTION IV
STEAM GENERATOR SUBSYSTEM RESEARCH EXPERIMENT

DESCRIPTION OF SUBSYSTEM

The baseline solar steam generator (Figure 19) uses existing fossil fuel boiler technology to reduce the risk of failure in critical design areas and expedite the experiment. It has these key features:

- A recirculating drum boiler to facilitate daily startup and shutdown
- Pump-assisted circulation to permit use of smaller boiler tubes
- A helical superheater for relatively free radial thermal expansion and minimization of heat flux maldistribution
- Spray attemperators to control steam temperature between the two stages of the superheater.

A flow schematic of the steam generator is shown in Figure 20.

OBJECTIVE OF THE EXPERIMENT

The steam generator SRE is designed to prove the validity of the preliminary design by:

- Demonstrating technical feasibility
- Identifying operating procedures
- Confirming fabrication techniques
- Verifying the applicability of standard components and materials and the structural, thermal, and hydraulic analysis of the steam generator
- Verifying the control of the subsystems
- Providing supportive data for system effectiveness studies

The SRE system generator will be scaled and matched to the dimensions and materials of the pilot plant version to ensure the validity of the findings of the experiment. A size comparison of the two is shown in Figure 21.

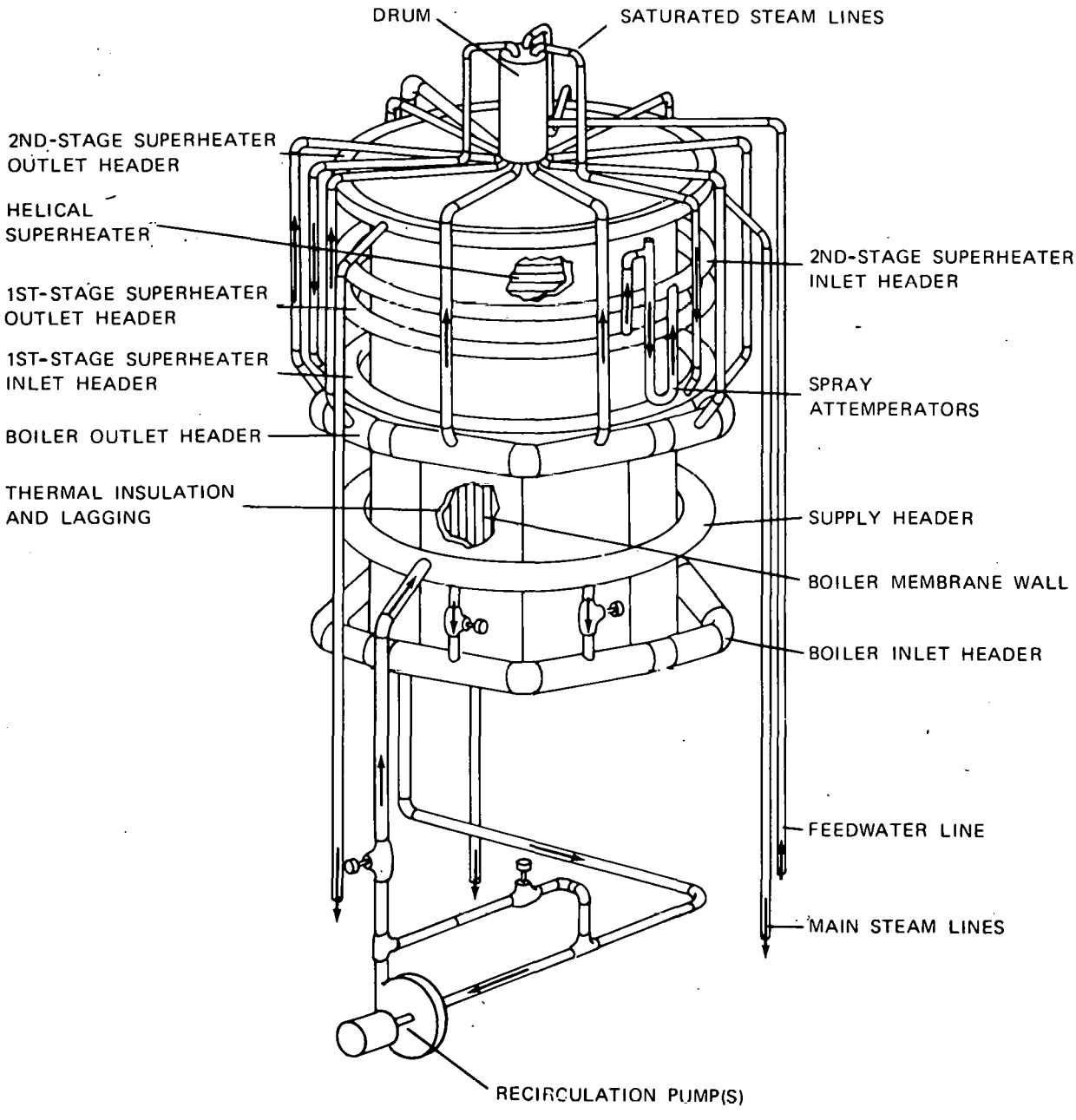

Figure 19. Pilot Plant Steam Generator Design Arrangement

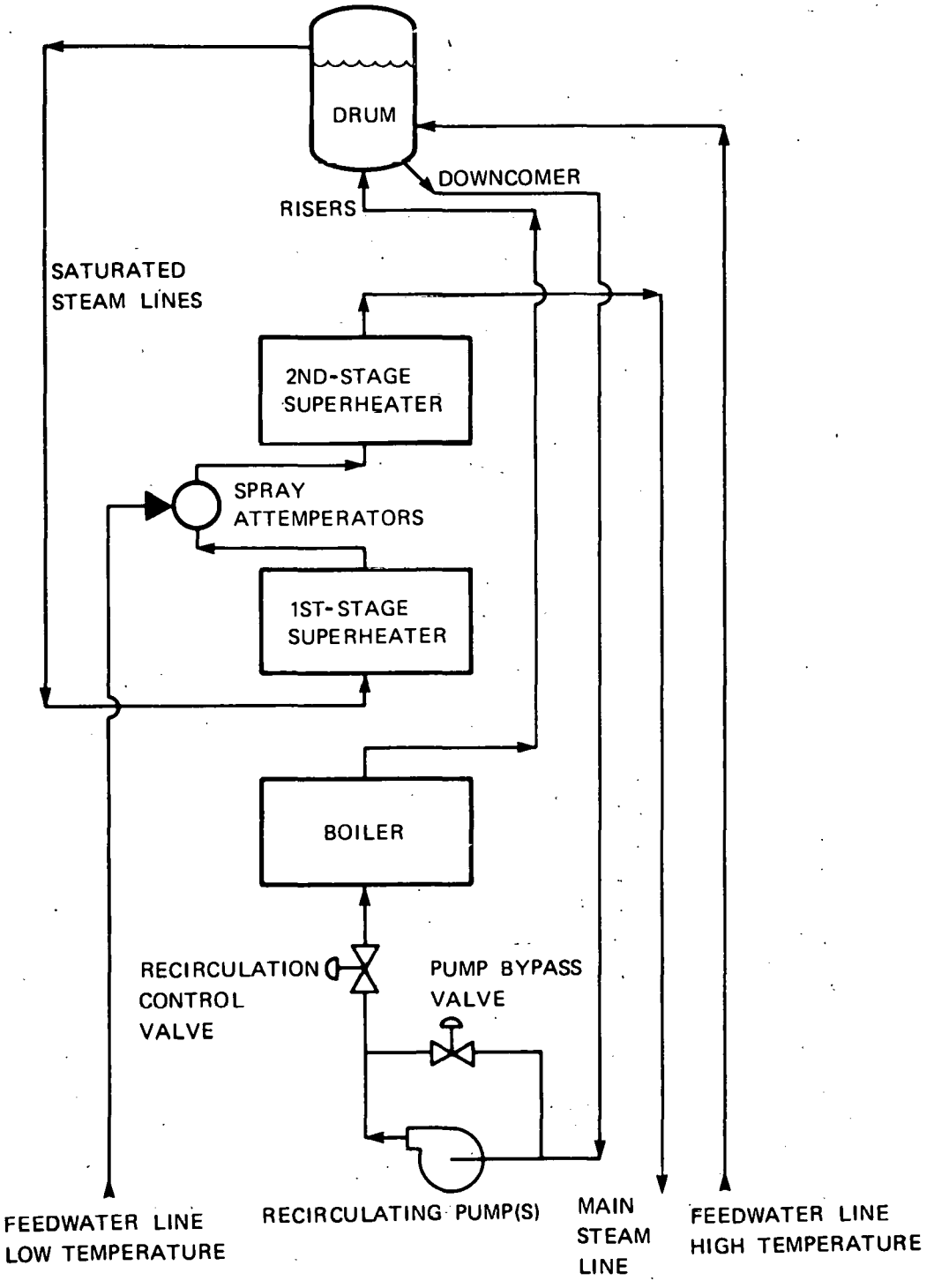

Figure 20. Solar Steam Generator Flow Schematic

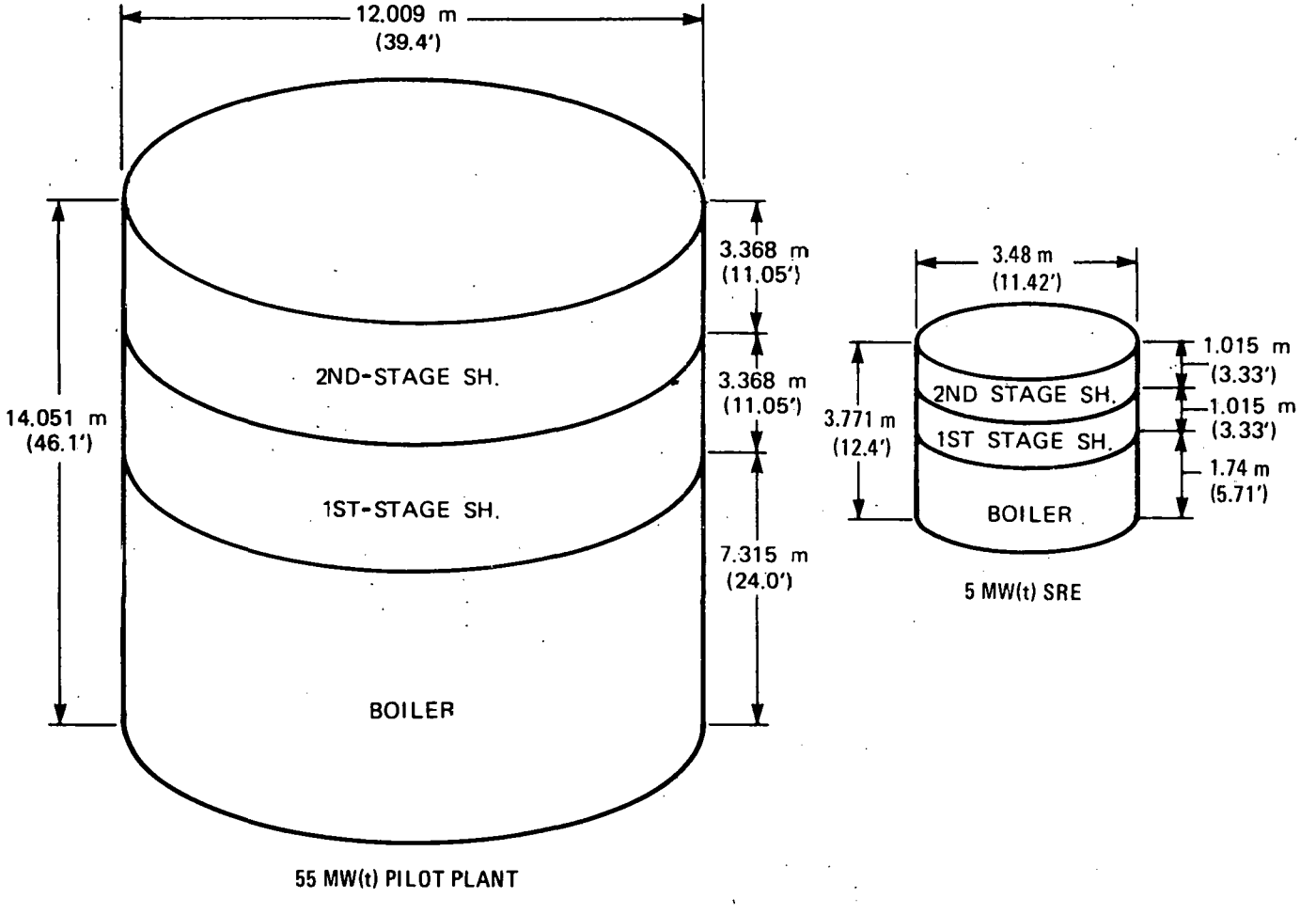

Figure 21. Pilot Plant and SRE Steam Generator Comparison

DEFINITION OF THE EXPERIMENT

As stated, critical design parameters of the experimental model are the same as or proportional to those of the pilot plant steam generator. The original parameters for the model were, however, changed in several instances to permit shipment of the model to the test site by truck and to refine the design (Table 10). The arrangement of the model (Figure 22) differs from that of the pilot plant version (Figure 19) only in that the recirculating pump is relocated to the side of the steam generator.

Table 10. Steam Generator Specifications Comparison

Parameter	Unit	PDBR SRE	Updated SRE
Cavity size	meters (feet)	3.62 (11.88)	3.48 (11.42)
Steam pressure at superheater outlet	bars (psig)	103 (1500)	109 (1575)
Drum operating pressure	bars (psig)	117 (1700)	122 (1775)
Boiler and superheater design pressure	bars (psig)	124 (1800)	130 (1875)
Boiler height	meters (feet)	2.21 (7.24)	1.74 (5.71)
Superheater tube material	---	Croloy 2-1/4	To be determined.
Superheater tube, OD	cm (inches)	1.27 (0.5)	2.54 (1.0)

Test Plan

The test plan calls for testing the experimental model steam generator and thermal storage subsystems at the Riverside Plant of Northern States Power Company (NSP) in Minneapolis. The test items will be installed following necessary modifications to piping in the plant. The subsystems control center will be assembled in Honeywell's Ridgway facility in Minneapolis and transported to the plant after the experiment is set up.

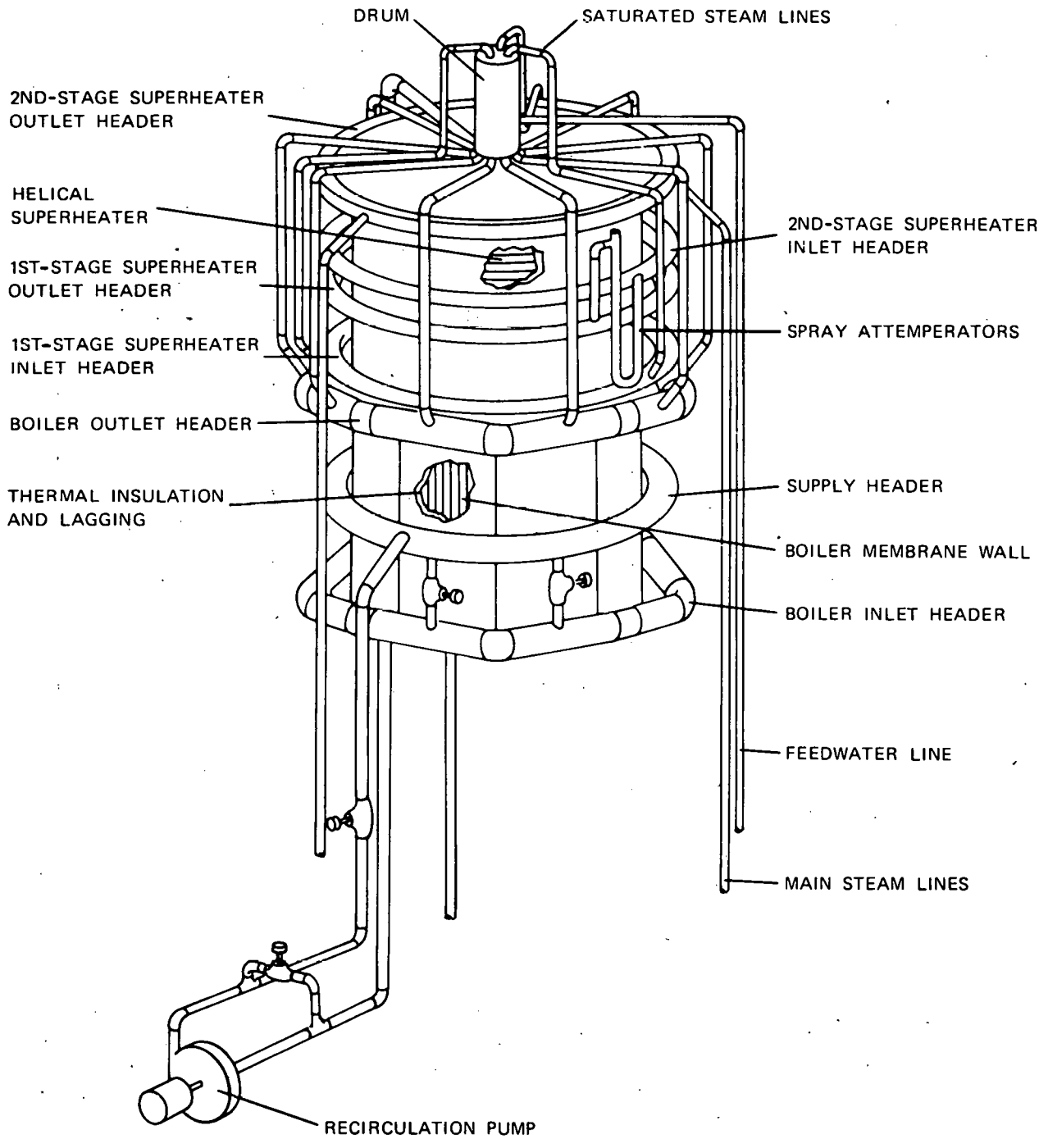

Figure 22. Steam Generator SRE Design Arrangement

The testing will consist of the following steps to ensure safety and proper instrumentation performance and to verify steady-state and transient performance of the steam generator:

- Initial debugging
- Cold checkout
- Hot checkout
- Control system tune-up
- Initial calibration tests
- Steady-state performance tests
- Transient performance tests

Appendix B contains stress and pressure analysis of the boiler section and superheater, made to evaluate the safety of the subsystem.

Test Site

Figure 23 is an outside view of the NSP plant. Figure 24 shows the steam generator test area, looking down from the turbine floor.

Test Arrangement

Figure 25 shows the steam generator and thermal storage test arrangement within the plant. Figure 26 shows the relative locations of the test areas, sources, and sinks. The feedwater available can be used without additional refinement. The water specification for the SRE model is compared with the available supply in Table 11.

The steam generator and solar simulator will be installed at the basement level, with the steam generator rising vertically through the 6.7- by 12.5-meter opening in the turbine floor. The transformer and power controllers for the solar simulator will also be installed at the basement level.

The mobile trailer housing the control and data acquisition systems will be installed alongside the steam generator on the turbine floor (Figure 27).

Solar Simulator

The solar simulator (Figure 28) will provide controlled radiant heat to the receiver for the steam generator. The lamp array tower will be inserted in the receiver cavity. The power controllers will be adjacent to the base of the receiver, and the control console will be inside the control center trailer.

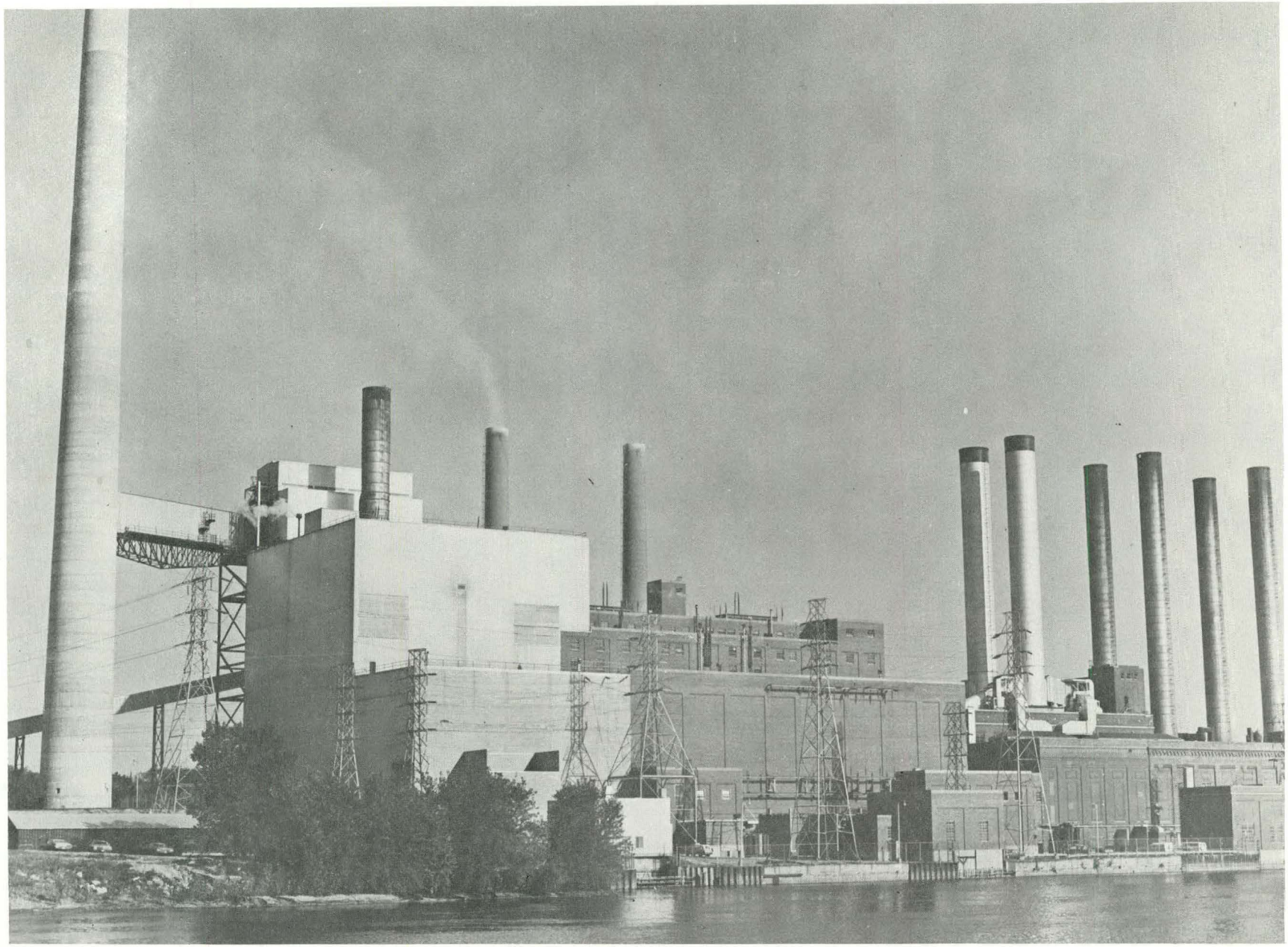

Figure 23. View of NSP Riverside Plant

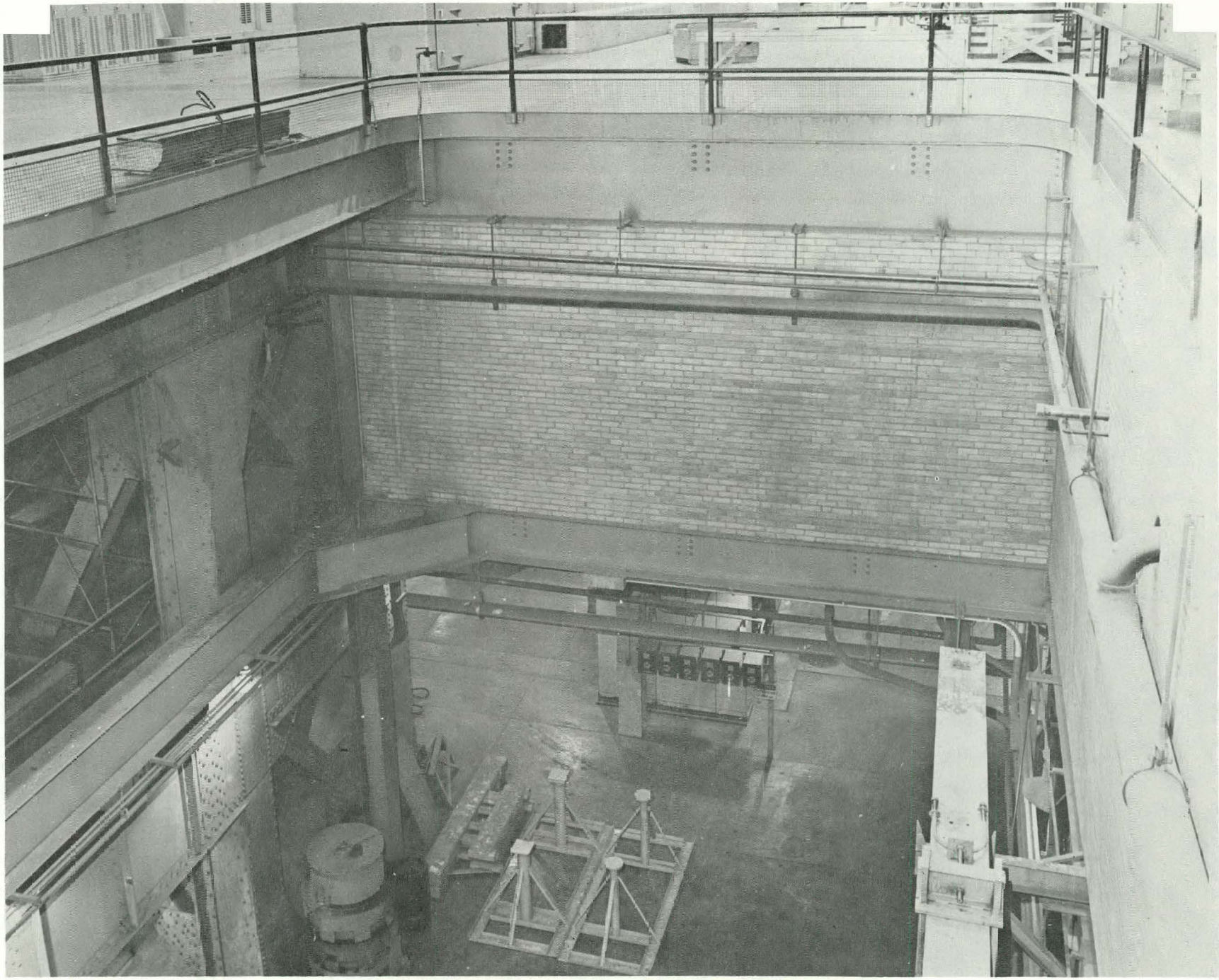

Figure 24. Steam Generator SRE Test Area

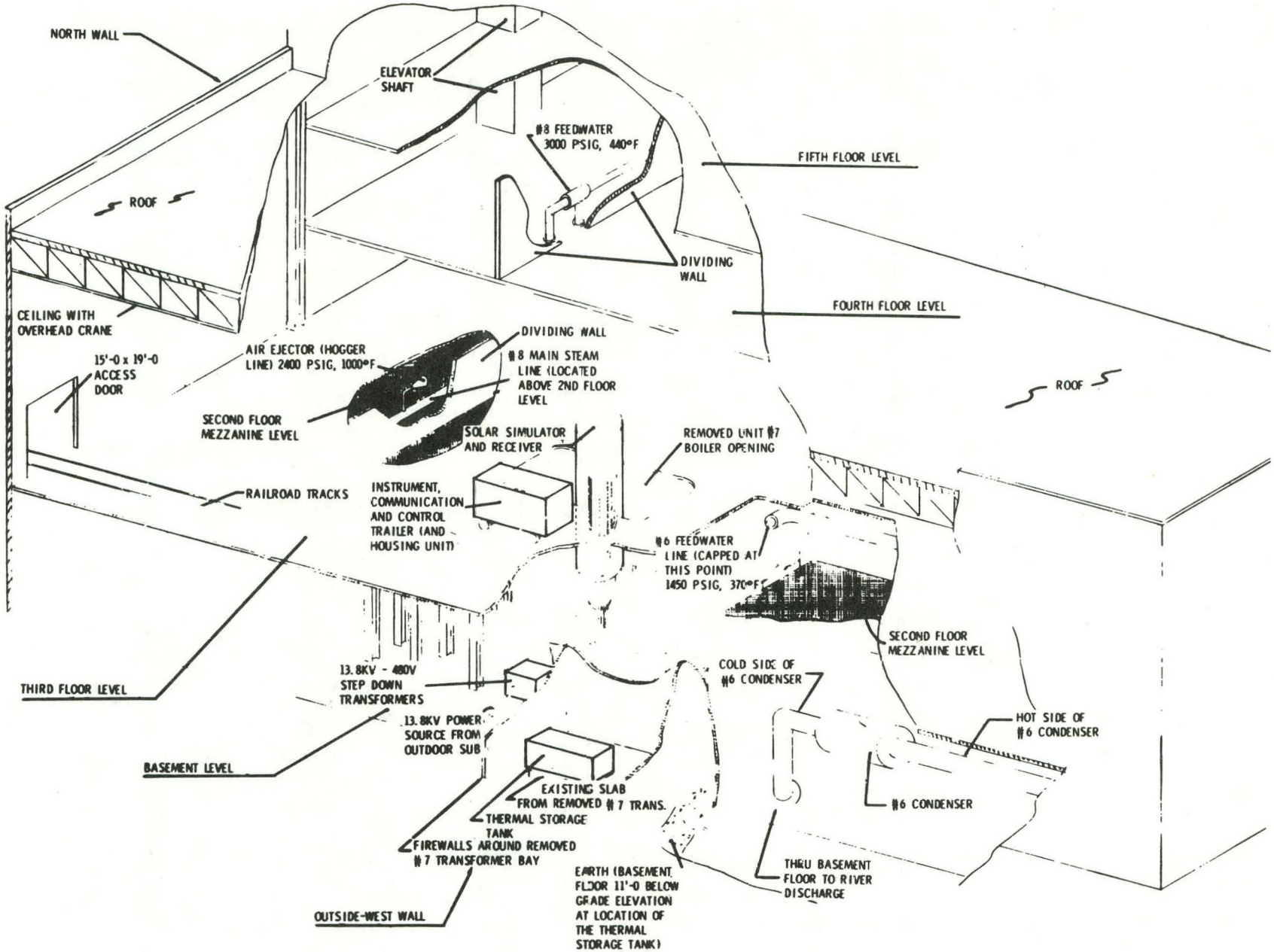

Figure 25. Steam Generator and Thermal Storage Test Facility

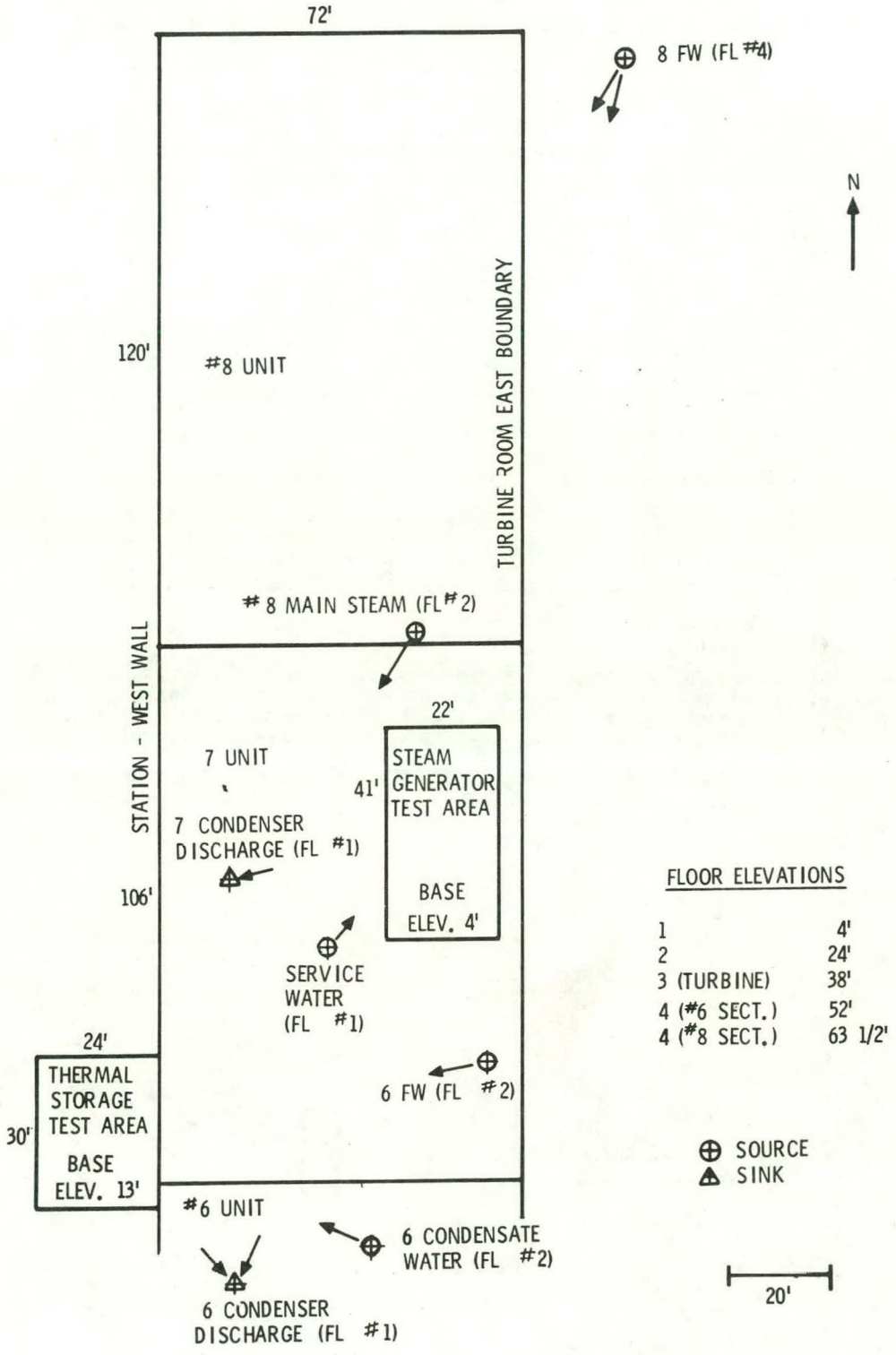

Figure 26. Relative Location of Test Areas, Sources, and Sink

Table 11. Steam Generator SRE Water Specifications

Item	Pilot Plant PDBR Spec	Riverside - NSP No. 8 Feedwater SRE
pH factor	9.3 → 9.5*	9.0 → 9.5
Oxygen (O_2), ppm	0.007	0.005
Iron (Fe), ppm	0.01 max	0.01
Copper (Cu), ppm	0.005 max	0.005 max
Sand (SiO_2), ppm	0.02 max	0.02 max
Total hardness, ppm	0.0*	Detection limit
Organics, ppm	0.0**	Detection limit
Total solids, ppm	0.05 max	0.05 max
Ammonia (NH_3)	As required	To be determined
Hydrazine (N_2H_4)	As required	To be determined

*With carbon-steel feedwater heaters

**The specification of 0 ppm is given as a recommendation to keep these contaminants completely out of the feedwater. Special analyses for these contaminants are available. Detection limits using these special analyses are 2.0 ppm for total hardness and 0.05 ppm for organics.

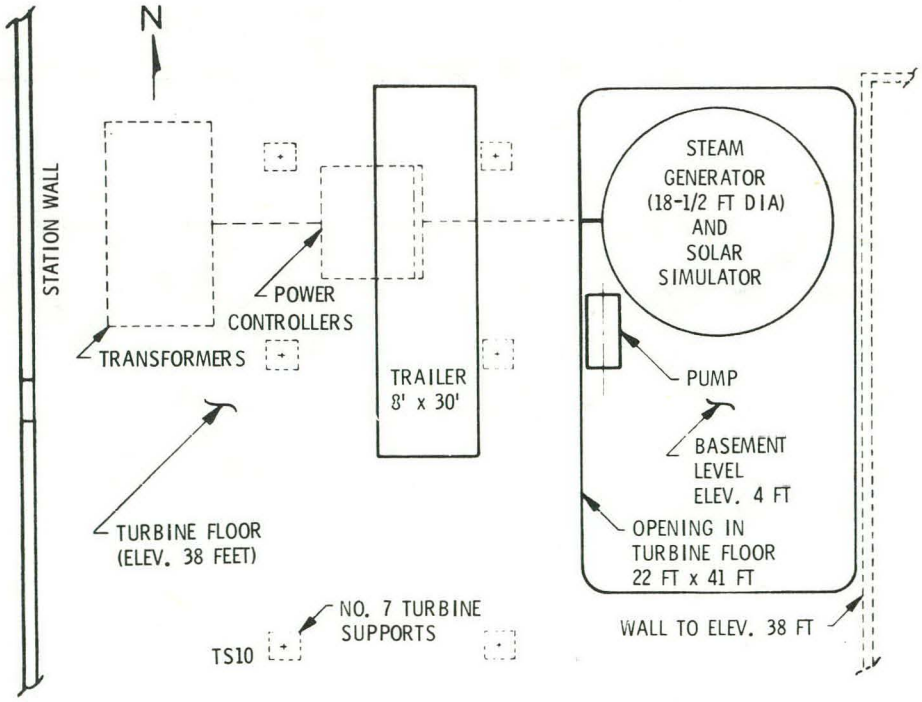

Figure 27. Steam Generator Test Installation

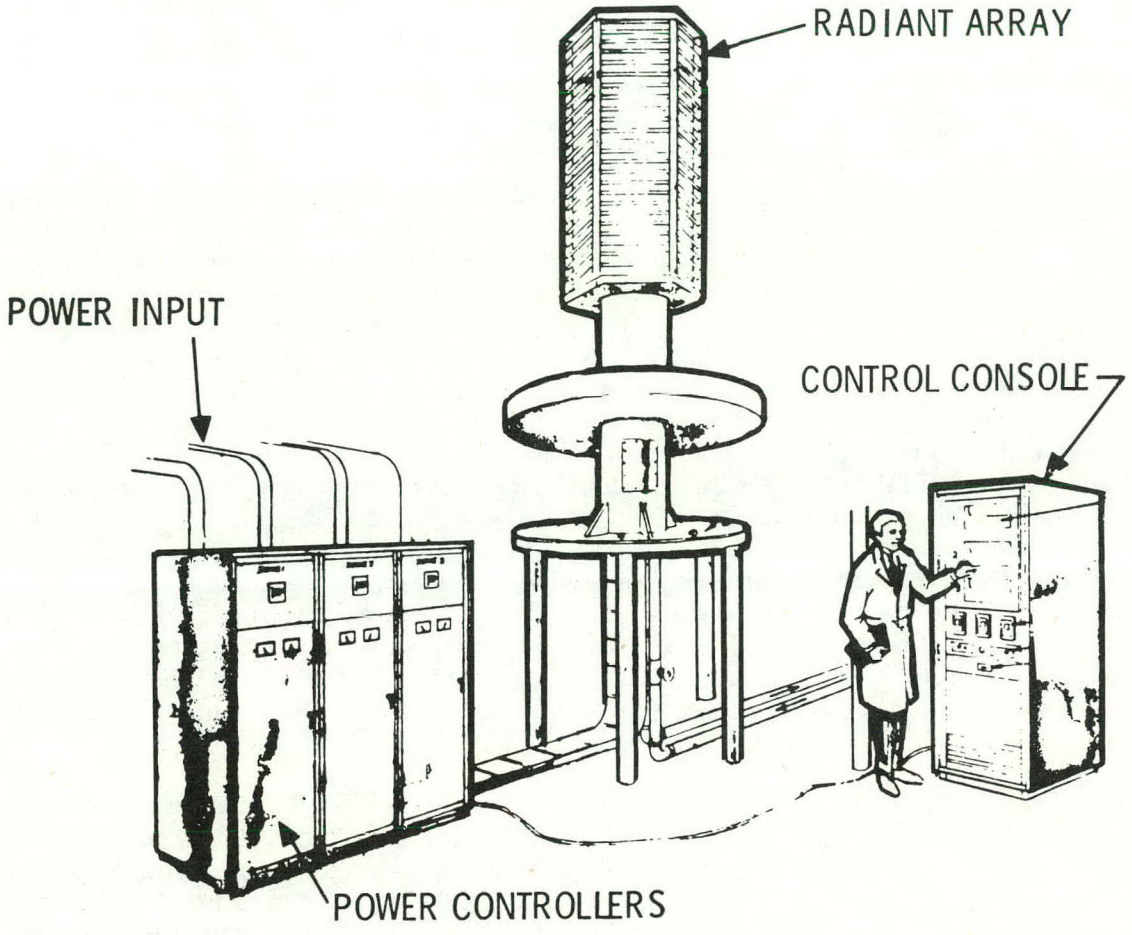

Figure 28. Solar Simulator System

The lamp array tower is a 27-facet cylinder with the facets positioned so the flux peaks are in the azimuthal center of each three-section segment of the boiler membrane wall (Figure 29).

The solar simulator power controllers require 310-volt rms, three-phase (A) 60-Hz power inputs. This requirement will necessitate a transformer substation to obtain those voltages from the 13.8-kV, three-phase (A) source available at the test site. A high-voltage fuzed switch will be used in the transformer substation rather than circuit breakers to reduce cost and voltage delivery time. The substation arrangement is shown in Figure 30.

Test Instrumentation and Data Acquisition

Instrumentation -- The test objectives determine the instrumentation. The types of measurements required are relatively certain, but the quantity is dependent on the detailed design. Minimum requirements are listed in Table 12. The data acquisition system can handle additional instrumentation if required.

Data Acquisition -- The data acquisition system is being designed to process all measurements from the steam generator and thermal storage SRE tests. They will not, however, be run concurrently. It is estimated that the steam generator tests will cover thirty 8-hour sequences involving 400 temperature points and 200 analog points (e.g., pressure differential).

The System 700 Process Analyzer (Figure 31) was selected for its flexibility. All measured and calculated data will be displayed. Measured data will also be converted to process dimensions and stored. The data processing sequence is shown in Figure 32. The plotter/line printer priority will be in this order: alarm messages, warning messages, and real-time data display. The data acquisition system will be controlled by a minicomputer.

Test Control -- The test control rationale covers considerations listed in Table 13. The testing will, as stated, be controlled from a mobile trailer adjacent to the steam generator test site. This central point, the layout of which is shown in Figure 33, will contain all of the control and display equipment necessary for test personnel to start, monitor, and conclude a test sequence without leaving the trailer. Emergency control procedures include the following:

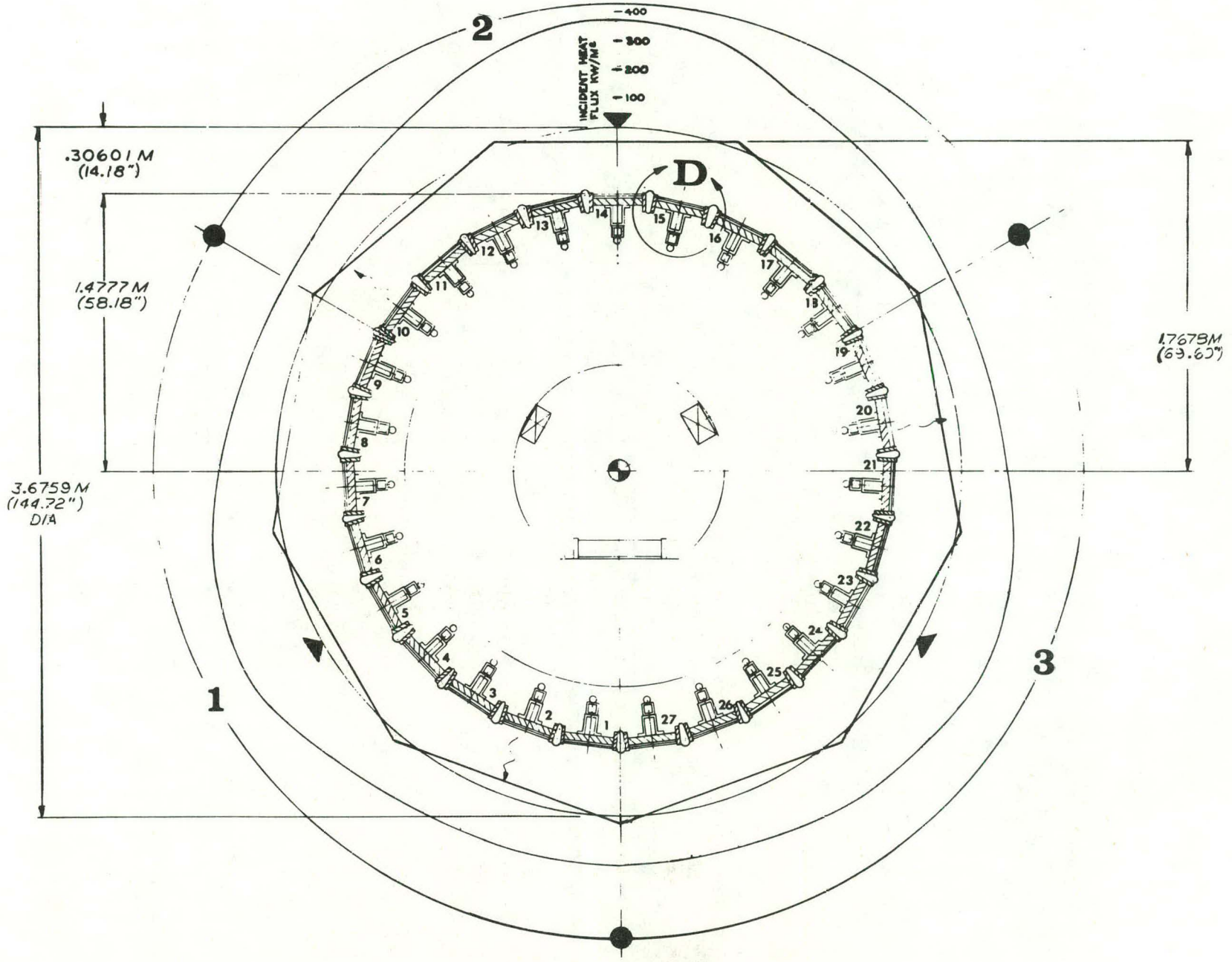

Figure 29. Lamp Array Horizontal Section

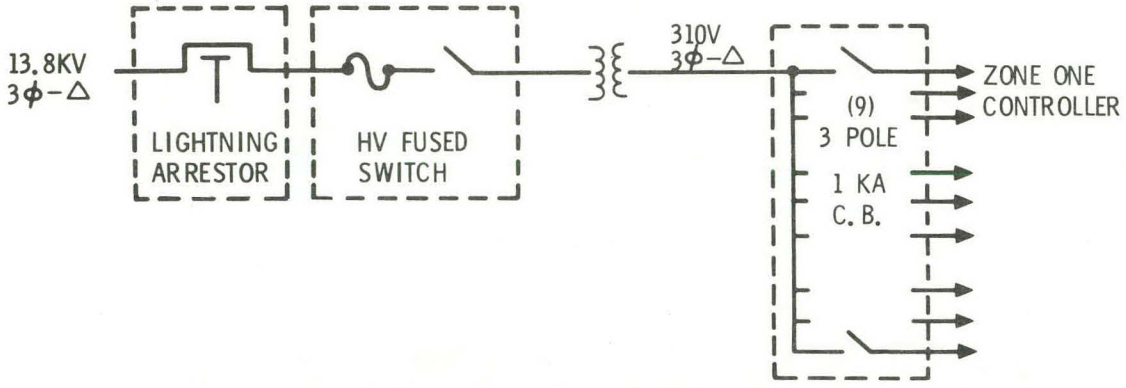

Figure 30. Solar Simulator Substation

Table 12. Steam Generator SRE Instrumentation Requirement

Type	Minimum Quantity
Temperature:	200
Headers	( )*
Drum	( )
Boiler	( )
Superheater	( )
Fluid	( )
Pressure	2
Flow	9
Drum level	1
Displacement	12

* Exact distribution to be determined

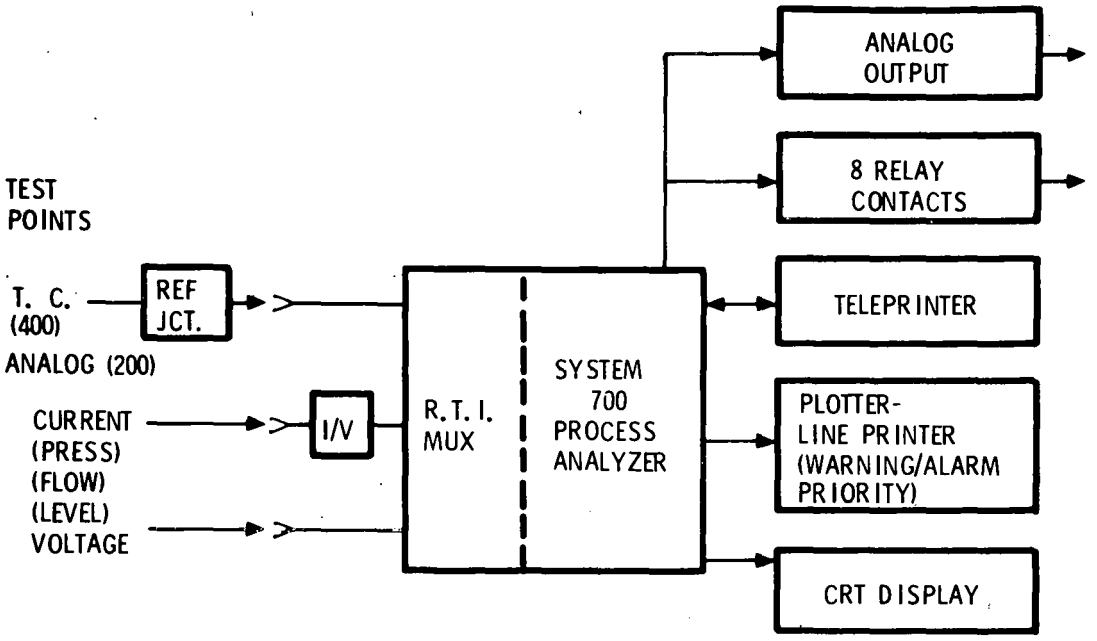

Figure 31. SRE Data Acquisition System Configuration

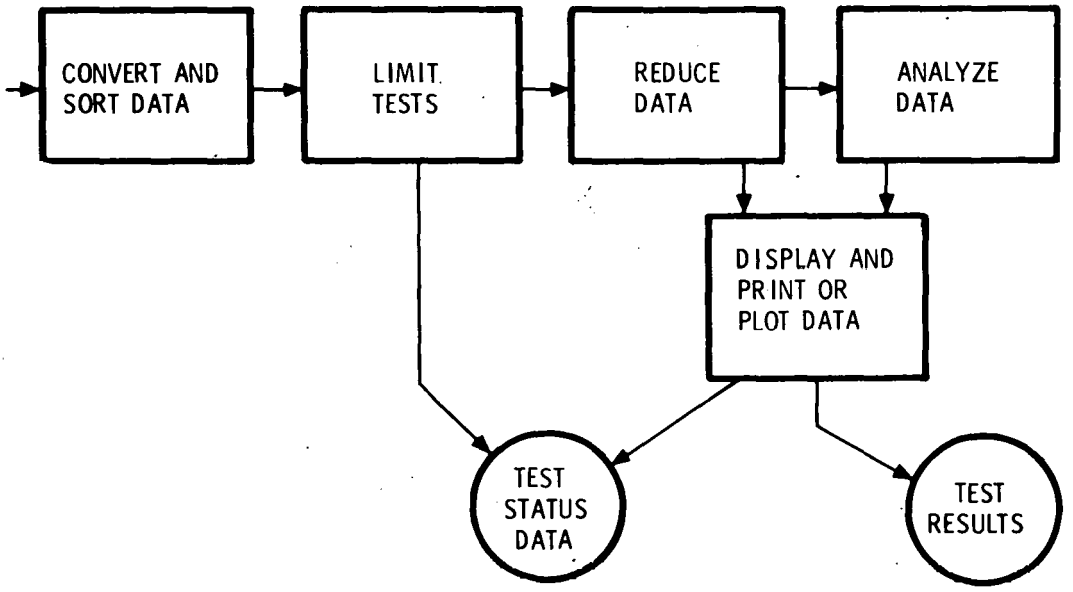

Figure 32. SRE Data Acquisition System
Data Processing

Table 13. SRE Test Control Rationale

Control Area	Feature/Benefit
Test control	• Central control of testing
Electronic control	• Fast response • Versatility as to control mode selection/adjustment • Minimizes instrument piping
Data acquisition system	• Accepts proportional 1-5V dc signals • Can provide real-time test performance information • Provides a test supervisory function in the indication and control of "alarm" situations
Measurement accuracy	• Setpoint accuracy secondary to readout accuracy • Separate temperature measurement for control and data acquisition • Pressure measurement by piezoresistive sensing elements (no mechanical linkages)
Emergency control	• Isolation of test sites from NSP operations • Automatic interlock controls

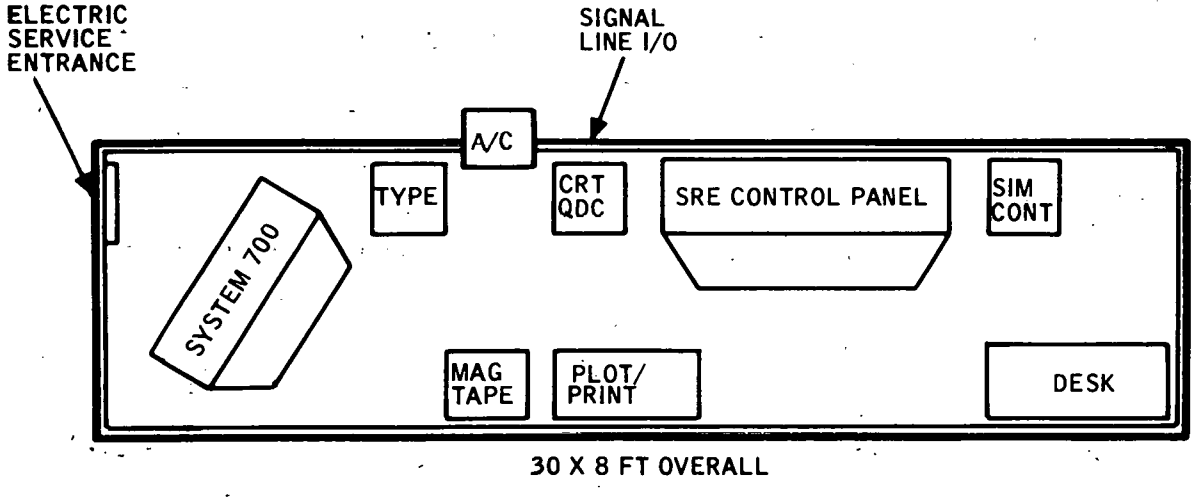

Figure 33. SRE Test Control Center

Emergency Condition	Interlock Action
Drum	
Low-level	- Operator warning - Trip solar simulator - Trip recirculation pump
High-level	- Operator warning - Shut off feedwater supply - Open blowdown - Trip solar simulator
Low Flow	
Boiler water circulation or feedwater	- Operator warning - Trip solar simulator
Recirculation pump	- Operator warning - Open pump bypass

Steam Generator SRE Schedule

The schedule for the steam generator research experiment is shown in Figure 34. Components and data and control equipment will be procured and checked out during 1976. Subsystem testing will be conducted during the early part of 1977. Maintenance of the schedule is, in part, dependent on acceptance of the conceptual design of the experiment by ERDA. Formal presentation of the design was made in mid-December.

PLANS FOR NEXT QUARTER

Plans for the first quarter of 1976 include:

- Preparing procurement specifications for the subsystem (January - March).
- Obtaining bids and letting orders for subsystem and support system components (January - March).
- Monitoring and expediting deliveries of close-in parts (January - March).
- Generating steam generator test procedures (February - March).
- Revision to the SRE conceptual design -- if and when required.

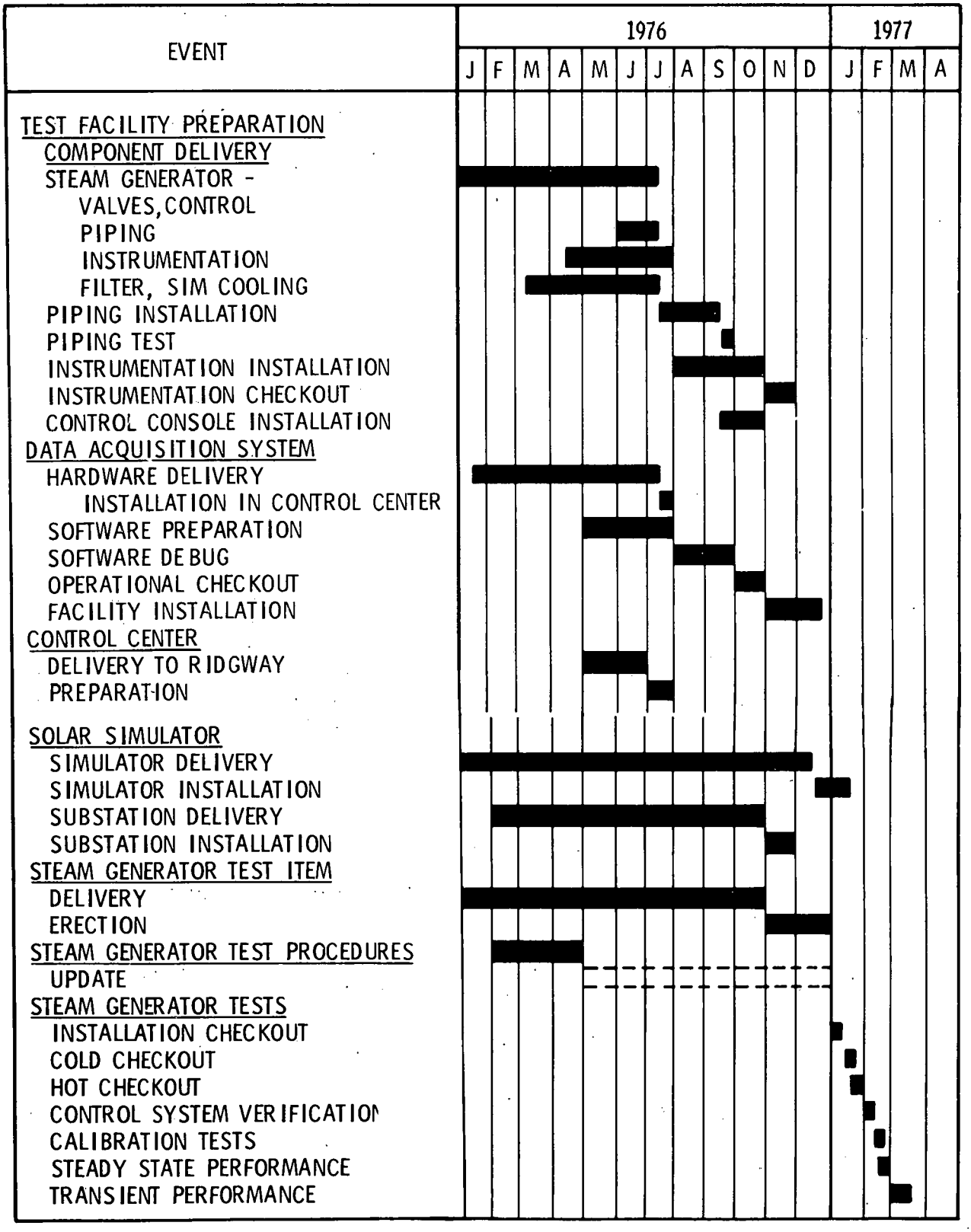

Figure 34. Steam Generator SRE Test Schedule

SECTION V
THERMAL STORAGE SUBSYSTEM RESEARCH EXPERIMENT

DESCRIPTION OF THE SUBSYSTEM

Storage Concept

The thermal storage concept uses the latent heat of fusion of a eutectic salt to store thermal energy. Energy to charge the salt is obtained as heat of condensation from steam supplied by the steam generator (receiver) subsystem. The banks of condenser tubes are located at the bottom of the storage tank. Heat transfer to the salt is by natural convection.

Heat energy in the tank is discharged by circulating feedwater through boiler tubes located at the top of the tank to obtain saturated steam. Salt buildup on the tubes is removed mechanically.

Pilot Plant Design and Performance Features

The basic design features of the pilot plant thermal storage subsystem are:

- 255-MWhr(t) storage capacity
- Salt phase change materials (including superheater)
- Battery of 12 unit cells
- Below-ground storage
- Self-regulating control system
- Modular heat exchangers
- One out main storage capacity
- 40-year storage life

The performance features are:

- Deliver 7 MW(e) net - 6 hours
- Provide 28°C superheat
- 40 bar/280°C discharge cycle
- 100 bar/510°C charge cycle
- Handle 49-MW(t) charge rate
- Heat loss < 0.1 percent per hour

Storage Salt

Figures 35 and 36 show the salt selections and selection criteria. The salt selected for the main storage is a ternary eutectic of $NaNO_3$-NO_2SO_4, melting at 287°C with a heat of fusion experimentally determined to be 94 kWhr(t)/m^3 (9100 Btu/ft^3).

The superheater storage salt is a binary eutectic of NaCl-NaOH, melting at 370°C, and with a heat of fusion in excess of 176 kWhr(t)/m^3 (17,000 Btu/ft^3).

OBJECTIVE OF THE EXPERIMENT

The objective of the thermal storage SRE is to confirm and/or expand the baseline concept to the point where preliminary design specifications can be prepared. This requires the design, construction, and test of a scale model of the pilot plant main storage cell. Geometric and dynamic similarity must be considered to achieve proper scaling and modeling of thermal and fluid dynamic phenomena. The experiment is designed specifically to:

- Provide geometric similarity of all significant dimensions
- Test at a heat flux and temperature differential (ΔT) the same as in the pilot plant for vaporizer performance
- Test at a heat flux and temperature differential the same as in the pilot plant for condenser performance
- Test at a heat flux the same as in the pilot plant for tank thermal performance

Table 14 compares the pilot plant characteristics with those of the SRE model.

DEFINITION OF THE EXPERIMENT

Test Plan

The SRE test model will contain the same phase change materials designated for the pilot plant and will exchange heat with scale models of the vaporizer and condenser heat transfer surfaces. An identical control system will be implemented to operate under the same basic charge and discharge cycle conditions. Table 15 summarizes the SRE design. Figure 37 is a schematic diagram of the experiment.

Thermal Storage Tank -- Figure 38 illustrates the scaling for the experiment. The design (Figure 39), which combines ease of construction with reasonable weight, cost, and thermal losses, requires that external stiffeners be located

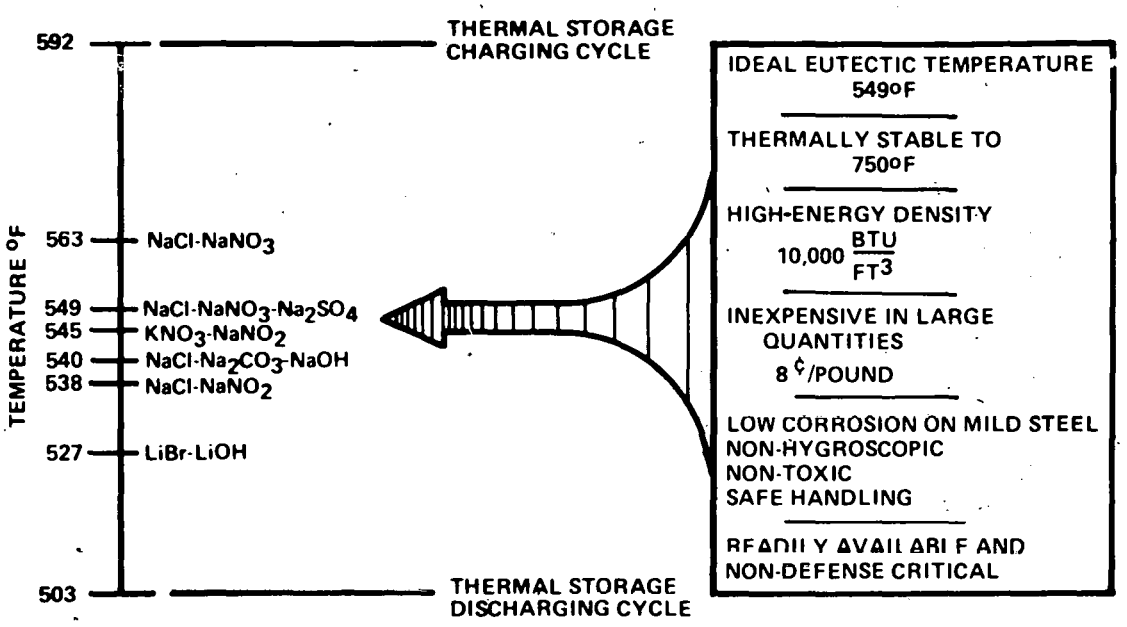

Figure 35. Phase Change Material Selected for Tank

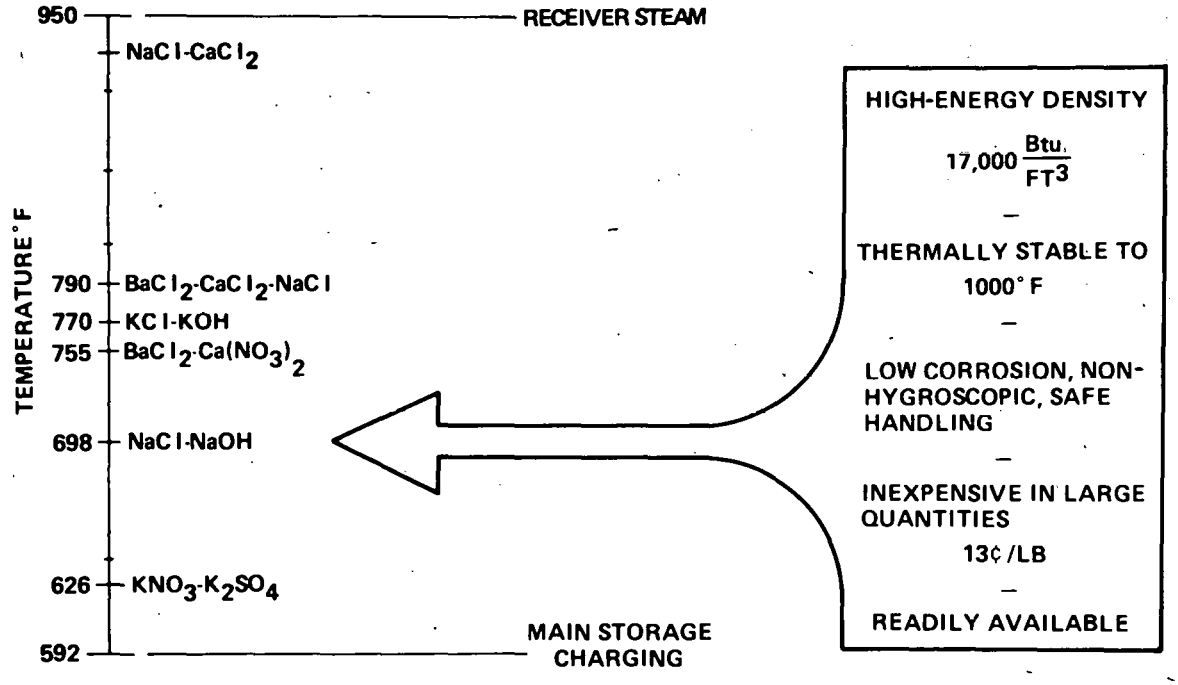

Figure 36. Phase Change Material Selected for Superheater

Table 14. Comparison of Pilot Plant and SRE Thermal Storage

Parameter	Pilot Plant Characteristics	Characteristics required in SRE Program
Design	• 255 MWhr(t) main storage capacity	• 1/4-scale model of quarter-unit cell
	• Salt PCM	• Same salt PCM
	• Battery of 12 unit cells	• 1/4-scale model of quarter-unit cell
	• 15-MWhr(t) superheater capacity	• Based on test results and analysis
	• Self-regulating control system	• Same control system
	• Below-ground storage	• Above-ground storage with insulation/variable heat loss measurements and analysis
	• Modular heat exchangers	• 1/4-scale model of quarter-unit cell
Performance	• Deliver 7 MW(e) net or 30 MW(t) net--6 hours	• 1/4-scale model of quarter-unit cell--270 kW(t)--4.6 hours
	• Provide 50°F superheat	• Based on test results and analysis
	• 575 psig/534°F discharge cycle	• Same discharge cycle
	• Handle 49 MW(t)--4 hours	• 1/4-scale model of quarter-unit cell--282 kW(t)--4.4 hours
	• 1450 psig/950°F charge cycle	• Same charge cycle
	• Heat loss 0.1%/hr	• Heat loss rate variable
Operating	• Parallel superheat units	• Based on test results and analysis
	• One out main storage capability	• Storage fill/drain capability demonstrated
	• Storage life	• Salt and material compatibility assessments

Table 15. Thermal Storage SRE Design Summary

Parameter	SI Units	English Engineering
Tank Size - Nominal	2.4 m x 2.4 m x 3 m	8 ft x 8 ft x 10 ft
Tank Weight	5,440 kg	12,000 lb
Boiler Weight	3,630 kg	8,000 lb
Condenser Weight	2,730 kg	6,000 lb
Salt Weight	23,200 kg	51,000 lb
Tank Weight	35,000 kg	77,000 lb
Thermal Storage Capacity	1.25 MWhr(t)	4.3×10^6 Btu
Charge Rate	282 kW(t)	9.6×10^5 Btu/hr
Charge Time	4.4 hr	4.4 hr
Discharge Rate	270 kW(t)	9.2×10^5 Btu/hr
Discharge Time	4.6 hr	4.6 hr
Condenser		
Charge Steam Rate	754 kg/hr	1664 lb/hr
Charge Steam Conditions	9500 kPa/307°C	1375 psi/585°F
Condensate Loading, W/L	3.05 kg/hr-m	2.05 lb/hr-ft
Pipe Size	1.91 cm O.D./1.47 cm I.D.	3/4 in. O.D./14 gauge
Configuration	4-28-leg serpentines with 1.18 fins/cm	4-28 leg serpentines with 3 fins/inch
Total Pipe Length	244 m	800 ft
Vaporizer		
Discharge Steam Rate	590 kg/hr	1300 lb/hr
Discharge Steam Conditions	5722 kPa/272°C	830 psi/522°F
Recirculation Rate	2/1	2/1
Pipe Size	1.59 cm O.D./1.4 cm I.D.	5/8 in./15 gauge
Configuration	1-44 leg serpentine with scrapers on	1-44 leg serpentine with scrapers on
Total Pipe Length	94 m	308 ft

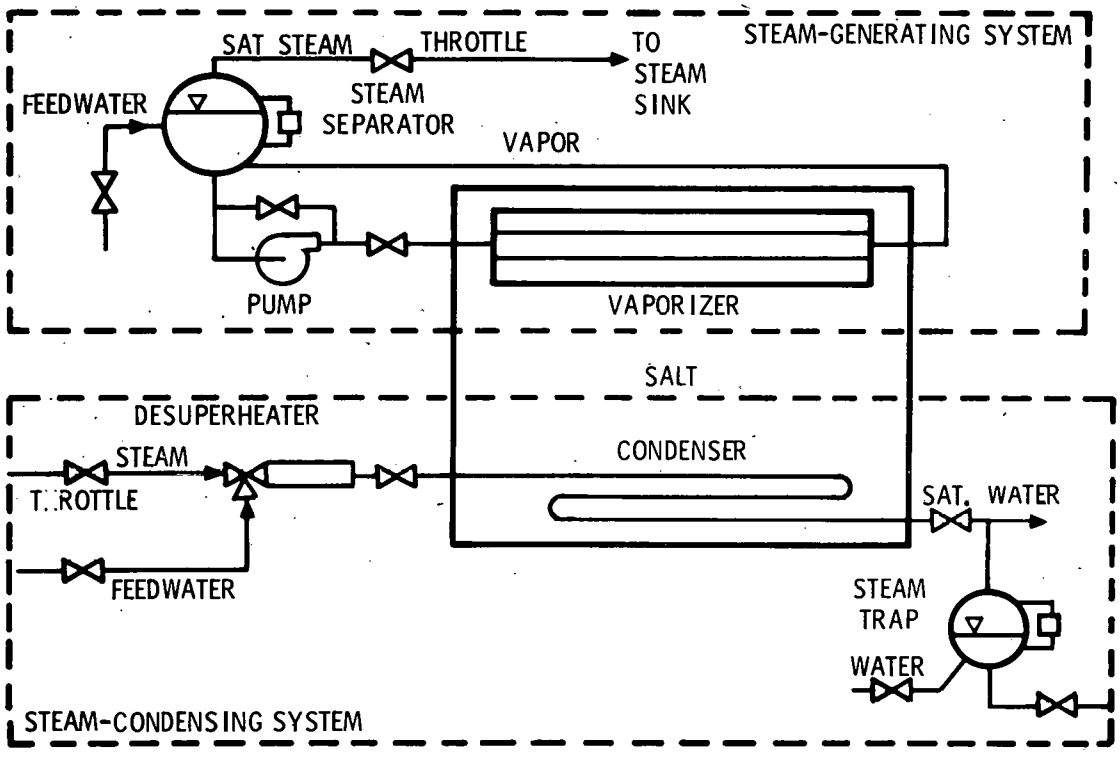

Figure 37. SRE Schematic

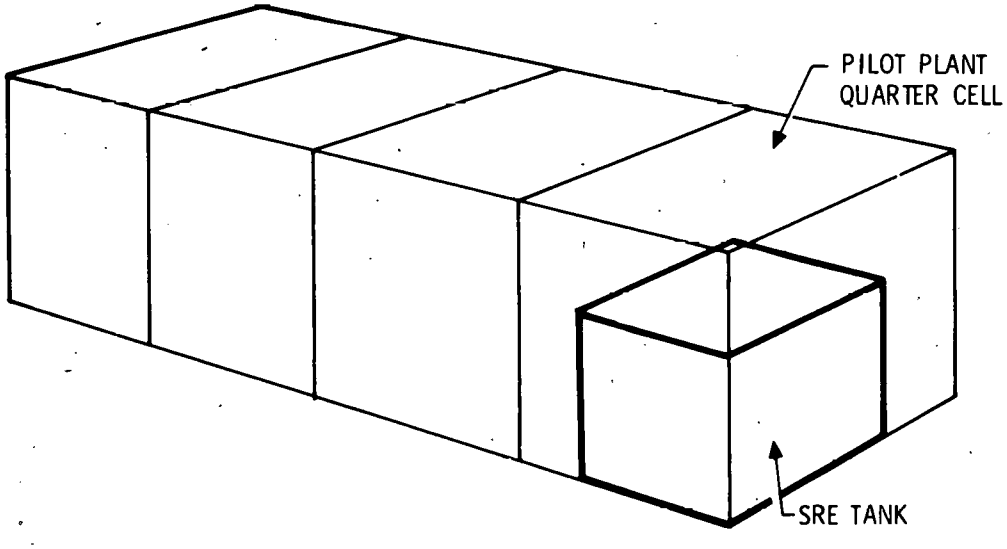

Figure 38. SRE Storage Tank Scaling

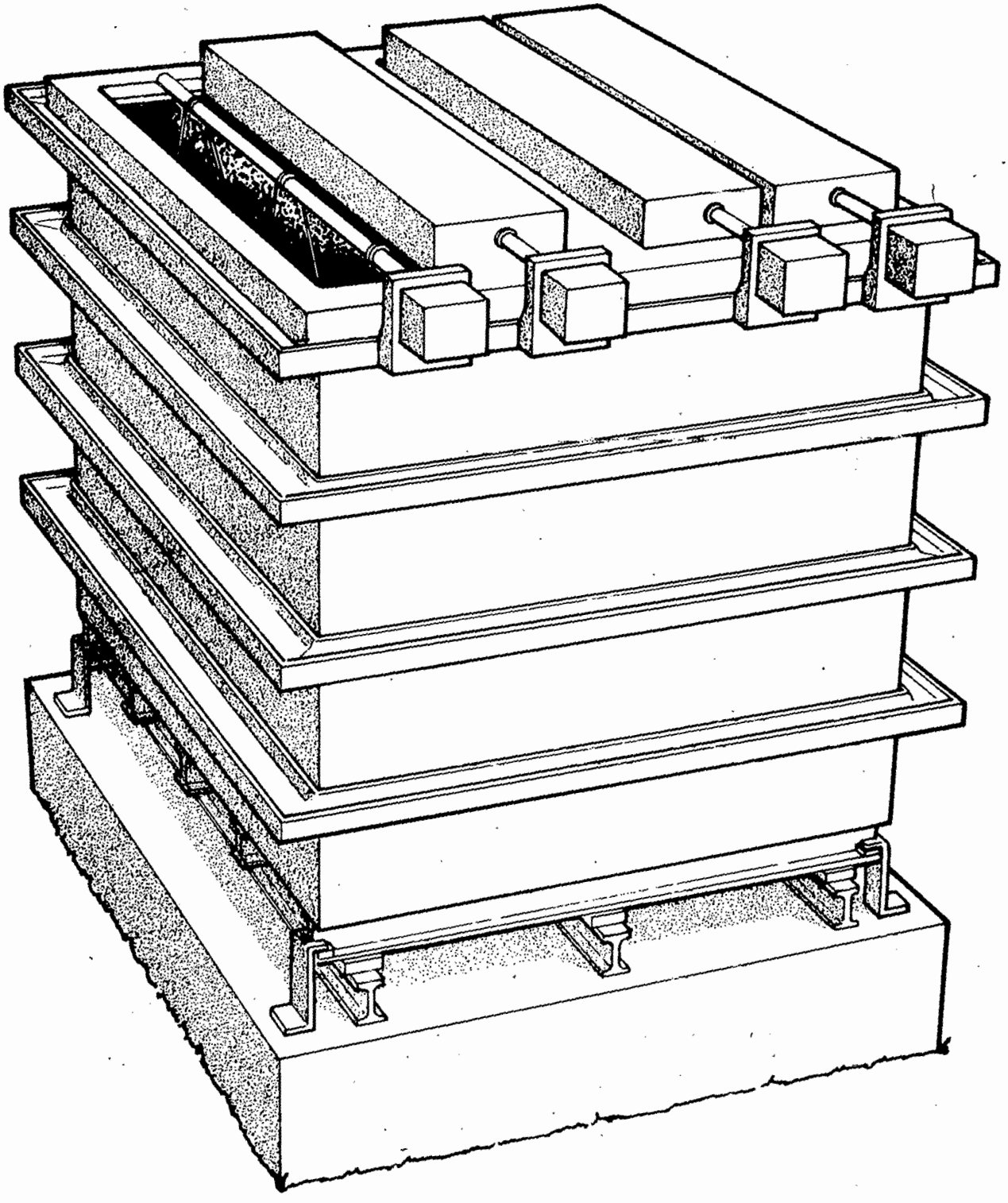

Figure 39. Thermal Storage Tank Configuration

around the tank. A tradeoff study of the number of stiffeners versus minimum weight plate wall thickness suggests a tank with 1.27 cm (0.5 inch) wall plate with four I-beams 20.3 cm x 34.2 kg/m (8 in. x 23 lb/ft) located 56.6 cm (22.3 in.) apart running around the tank.

Vaporizer -- The SRE vaporizer unit is a scale model of that for the one-quarter pilot plant cell. The general arrangement is shown in Figure 40. The design parameters are listed in Table 16.

Continuous removal of salt from the vaporizer tube is necessary to maintain satisfactory heat transfer rates. Small-scale experiments have been conducted using several types of scrapers, one configuration of which is shown in Figure 41. The test results are documented in Appendix C. They were generally successful, being, as would be expected, indicative rather than definitive.

Condenser -- The SRE condenser is designed for a steam rate of 756 kg/hr (1664 lb/hr), which will yield a heat flux (q/A) identical to that in the pilot plant condenser module. Details of the module are shown in Figure 42. Condenser design parameters are listed in Table 17. The proposed condenser tube fin configuration is cylindrical, though another might be selected based on detailed design work. Candidate configurations are shown in Figure 43. An engineering module condenser will be used to investigate their relative merits prior to committing one to the SRE model.

Phase Change Material -- Experiments conducted in the laboratory showed that both $NaNO_3$-NaOH and NaCl-$NaNO_3$-Na_2SO_4 seemed to undergo thermal degradation when stored at 475°C and 500°C, respectively. Known amounts of $NaNO_2$ were added to the ternary eutectic with a view of slowing down the decomposition process. When 0.5 percent by weight of $NaNO_2$ was added, there was a slight decrease in the heat of fusion. That trend became more pronounced with 1- and 5-percent additions by weight of $NaNO_2$ (Figure 44).

Addition of a small quantity of $NaNO_2$ to the ternary eutectic did not appear to prevent decomposition of $NaNO_3$ or 500°C and above. Initial findings of long-term life studies of the pure eutectics $NaNO_3$-NaOH and NaCl-$NaNO_3$-Na_2SO_4 indicate no significant changes in thermal stability.

The above eutectics were placed in mild steel (AISI 1020) tubes that were closed and cycled between 50°C and 450°C through 140 cycles. After cooling, the material inside each tube was examined by differential scanning calorimeter. The initial findings showed the melting points of both eutectics remained virtually unchanged. There were no significant changes in heats of fusion when compared with fresh samples. The small depression in the thermogram for the NaCl-$NaNO_3$-Na_2SO_4 at about 270°C (Figure 45) could be attributed to the reversible phase transformation of Na_2SO_4 from orthorhombic to hexagonal. (Further information on characteristics and test plans for the eutectic materials is contained in Appendix C.)

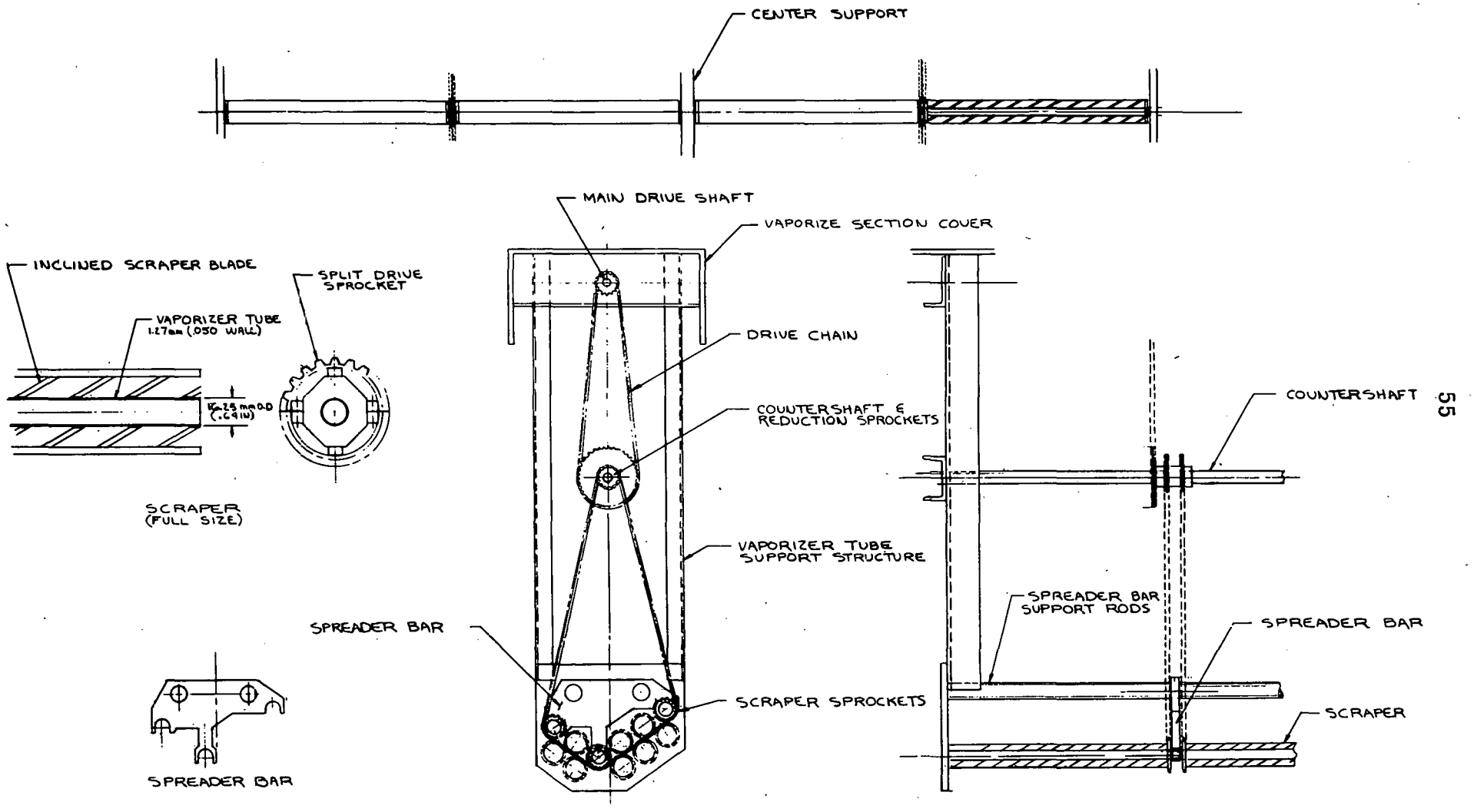

Figure 40. Thermal Storage Tank Vaporizer Arrangement

Table 16. Vaporizer Design Parameters

Parameter	SI Units		English Engineering Units	
	Pilot Plant	SRE	Pilot Plant	SRE
Geometric Similarity:				
Tank size	4.6 x 3.7 x 3.7 m	2.9 x 2.3 x 2.3 m	15 x 12 x 12 ft	9.5 x 7.6 x 7.6 ft
Vaporizer module size	(4) 0.53 x 3.4 m	(4) 0.34 x 2.13 m	(4) 1.75 x 11 ft	(4) 1.1 x 7 ft
Total tube length	147 m	94 m	484 ft	308 ft
No. of tubes	1	1	1	1
No. of rows	2	2	2	2
No. of legs	44	44	44	44
Distance between centers	10.2 cm	6.4 cm	4 in.	2.5 in.
Tube I.D./O.D.	2.21 cm/2.54 cm	1.4 cm/1.59 cm	0.87 in./1.0 in.	0.55 in./0.625 in.
Solid salt clearance/ thickness	0.015 cm	0.01 cm	0.006 in.	0.004 in.
Dynamic Similarity:				
Steam output rate	1475 kg/hr	590 kg/hr	3250 lb/hr	1300 lb/hr
Water inlet velocity	3.4 in/sec	3.4 in/sec	11 ft/sec	11 ft/sec
Mass velocity	9.6×10^6 kg/hr-m^2	9.6×10^6 kg/hr-m^2	1.96×10^6 lb/hr-ft^2	1.96×10^6 lb/hr-ft^2
Exit steam quality	0.4	0.4	0.4	0.4
Overall ΔT	24.5°C	15°C	44°F	27°F
Overall coefficient, U_i	3123 W/m^2-°C	4970 W/m^2-°C	500 Btu/hr-ft^2-°F	875 Btu/hr-ft^2-°F
Heat flux, q/A_i	76,300 W/m^2	76,300 W/m^2	2.4×10^4 Btu/hr-ft^2	2.4×10^4 Btu/hr-ft^2

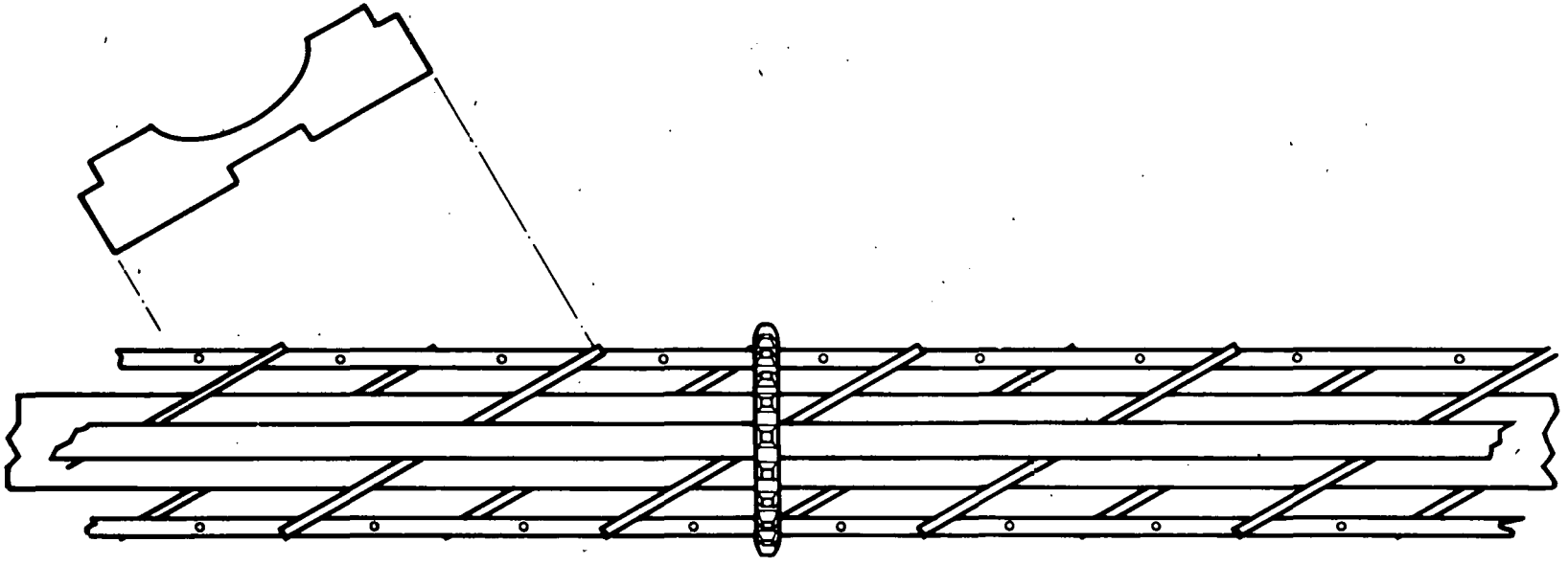

Figure 41. Split-Design, Inclined-Plate, Rotary Scraper

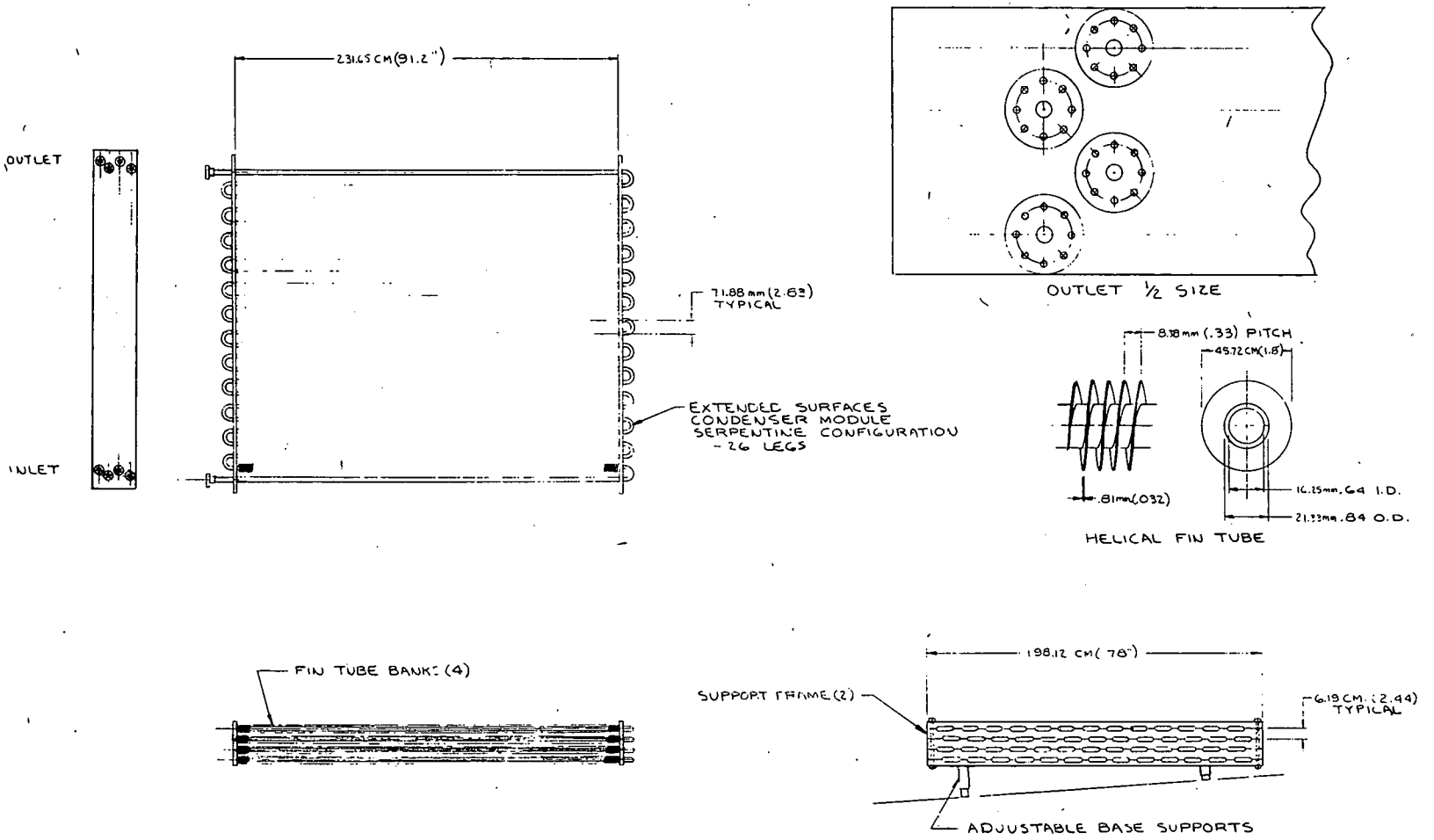

Figure 42. Thermal Storage Tank Condenser Module

Table 17. Condenser Design Parameters

Parameter	Symbol	SI Units			English Engineering Units		
		Units	Pilot Plant	SRE	Units	Pilot Plant	SRE
Storage Capacity	L	MWhr(t)	5	1.25	Btu	17.1×10^6 Btu	4.27×10^6
Tank Size:							
Length	L	m	4.57	2.90	ft	15	9.5
Width	W	m	3.66	2.32	ft	12	7.6
Height	H	m	3.66	2.32	ft	12	7.6
Pipe Size:							
Outside diameter	D_o	m	0.0318	0.0191	in.	1.250	0.750
Inside diameter	D_i	m	0.0264	0.0147	in.	1.040	0.580
Wall thickness	t_w	m	0.0027	0.0022	in.	0.105	0.085
Exterior area/length	A_o/L	m^2/m	0.0997	0.0598	ft^2/ft	0.3271	0.1963
Interior area/length	A_i/L	m^2/m	0.0829	0.0463	ft^2/ft	0.272	0.152
Pipe Fins:							
Fin height	h_f	m	0.0191	0.0114	in.	0.750	0.450
Fin thickness	t_f	m	1.27×10^{-3}	7.62×10^{-4}	in.	0.050	0.030
Fins/length	--	m^{-1}	78.74	118.11	in^{-1}	2	3
Fin area	--	m^2	6.36×10^{-3}	2.29×10^{-3}	in^2	9.86	3.55
Fin area/length	A_F	m^2/m	0.501	0.271	ft^2/ft	1.643	0.888
Fin effectiveness	--	--	0.45	0.5	--	0.45	0.5
Bare tube area	A_b	m^2/m	0.0896	0.0546	ft^2/ft	0.294	0.179
Effective area	A_o	m^2/m	0.315	0.190	ft^2/ft	1.034	0.623
Outside/inside area	--	--	3.8	4.1	--	3.8	4.1
Condenser Module:							
Total pipe length	--	m	409.7	245.7	ft	1344	806
No. of serpentines	--	--	4	4	ft	4	4
Length/serpentine	L	m	102.4	61.6	ft	336	202
No. of legs	--	--	28	28	--	28	28
Length/leg	--	m	3.66	2.19	ft	12	7.2
Spacing of legs (center to center)	--	m	0.10	0.06	m	4	2.4
Module Size:							
Length	--	m	3.96	2.38	ft	13	7.8
Width	--	m	2.90	1.74	ft	9.5	5.7
Height	--	m	0.37	0.23	--	1.23	0.74

Table 17. Condenser Design Parameters (Concluded)

Parameter	Symbol	SI Units			English Engineering Units		
		Units	Pilot Plant (Quarter Cell)	SRE	Units	Pilot Plant (Quarter Cell)	SRE
Input Parameters:							
Steam rate	--	kg/hr	2304	755	lb/hr	5080	1664
Steam rate/serpentine	W	kg/hr	576	189	lb/hr	1270	416
Steam velocity (entrance)	--	m/sec	5.33	5.88	ft/sec	17.5	19.3
Mass velocity	G	$kg/sec^{-1}m^{-2}$	295.7	306.5	$lb/hr^{-1}ft^{-2}$	218,000	226,000
Condensate loading	Γ	$kg/sec^{-1}m^{-1}$	1.56×10^{-3}	8.52×10^{-4}	$lb/hr^{-1}ft^{-1}$	3.78	2.06
Heat rate	--	W	8.43×10^{5}	2.84×10^{5}	Btu/hr	2.88×10^{6}	0.97×10^{6}
Heat rate/serpentine	q	W	2.11×10^{5}	0.709	Btu/hr	7.2×10^{5}	2.42×10^{5}
Heat rate/unit length	q/L	W/m	2056	1149	$Btu/hr^{-1}ft^{-1}$	2140	1106
Heat Flux to:							
Effective outside area	q/A'_o	W/m^2	6526	6053	$Btu/hr^{-1}ft^{-2}$	2070	1920
Inside tube area	q/A_i	W/m^2	24,810	6053	$Btu/hr^{-1}ft^{-2}$	7870	1920
Charge time	--	hr	5.94	4.41	hr	5.94	4.41
Heat Transfer Coefficients:							
Inside	h_i	W/m^2-°C	11,215	13,856	Btu/hr-ft^2-°F	1975	2440
Tube wall conductance	h_w	W/m^2-°C	17,808	22,856	Btu/hr-ft^2-°F	3136	4025
Fooling coefficient (assumed)	h_d	W/m^2-°C	5678	8518	Btu/hr-ft^2-°F	1000	1500
Outside - bare tube	h_{ob}	W/m^2-°C	411	449	Btu/hr-ft^2-°F	72.4	79
Effective outside coefficient based on inside area	h_{ofi}	W/m^2-°C	1562	1840	Btu/hr-ft^2-°F	275	324
Overall coefficient based on inside area	U_i	W/m^2-°C	1039	1283	Btu/hr-ft^2-°F	183	226
Estimated Temperature Drops:							
$t_{sat} - t_{wi}$	Δt_i	°C	2.2	1.8	°F	4	3.2
$t_{wi} - t_{wo}$	Δt_{wo}	°C	5.8	13.5	°F	10.5	24.3
$t_{wo} - t_{salt}$	Δt_o	°C	9.0	4.0	°F	28.5	7.2
Overall temperature differential	Δt	°C	23.9	19.3	°F	43.0	34.7
Salt temperature	T_{salt}	°C	287.2	287.2	°F	549	549
Steam temperature	T_{sat}	°C	311.1	306.7	°F	592	584
Steam pressure	P	kPa	9998	9481	psi	1450	1375

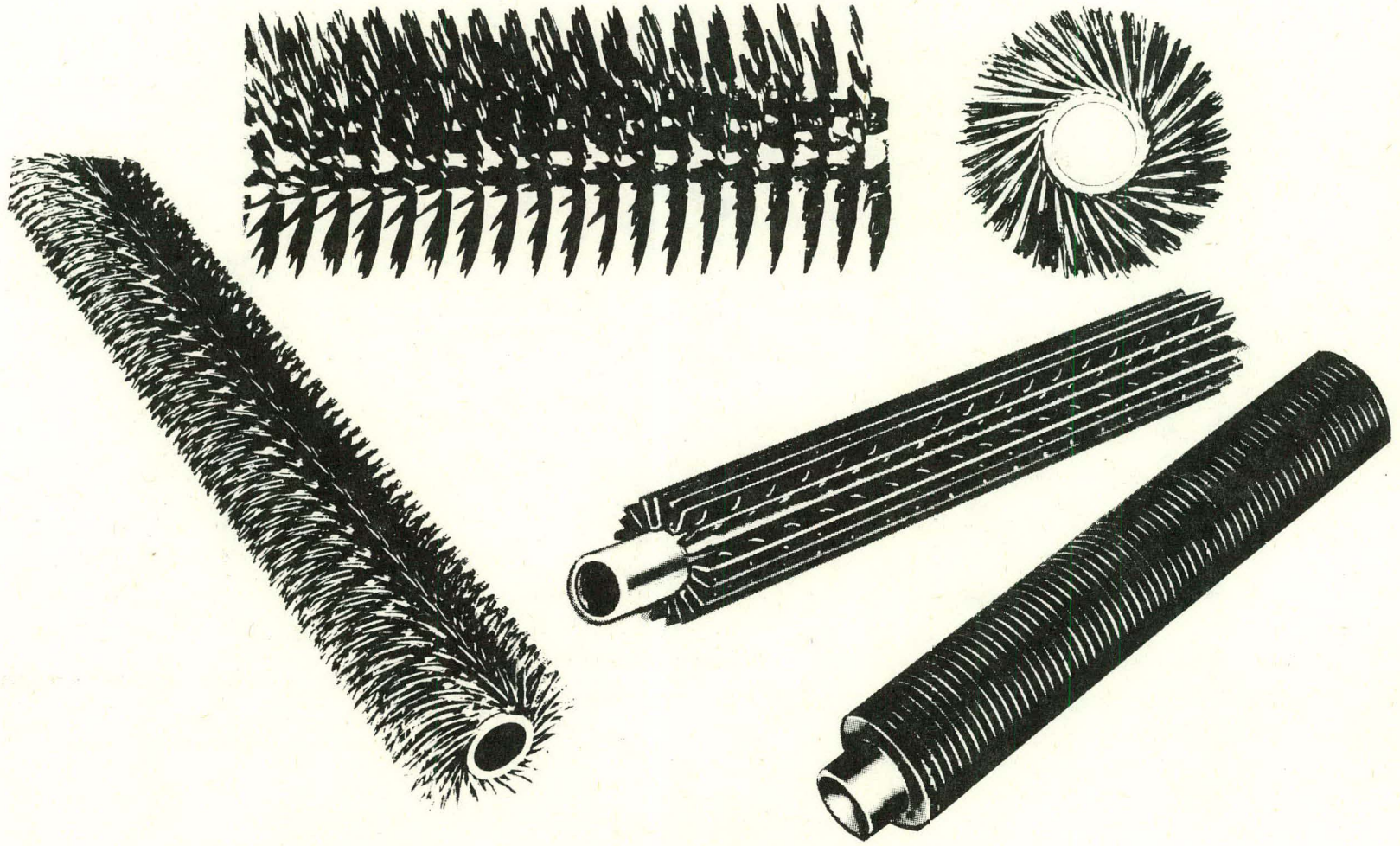

Figure 43. Condenser Tube Configurations

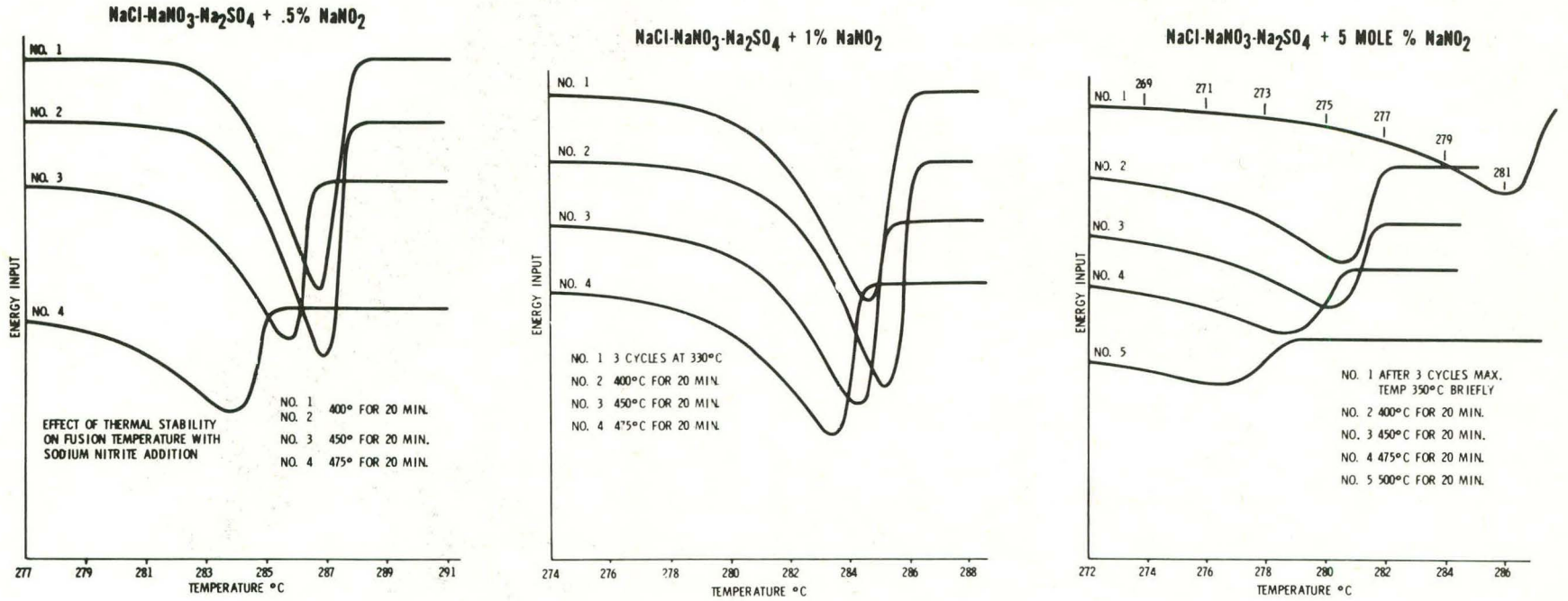

Figure 44. Effect of $NaNO_2$ Addition on Salt Stability

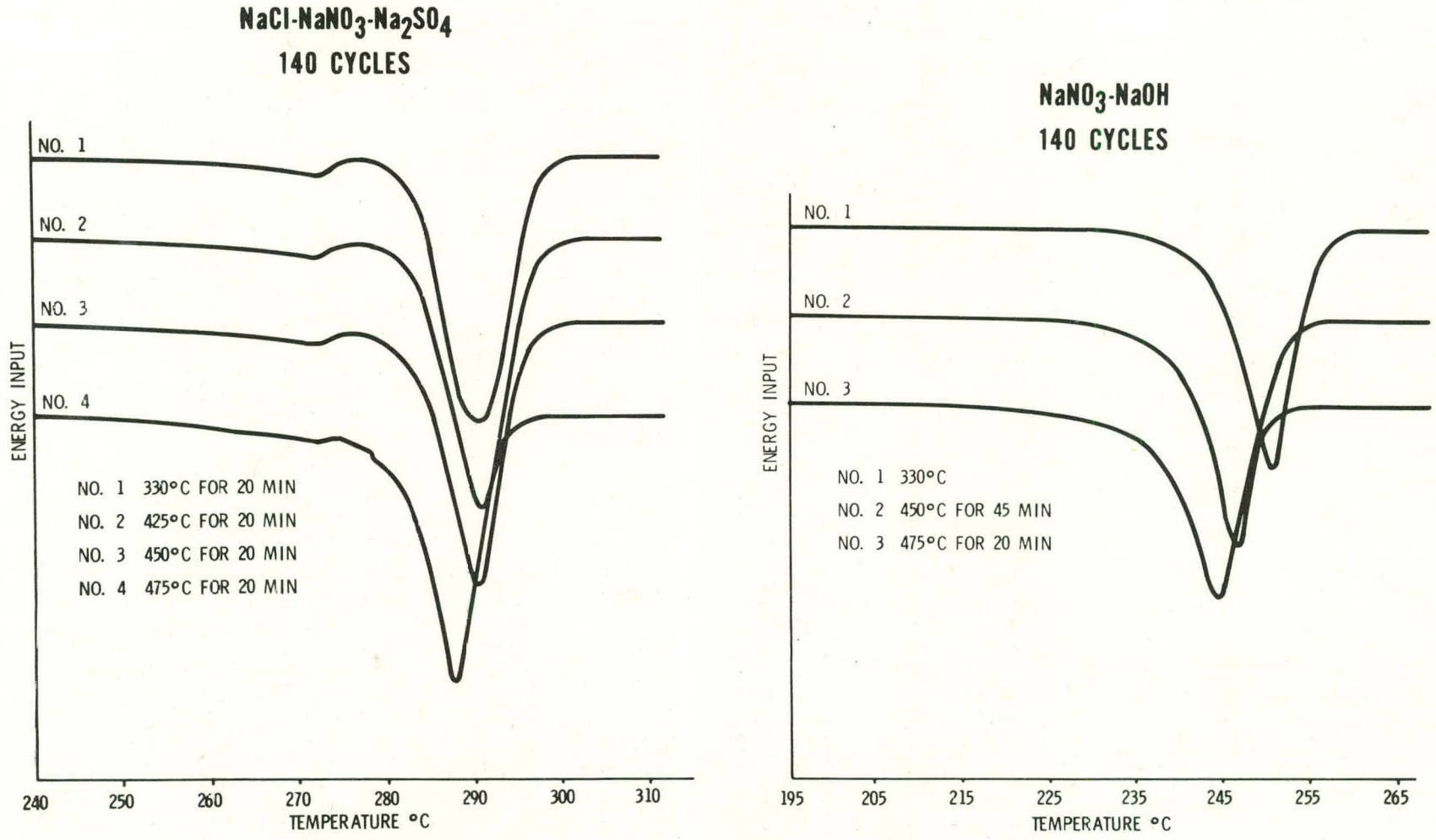

Figure 45. Effects of Cycling on Thermal Stability

Test Site

The Riverside Plant of NSP in Minneapolis will be used for the thermal storage SRE, as for that for the steam generator. The test items will be installed following necessary modifications to piping in the plant. The test control center will be assembled in Honeywell's Ridgway facility in Minneapolis and transported to the plant after the experiment is set up. Figure 46 shows the thermal storage test area on an outside wall of the plant. Temporary construction will be used to enclose the test space (i.e., one wall and a roof will be required).

Test Arrangement

The thermal storage and steam generator test arrangement is shown in Figure 25, and the locations of the test areas relative to sources and sinks are shown in Figure 26.

As those figures indicate, the input steam is from the No. 8 unit -- 163 bar/ 538°C. The steam will be expanded through a pressure regulator to 100 bar/ 510°C to meet design conditions. An air failure-to-close isolation valve will protect the SRE test equipment. The steam will then go through a desuperheater to reduce the temperature to the saturation condition of 310°C. The feedwater flow rate will be governed by the energy balance. Calculations show that the steam input to the condenser will be 1.37 times the mass flow into the superheater.

The mobile trailer housing the control and data acquisition systems will be installed alongside the steam generator on the turbine floor of the plant (Figure 27). The relative positions of the thermal storage tank and No. 7 turbine (control trailer) area are shown in Figure 47.

Test Instrumentation and Data Acquisition

Instrumentation -- Types and approximate quantities of instruments are listed in Table 18. The data acquisition system can handle additional instrumentation if required.

Data Acquisition -- The data acquisition system is being designed to process all measurements from the thermal storage and steam generator SRE tests; however, they will not be conducted simultaneously. The System 700 Process Analyzer, as shown in Figure 31, will be used, except that the thermal storage tests will cover an estimated thirty 1- to 6-hour sequences involving 57 temperature points and 16 analog points, as opposed to the estimated thirty 8-hour sequences involving 400 temperature points and 200 analog points for the steam generator subsystem tests. The data processing sequence is as shown in Figure 32. All data will be available in real time and will be converted to process dimensions and stored.

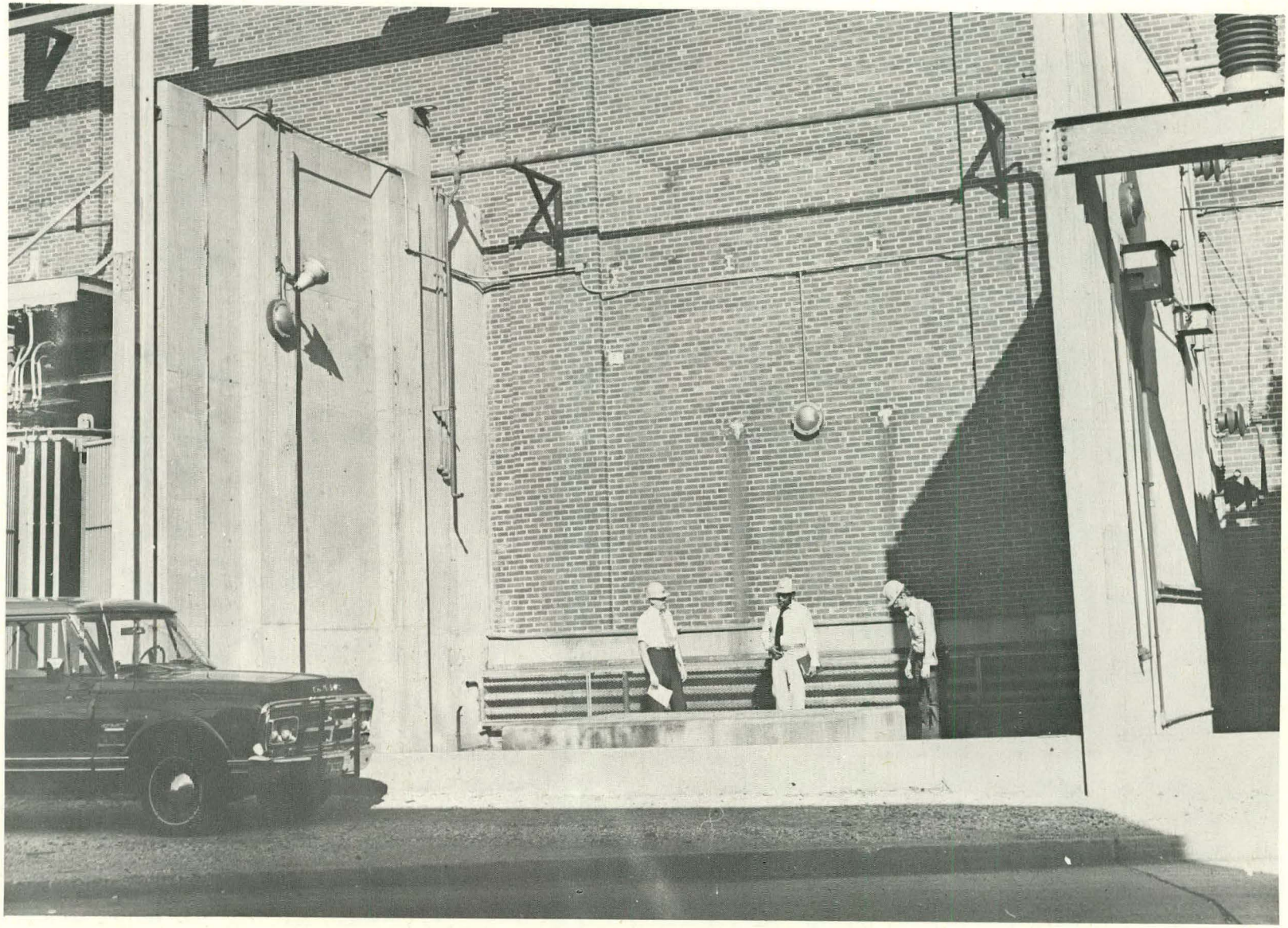

Figure 46. Thermal Storage SEE Test Area

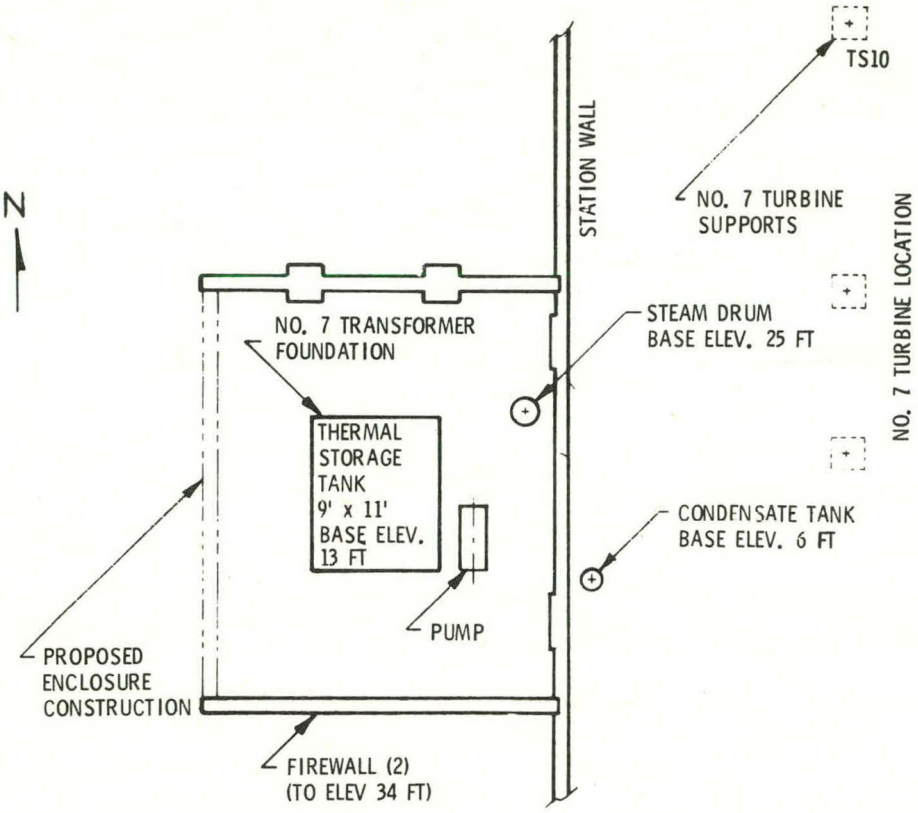

Figure 47. Thermal Storage Test Installation

Table 18. Thermal Storage SRE Instrumentation Requirements

Type	Quantity Required (approx.)
Temperature (thermocouple):	122
Tank	(28)
Condenser	(26)
Boiler	(10)
Fluid	(58)
Pressure (gauge)	To be determined
Flow rate (meter)	To be determined
Liquid level in tank*	1
Heat loss (gauge)	15
Salt buildup on tank walls (rad)	1

*As indicator of stored energy in tank.

Test Control

The test control rationale includes the same considerations as are listed in Table 13. The arrangement of the test control center is as shown in Figure 33.

The experimental nature of the equipment requires that close consideration be given the following safety related factors:

- Personnel protection
- Electrical grounds and circuit cutouts
- Fire
- Condenser system leakage or failure
- Steam generator leakage or failure
- Seismic or mechanical shock effects
- Gas blanketing failure
- Tank leakage or failure

Suitable safety precautions will be taken in all of the above areas.

Test Support Equipment

Table 19 lists support equipment required for the thermal storage (and steam generator) research experiment. In addition to the items listed, the experiment requires dry nitrogen to keep the molten salts clean and dry and an observation platform and viewing ports in the tank cover. The latter also implies adequate interior lighting.

Thermal Storage SRE Schedule

The schedule for the thermal storage subsystem research experiment is shown in Figure 48. The SRE concept was presented formally to ERDA in mid-December 1975. Procurement activities will begin in January 1976. Subsystem testing will be completed in the first quarter of 1977.

PLANS FOR NEXT QUARTER

Plans for the first quarter of 1976 include:

- Conducting engineering model tests
- Preparing procurement specifications for the subsystem (January - March)

Table 19. SRE Supplemental Equipment and Tool Needs

Item	Description
1	Overhead crane and necessary lifting attachments
2	Test frame for vaporizer sections for repair and listing
3	Washing equipment to remove salts from probes and vaporizer section
4	Portable potentiometers
5	Probe-type thermocouples
6	Power measuring equipment: a) Wattmeter b) Tachometer c) Torque meter
7	Test sampling probes
8	Pressure gauges
9	Electrical control panels/local control: a) Switch gear for drives b) Lighting panels c) Auxiliary heaters
10	Ladders
11	Storage cabinets
12	Miscellaneous tools
13	Salt mixer
14	Weighing scales for mixing
15	Transfer containers for supplying salt to SRE

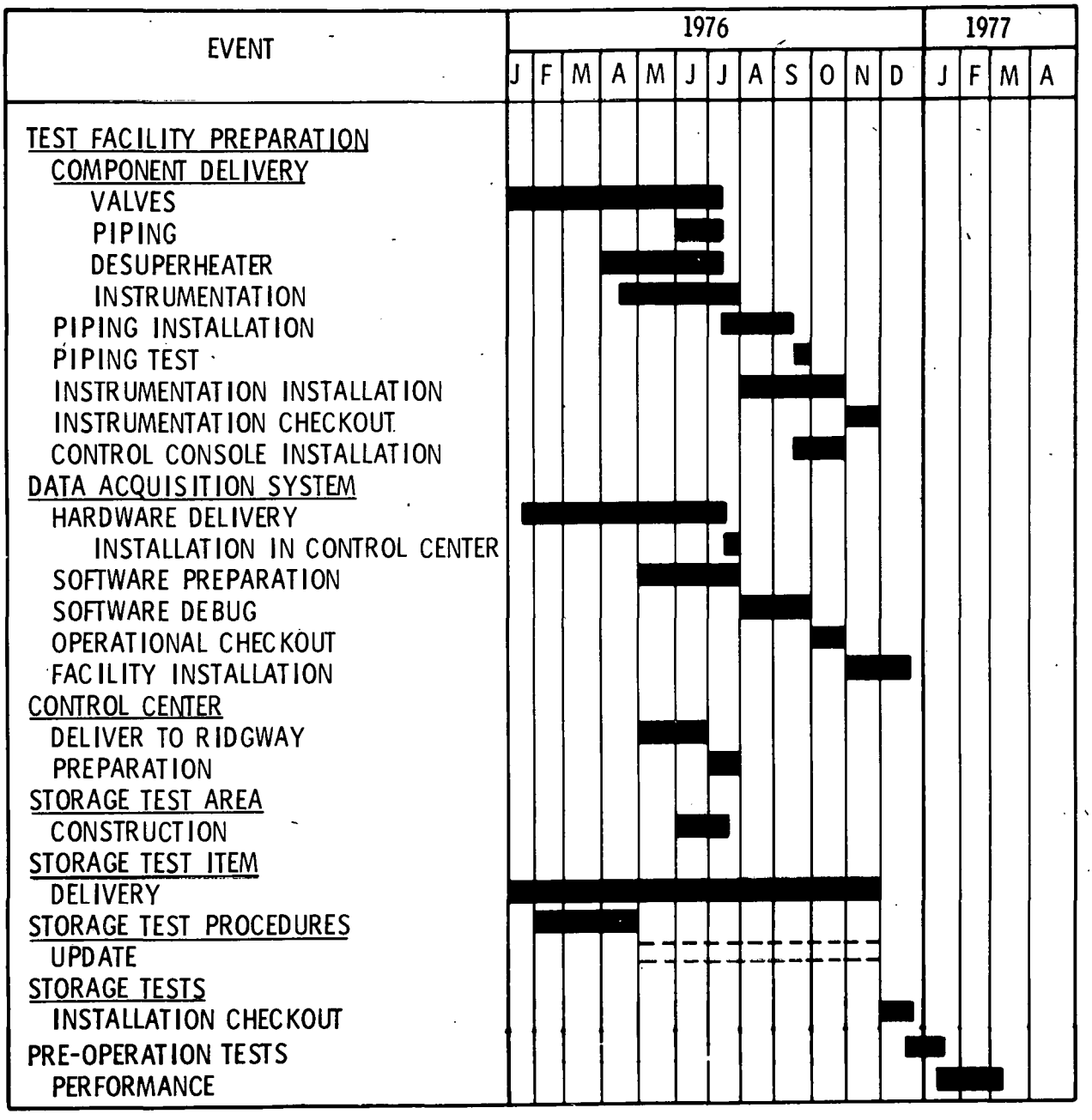

Figure 48. Thermal Storage SRE Test Schedule

- Obtaining bids and letting orders for subsystem and support system components (January - March)
- Monitoring and expediting close-in deliveries (January - March)
- Generating thermal storage test procedures
- Continuing engineering model experiments
- Revising the SRE conceptual design -- if and when required.

SECTION VI
PROGRAM DOCUMENTATION

In addition to this report, the Solar Pilot Plant program was documented by the following during the first 6 months:

- Program Plan, CDRL Item 9, 3 July 1975, and Program Plan, Revised, 10 September 1975
- Preliminary Design Baseline Report (PDBR), CDRL Item 1, 30 September 1975, and PDBR Supplement, 17 December 1975
- Collector SRE Conceptual Design Report (CDR), CDRL Item 3, 1 October 1975, and Collector SRE CDR, Revised, 17 December 1975
- Steam Generator SRE Conceptual Design Report (CDR), CDRL Item 4, 17 December 1975
- Thermal Storage SRE Conceptual Design Report (CDR), CDRL Item 5, 17 December 1975

A revised edition of the PDBR, incorporating information in the PDBR supplement and changes requested by ERDA, will be published at the end of January 1976.

The Collector Detailed Design Report (CDDR), CDRL Item 6, is scheduled to be presented orally in March 1976.

The next Quarterly Report, covering the first quarter of 1976, will be issued on 20 April 1976.

THIS PAGE

WAS INTENTIONALLY

LEFT BLANK

APPENDIX A

HELIOSTAT SELECTION BY PARAMETRIC ANALYSIS

A parametric analysis, based in part on a ray-trace analysis made earlier, was made of the azimuth-elevation and tilt-tilt heliostat configurations. The basic criterion for selection was cost per unit energy. Elements entering the consideration and sources for cost estimates are summarized in Table A-1. The first five elements listed in Table A-1 are shown in Figure A-1.

Table A-1. Heliostat Cost Elements and Basis for Estimates

Basis for Estimate	Cost Element
Concepts evaluated	• Azimuth-Elevation • Tilt-Tilt
Cost elements analyzed	• Mirror module • Mirror module drive • Outer gimbal • Outer gimbal drive • Foundation • Control • Assembly and installation
Cost estimates based on	• Catalog items 60% • Suppliers' estimates 21% • Engineering estimates 19%

Table A-2 is an optimization of the two heliostat configurations, made for the cost-effectiveness comparison. It will be noted that both have the same values for pointing accuracy and operational capability in wind. Using the values shown, the tilt-tilt configuration is more cost-effective, as indicated in Table A-3. On a square-meter basis (based on commercial scale quantities), the tilt-tilt configuration is 15 percent cheaper. On a cost per unit energy basis (the ultimate factor for selection), the tilt-tilt configuration is 15.7 percent more effective.

The ray-trace analysis showed a relationship between annual energy and mirror area, with energy varying inversely with area, due primarily to optical aberations (Figure A-2). Figure A-3 shows heliostat cost as a function of mirror area.

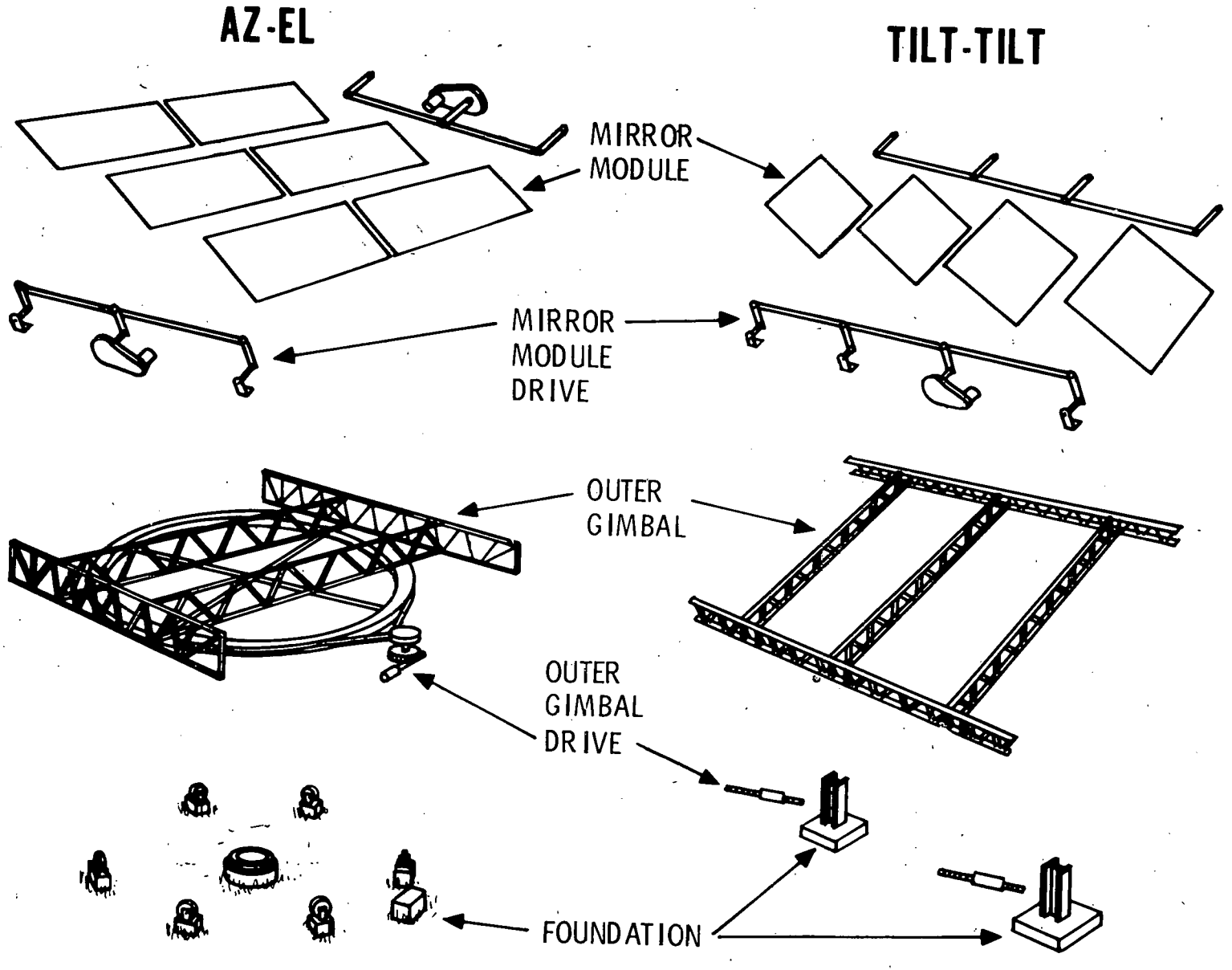

Figure A-1. Azimuth-Elevation and Tilt-Tilt Heliostat Configurations

Table A-2. Optimization of Candidate Heliostat Configurations

Factor	Az-El	Tilt-Tilt
Area (m^2)	50	40
Accuracy (mr)	2	2
Wind (m/s)	13.5	13.5
Mirror module spacing	1.9	1.6
Aspect ratio	2.4	1.0
Number of facets	6	4

Table A-3. Heliostat Cost as Function of Effective Mirror Area

Heliostat	Efficiency (m^2/MWhr)		Cost ($/$m^2$)		Fixed Charge Rate		Mils/kWhr
Tilt-Tilt	$\frac{1}{1.980}$	X	59.83	X	0.16	=	4.83
Az-El	$\frac{1}{1.967}$	X	70.45	X	0.16	=	5.73

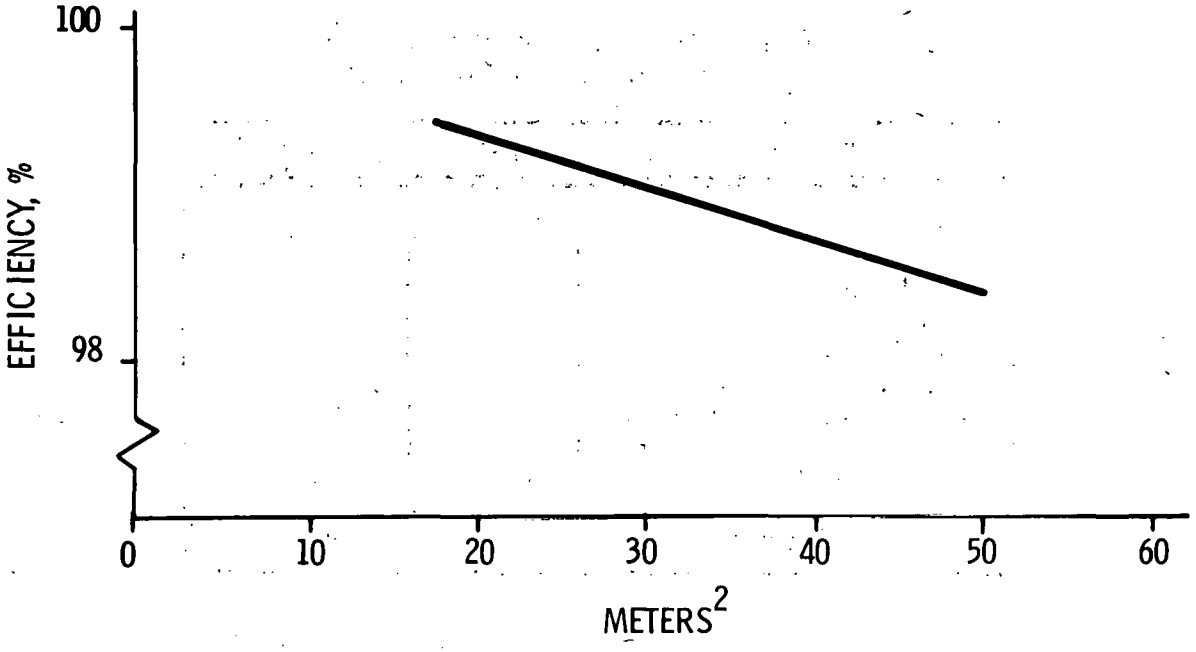

Figure A-2. Heliostat Efficiency as a Function of Mirror Area

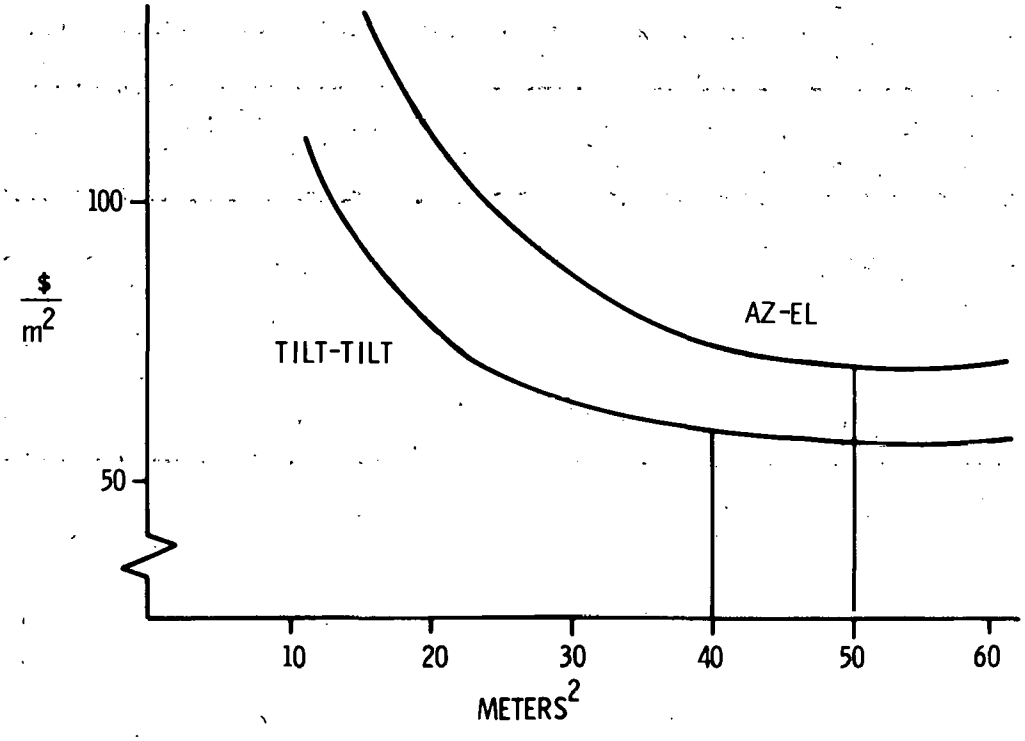

Figure A-3. Heliostat Cost as a Function of Mirror Area

Using 2 milliradians as the cost-effective point in pointing accuracy, Figure A-4 shows heliostat cost as a function of pointing accuracy.

Data checked in the Inyokern Valley in 1962 were used to calculate annual energy loss as a function of wind speed (Figure A-5). Figure A-6 shows heliostat effective cost as a function of wind speed operating capability using 13.5 meters per second wind speed as optimal.

Figure A-7 shows heliostat cost as a function of aspect ratio, and Figure A-8 shows cost as a function of module spacing.

Table A-4 is a summary of heliostat cost distribution based on the factors listed.

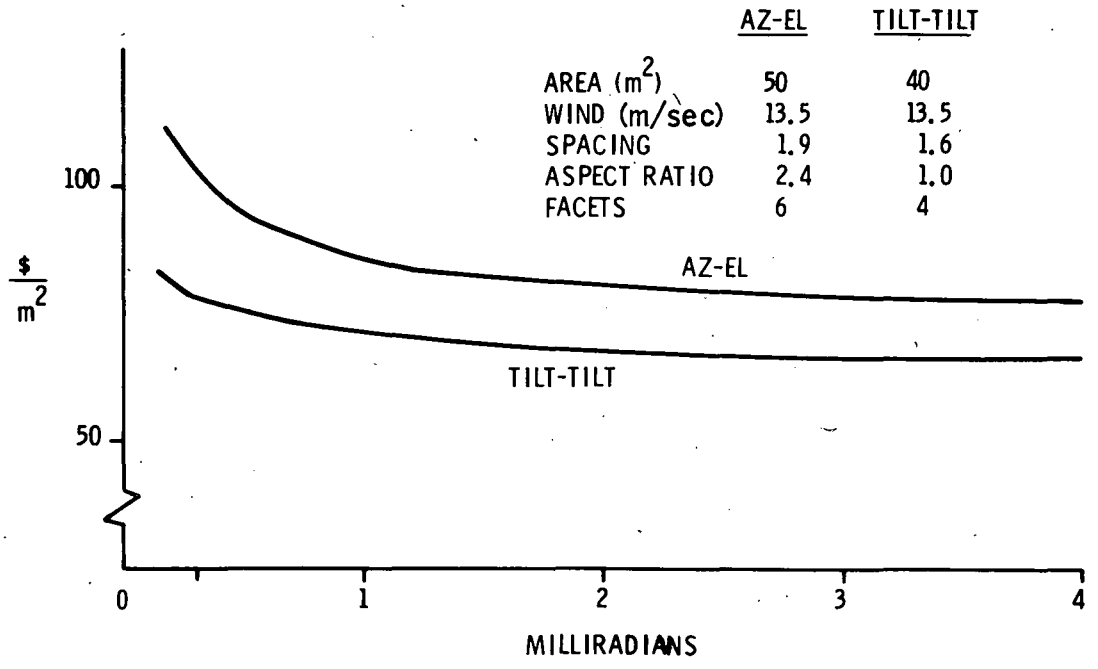

Figure A-4. Heliostat Cost as a Function of Pointing Accuracy

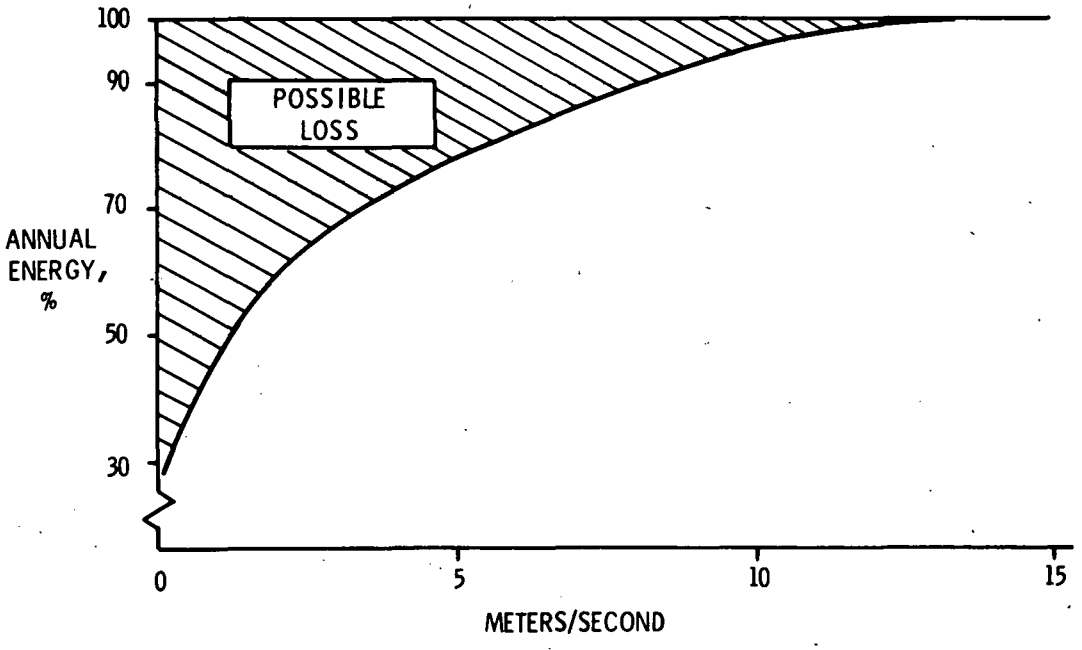

Figure A-5. Annual Energy Loss as a Function of Wind Speed

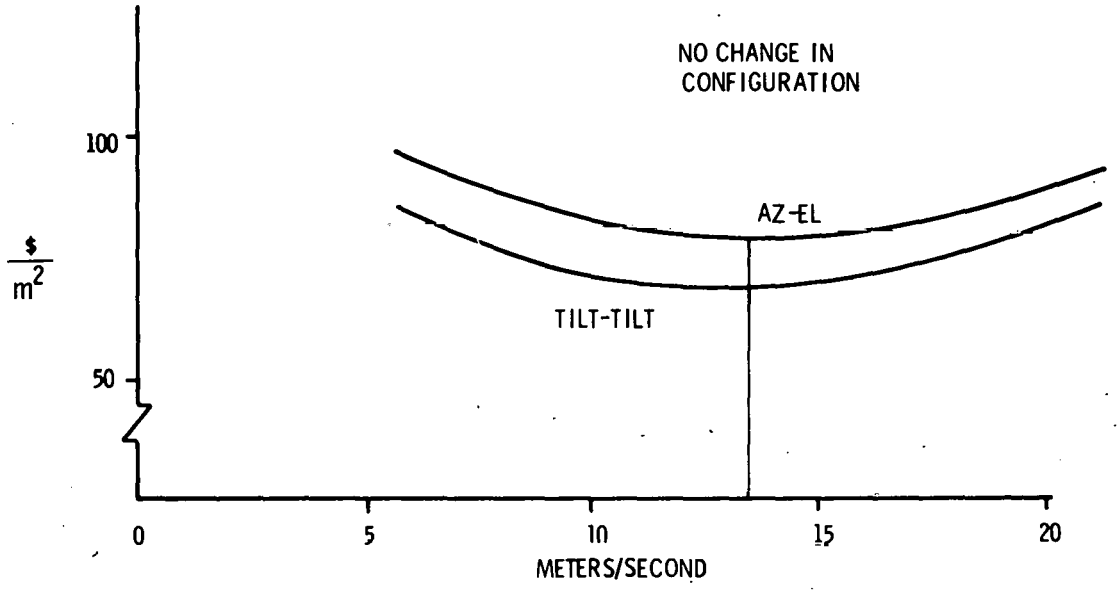

Figure A-6. Heliostat Effective Cost as a Function of Wind Speed Operating Capability

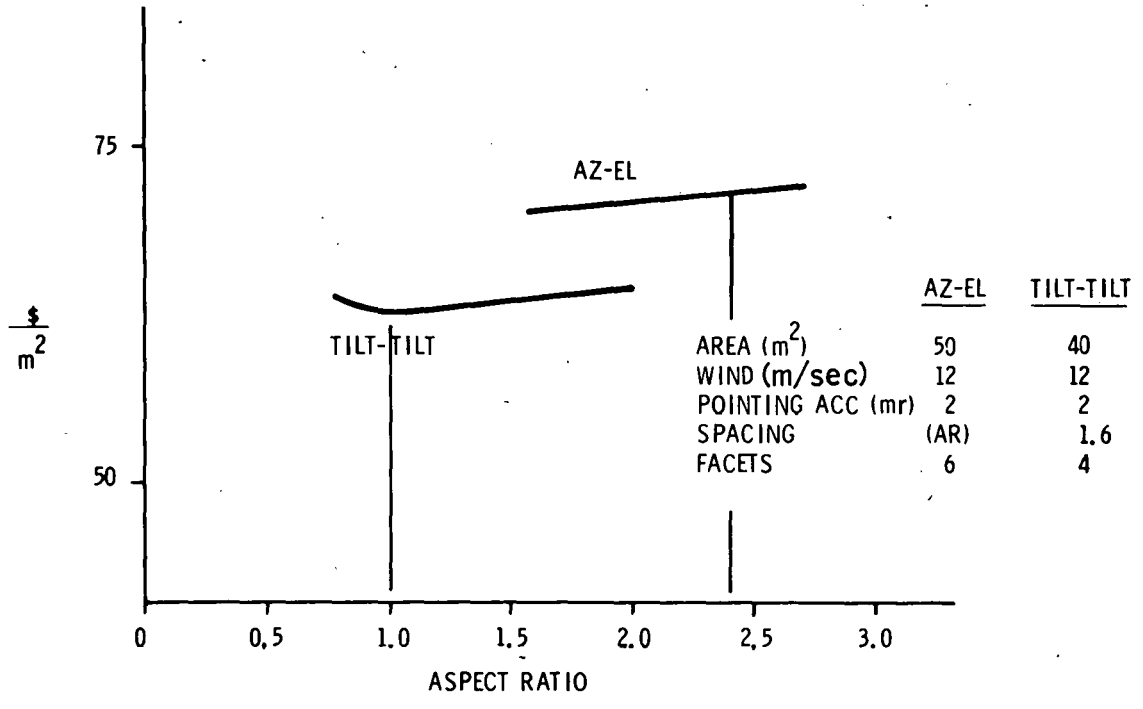

Figure A-7. Heliostat Cost as a Function of Aspect Ratio

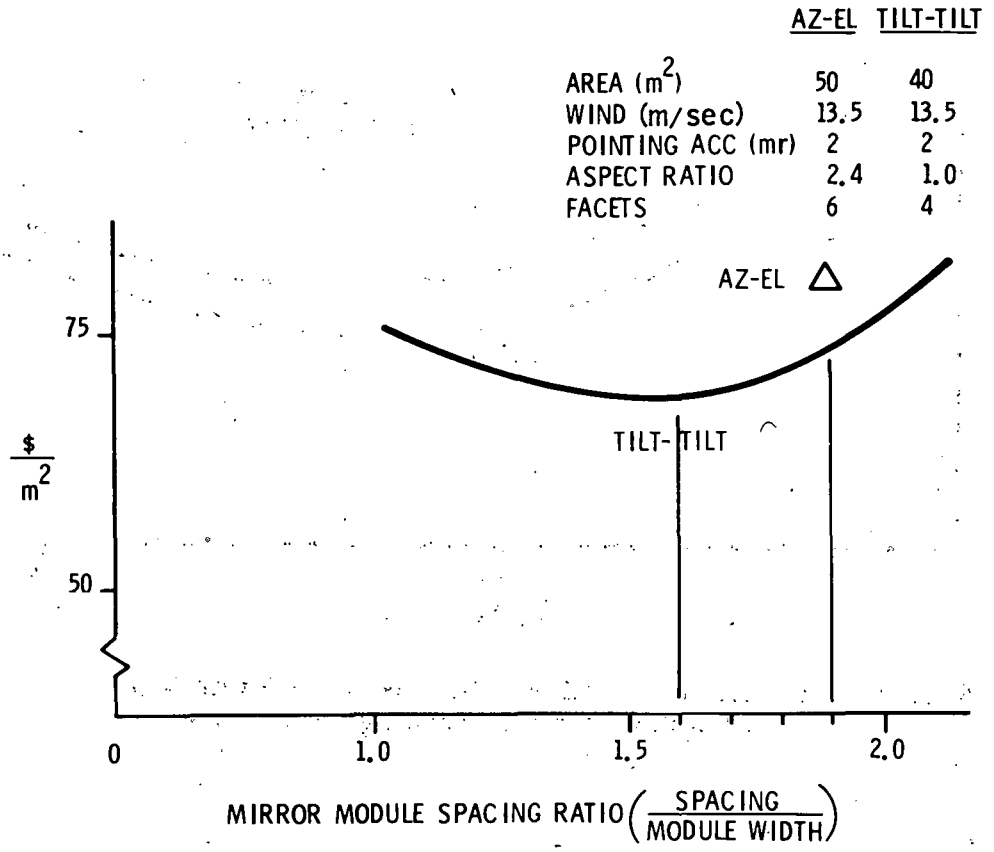

Figure A-8. Heliostat Cost as a Function of Mirror Module Spacing

Table A-4. Heliostat Cost Distribution

Cost Item	Az-El	Tilt-Tilt
Mirror module	$14.17	$13.78
Mirror module drive	14.95	13.09
Outer gimbal	14.12	9.06
Outer gimbal drive	16.82	14.23
Foundation	3.24	2.42
Control	6.24	6.41
Assembly and installation	.91	.84
Total	$70.45	$59.83

APPENDIX B

THERMAL STRESS AND PRESSURE ANALYSES OF THE STEAM GENERATOR SUBSYSTEM

BOILER SECTION

The integrity of the boiler section is maintained by avoiding tube failures due to departure from nucleate boiling (DNB). DNB occurs when the heat transfer mechanism in the tubes changes from nucleate boiling with a high heat transfer coefficient to film boiling with a low heat transfer coefficient. If operating conditions exceed the DNB limit, excessive tube temperature followed by failure will result. Figure B-1 shows the DNB limit for the boiler tube in the membrane wall of the solar steam generator. Figure B-2 shows the safety margin (DNB ratio) for the pilot plant boiler tubes under the operating conditions listed. Identical steam quality in the SRE steam generator is achieved by maintaining the same circulation ratio (i.e., the ratio of boiler flow to steam flow).

Results of a preliminary stress analysis of the boiler section are shown in Figures B-3 and B-4. In Figure B-3 the calculated stress due to pressure loading is compared with the allowable stress. It should be noted that the heat fluxes and ensuing temperatures are, in part, in excess of those anticipated. In Figure B-4, combined pressure and thermal stress are compared with the allowable stress ($3S_m$, equivalent to twice the yield stress, S_y). On the basis of this analysis, the boiler design is feasible from the stress standpoint.

SUPERHEATER SECTION

Results from preliminary analyses of the SRE and pilot plant superheater sections are shown in Figures B-5 and B-6 (SRE), and B-7 and B-8 (Pilot Plant). Combined pressure and thermal stress is compared with the yield stress (S_y) to show total stress as opposed to only the cyclic portion of the stress. The results indicate that the helical superheater concept is feasible for the anticipated operating conditions.

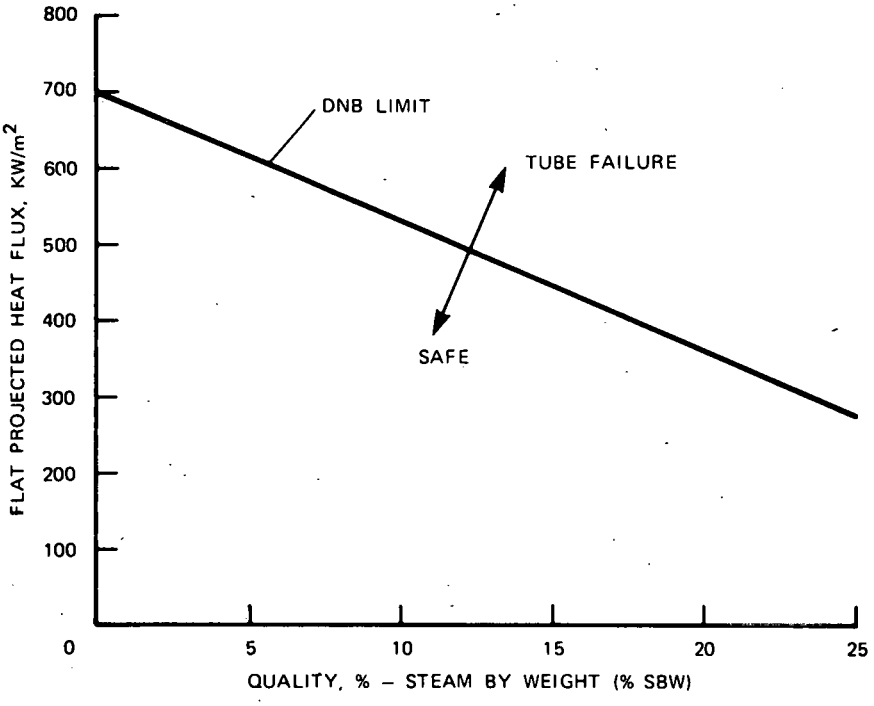

Figure B-1. DNB Limit for Boiler Section

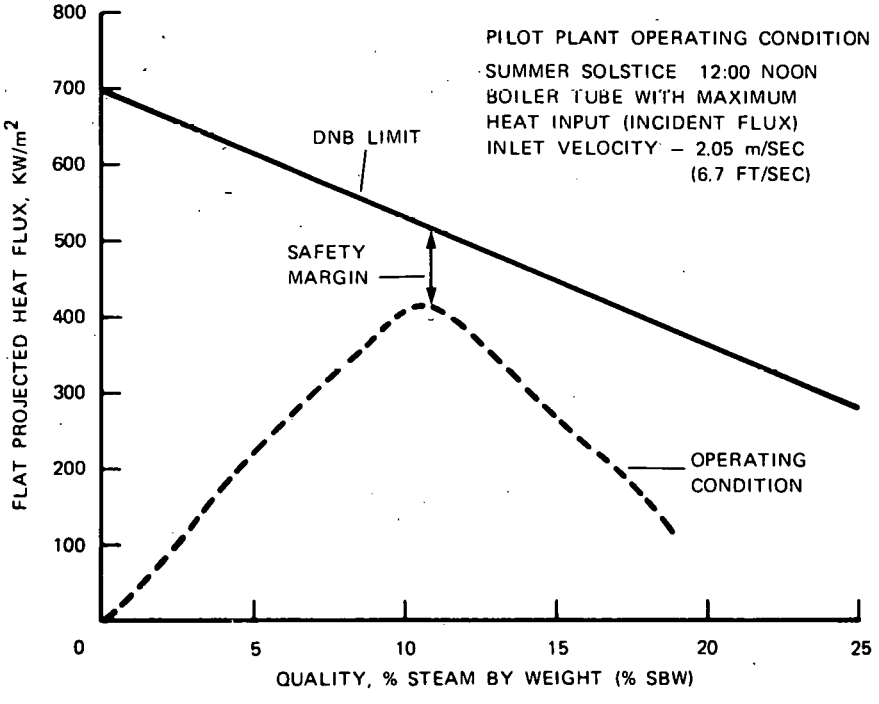

Figure B-2. Comparison of an Operating Condition with the DNB Limit

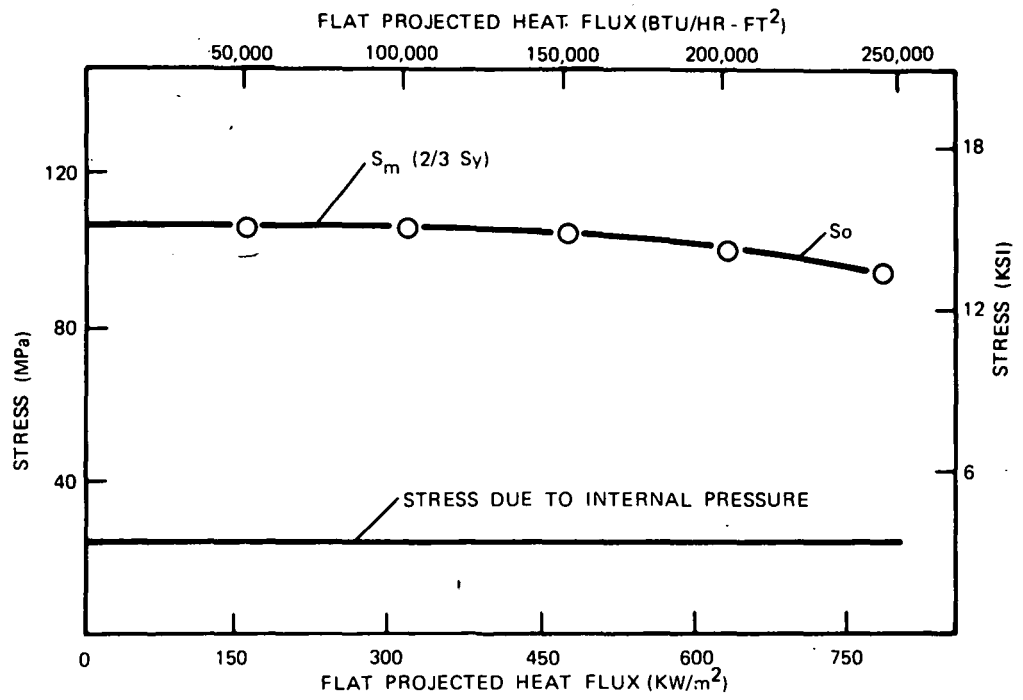

Figure B-3. Comparison of Stress Due to Pressure in Boiler Section with Allowable Stress

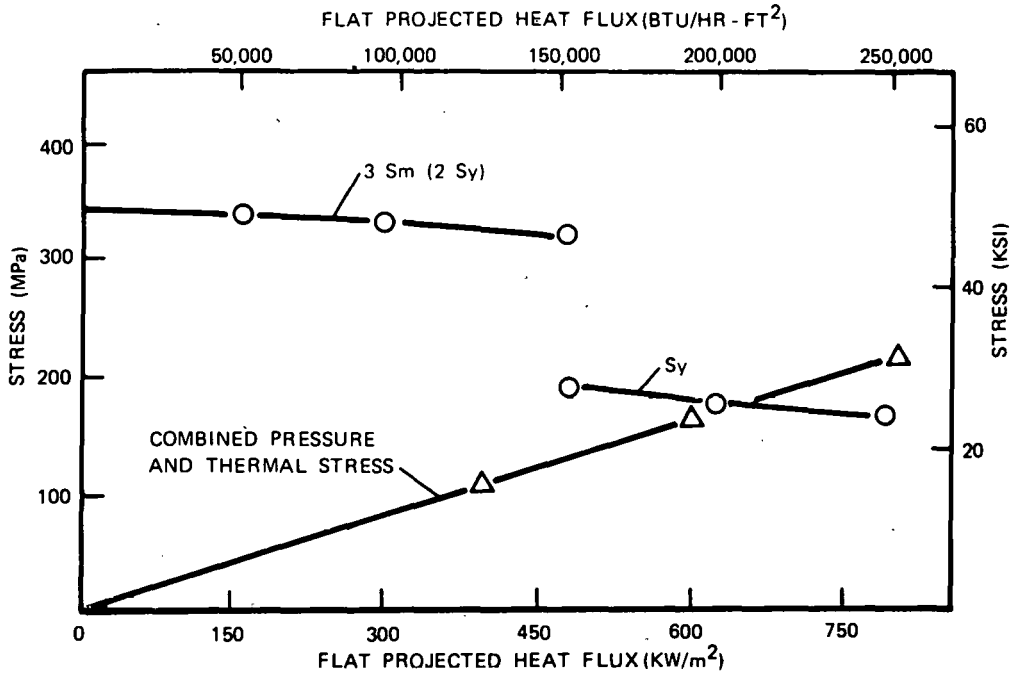

Figure B-4. Comparison of Combined Pressure and Thermal Stress in Boiler Section with Allowable Stress

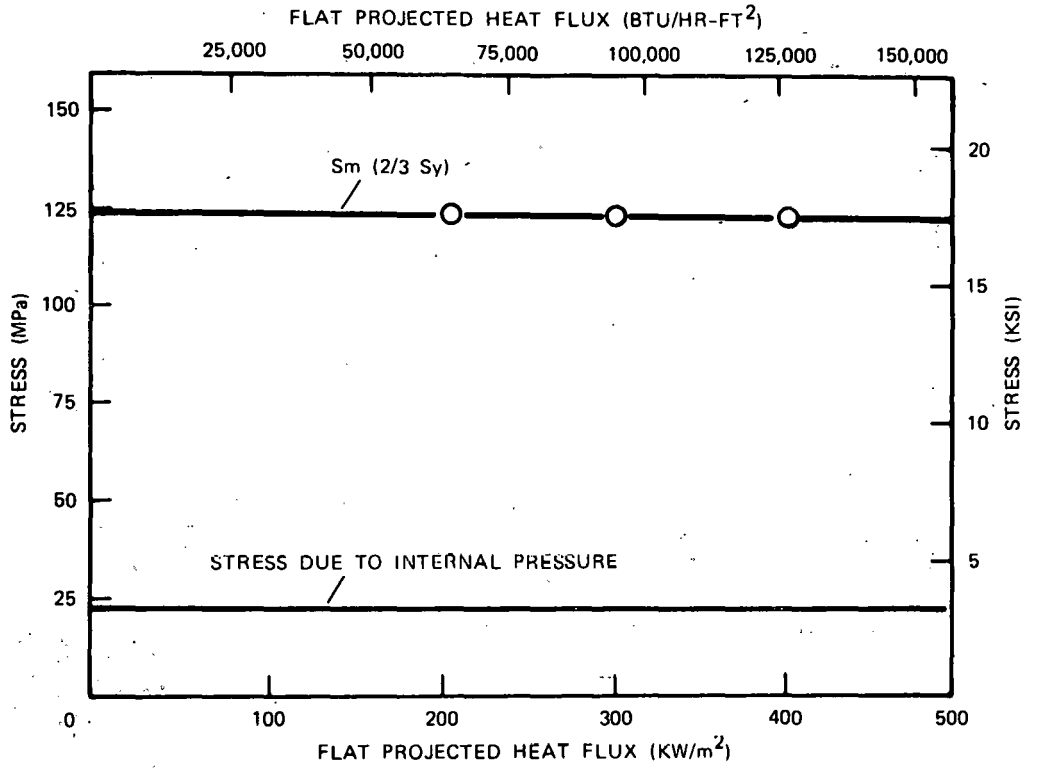

Figure B-5. Comparison of Pressure Stress in SRE Superheater Section with Allowable Stress

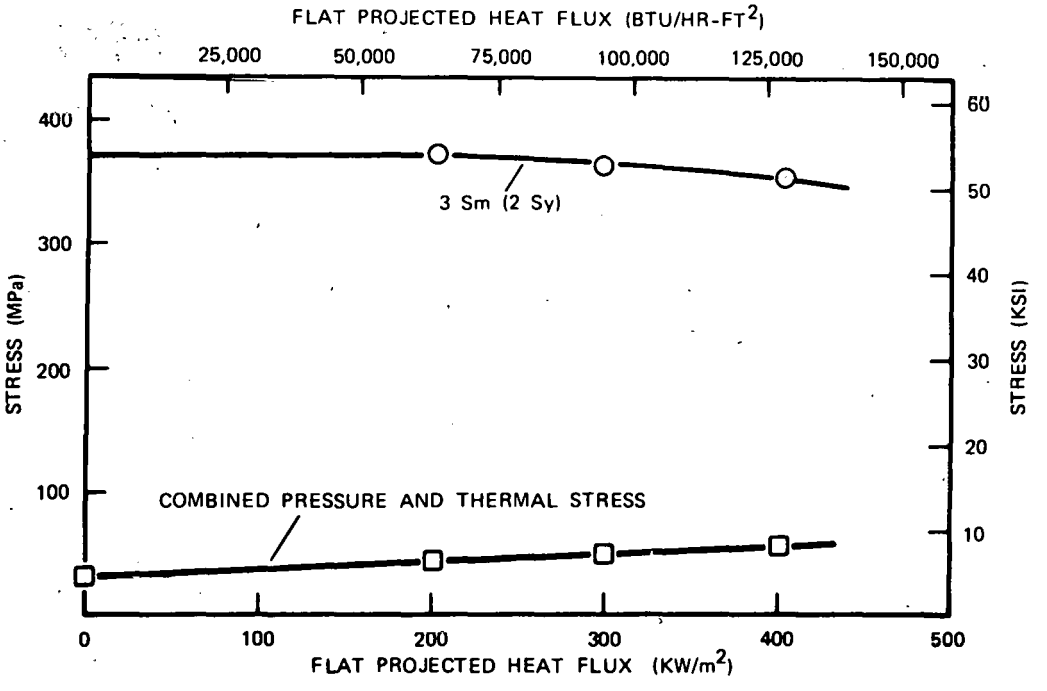

Figure B-6. Comparison of Combined Pressure and Thermal Stress in SRE Superheater Section with Allowable Stress

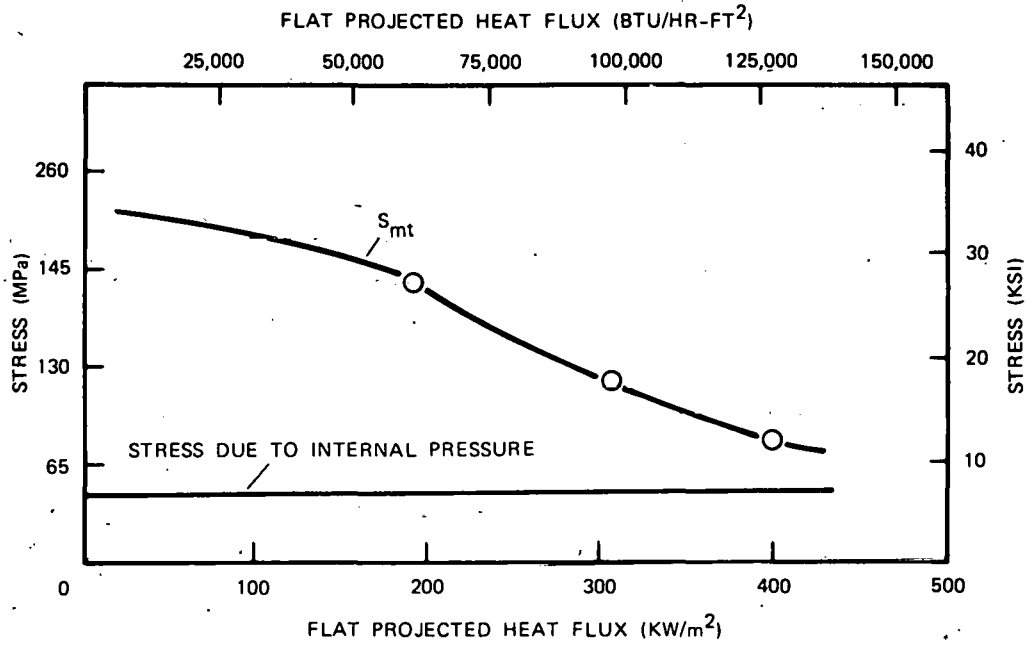

Figure B-7. Comparison of Pressure Stress in Pilot Plant Superheater Section with Allowable Stress

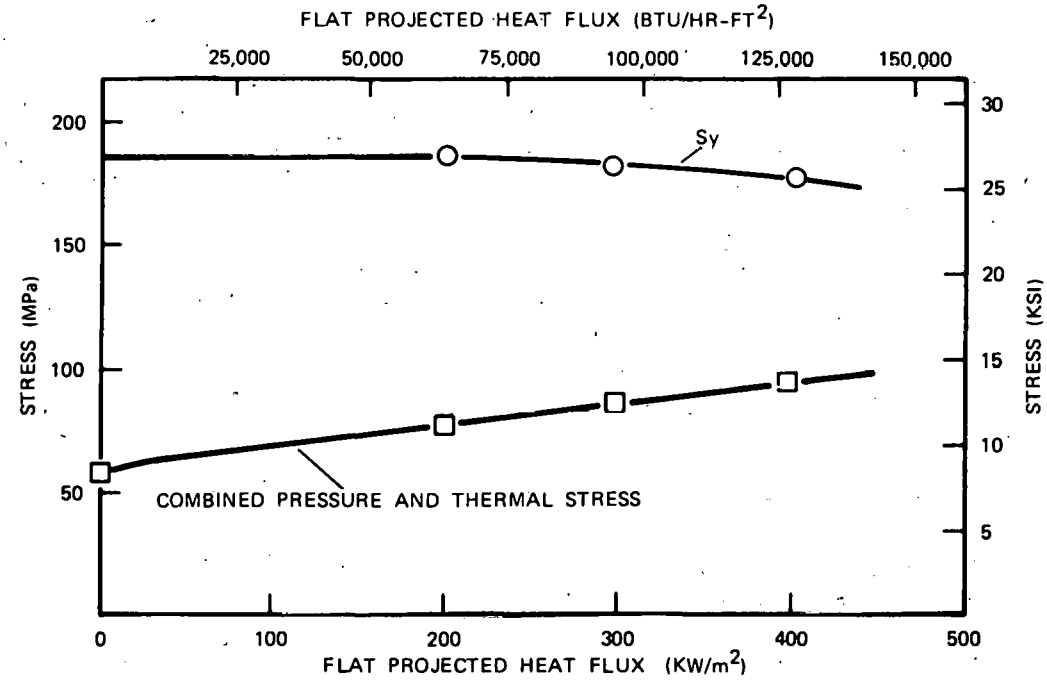

Figure B-8. Comparison of Combined Pressure and Thermal Stress in Pilot Plant Superheater Section with Allowable Stress

APPENDIX C
THERMAL STORAGE ENGINEERING MODEL PROGRAM

DESCRIPTION AND TESTS

In order to specify the design of the SRE and assure a measure of confidence in the overall feasibility, there needed to be a technical basis from which to formulate the design. The Engineering Model (EM) Program was created to serve this purpose.

At least two model configurations - condenser model and vaporizer model - were planned.

The vaporizer model (VM) was used to investigate various salt removal techniques and the attendant heat transfer coefficient. In addition, various vaporizer tube configurations and mechanisms were evaluated. The nucleation process was studied on a bulk scale and the effects of impurities evaluated.

The condenser model (CM) was used to investigate the capability of various pipe configurations, with and without extended surfaces, to transfer heat from condensing steam inside tubes to the salt mixture outside. The primary objective to be met with this model was an assessment of the heat transfer coefficient of a single tube and an estimate of the effects of multiple-tube arrangements. It was also expected that the heat transfer mechanisms currently being hypothesized would be substantiated or modified in light of the experiments. These data would make it possible to specify the EM condenser heat exchanger with high confidence or to specify an alternate or augmented scheme. EM testing would demonstrate the design sepcified by the CM and the SRE testing would evaluate the performance capability when used in several modules or banks.

Both models provided valuable information on salt handling and properties, test methods and techniques, materials compatibility, and operating and safety procedures.

Based on the scope of the experimental effort, a set of priorities was established as follows:

1) Investigate various salt scraping techniques and heat transfer.

2) Investigate various condenser tube configurations and tube bank arrangements and the attendant heat transfer

3) Investigate the thermal convection of the bulk salt in the bank.

The following discussion is a summary of accomplishing the first priority.

A series of preliminary tests was made to study the scraping problem and heat transfer on a small tank approximately 38 cm (15 in.) long, 23 cm (9 in.) deep and 27 cm (10.75 in.) wide. The tank was equipped with five 1.3-cm- (0.5 inch) diameter stainless-steel tubes on 5.1-cm (2-in.) centers near the upper surface of the tank. The tubes were connected in series. Three immersion heaters supplied heat for melting down the charge.

An air supply regulator, Rotometer, and an air preheater were connected to the tank heat exchangers, which permitted a low flow of heated air to be used for cooling. The tank was filled with an 83-percent $NaNO_3$ and 17-percent NaOH (by weight) salt mixture and melted down. Temperatures were measured with the use of in-line thermocouples.

Figure C-1 shows a schematic of the system. An additional element was added to the system, a stirring device consisting of a 7.6-cm-diameter (3 in.) impeller. This allowed vigorous flow of molten salt over the heat transfer tubes. Figure C-2 is a photograph of the test set. Figure C-3 is a closeup of the tank, stirring rod, and heaters. A leak in the tank sealed itself by freezing during a test.

The small size of the preliminary tank and practical problems with the heat exchanger and heaters led to the design and construction of a considerably larger and more flexible system. Figure C-4 is a schematic view of the larger system. The steel salt storage tank 61 cm x 45.7 cm x 45.7 cm (24 in. x 18 in. x 18 in.) was set into a large steel pan mounted on a movable base. A close-fitting cover was designed and built to carry the necessary heat exchangers, and electric bayonet-type immersion heaters were used to supply heat. A separate pump, oil lines, and Rotometer allowed the circulation of controlled quantities of oil at various temperatures for cooling the bath heat exchangers. A serpentine cooling system of five 45.7-cm by 1.3-cm (18-in. by 0.5-in.) pipe lines was fitted on a vertically adjustable frame. Mechanical rotary scrapers were fitted to these tubes and driven from an overhead sprocket through a 0.95-cm (0.375-in.) roller chain with sprockets on each scraper. The initial scrapers were two simple straight blades mounted on bearings on each end and also on the sprocket at the center. A different design consisted of a zig-zag scraper consisting of small plates of steel machined with elliptical holes to closely fit the tube and driven by a central sprocket. Figure C-5 shows both designs mounted on the heat transfer tubing and driven together.

Instrumentation was acquired consisting of two precision millivoltmeters, a recording millivoltmeter, and several digital thermocouple readouts. A differential thermopile arrangement for measuring temperature changes in the oil was connected to the input and output locations of the coolers.

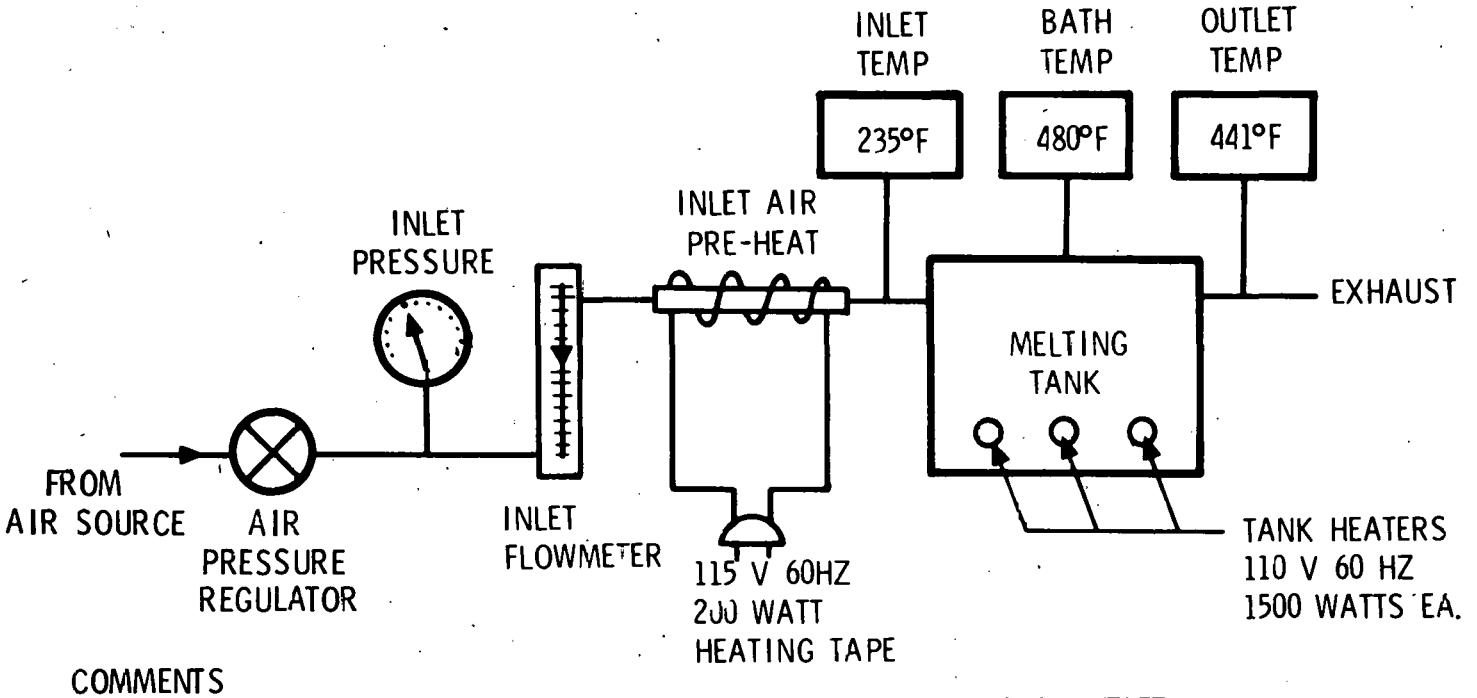

COMMENTS

1. THERMOCOUPLES ARE 1/16 IN. DIAMETER TYPE K CHROME-ALUMEL MATERIAL
2. MELTING TANK HAS 5 1/2 IN. DIAMETER STEEL TUBES USED AS A HEAT EXCHANGER
3. INITIAL SALT SOLUTION IS 83% $NaNO_3$ AND 17% NaOH
4. INLET AIR LINE IS 1/4 IN. O.D. TUBING

INLET AND OUTLET THERMOCOUPLE CONFIGURATION

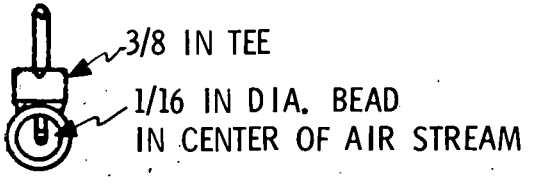

Figure C-1. Initial Experimental Salt Melt Test Setup

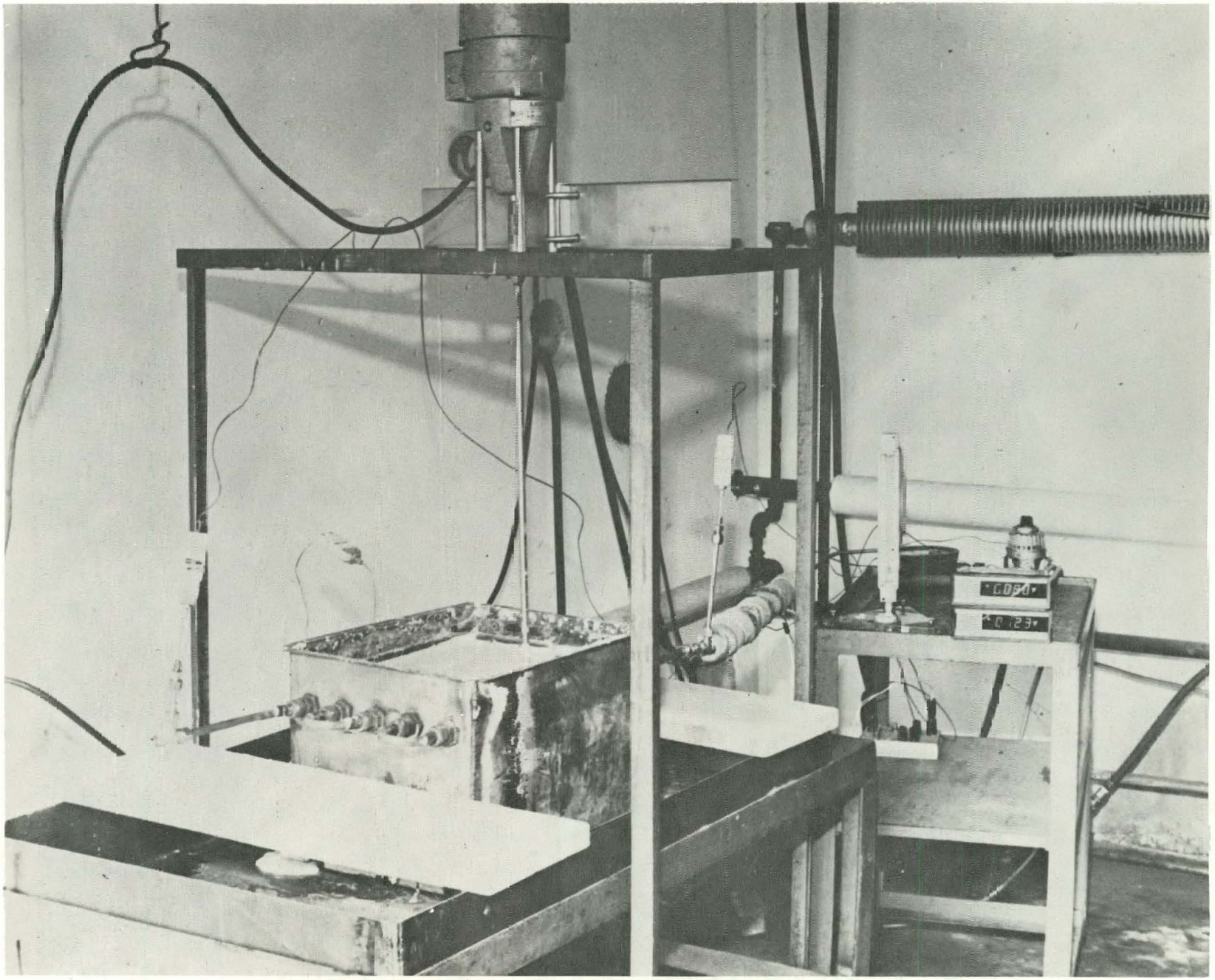

Figure C-2. Preliminary Test Facility

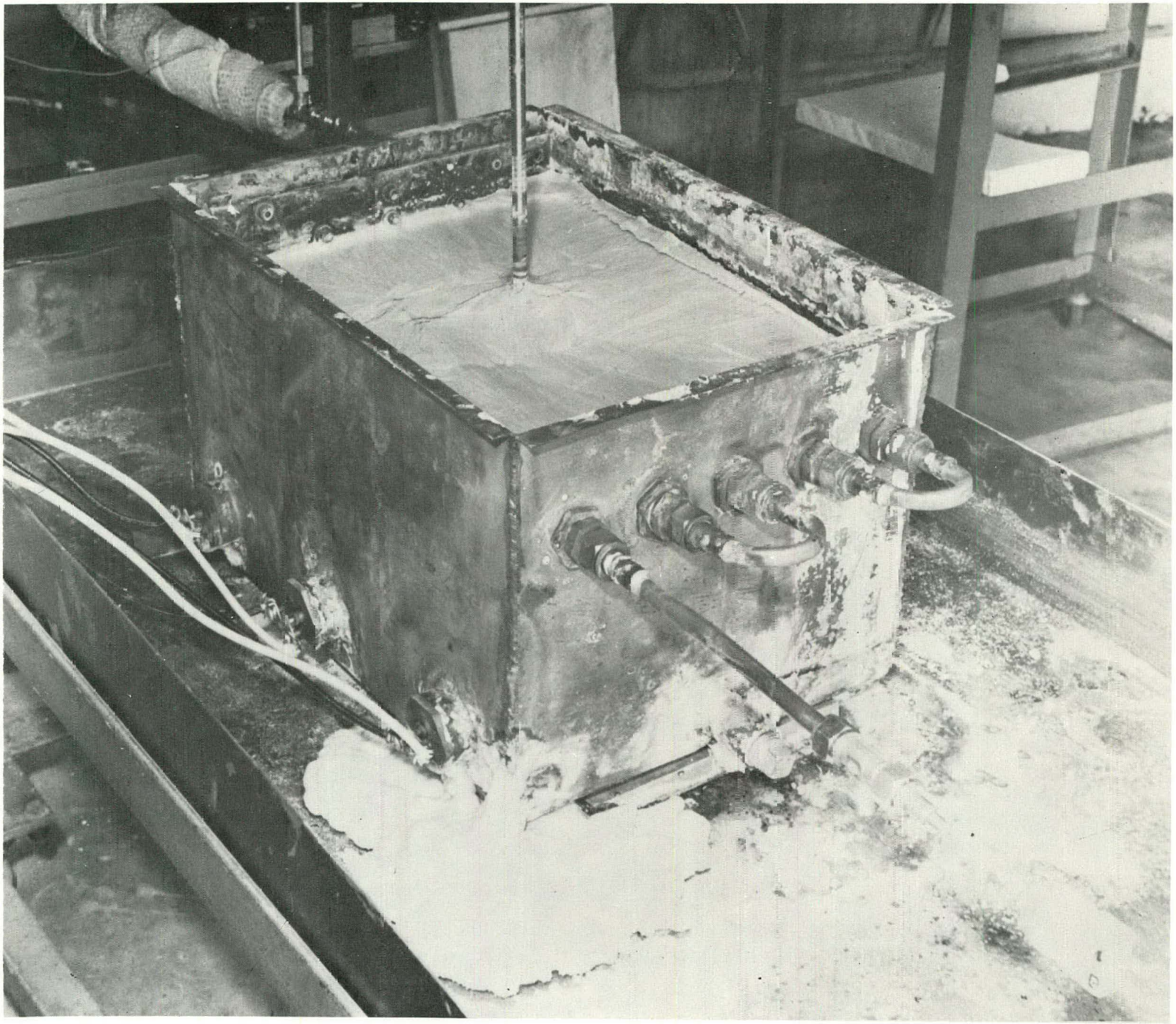

Figure C-3. Closeup of Tank, Stirring Rod, and Heaters

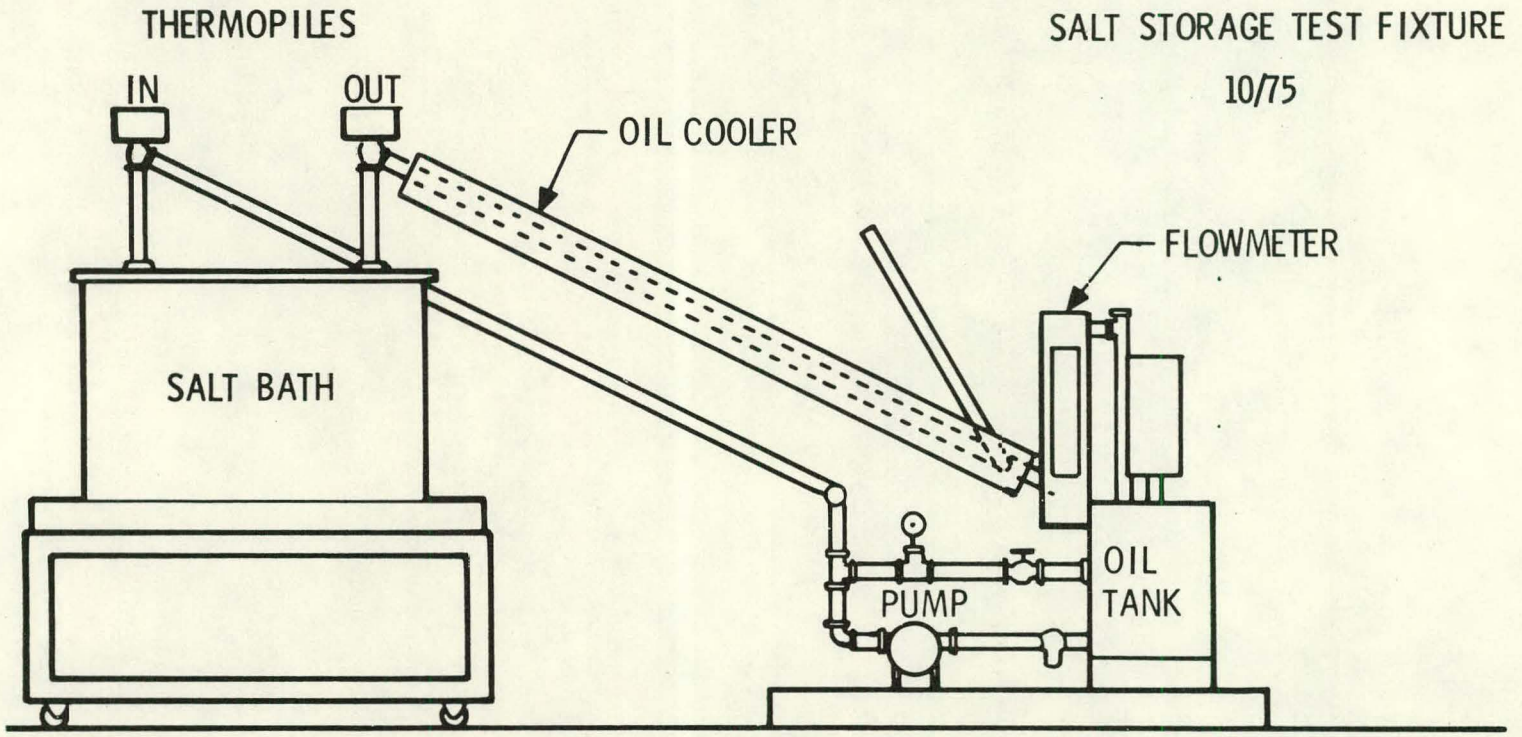

Figure C-4. Phase Change Heat Transfer Test Apparatus Engineering Model

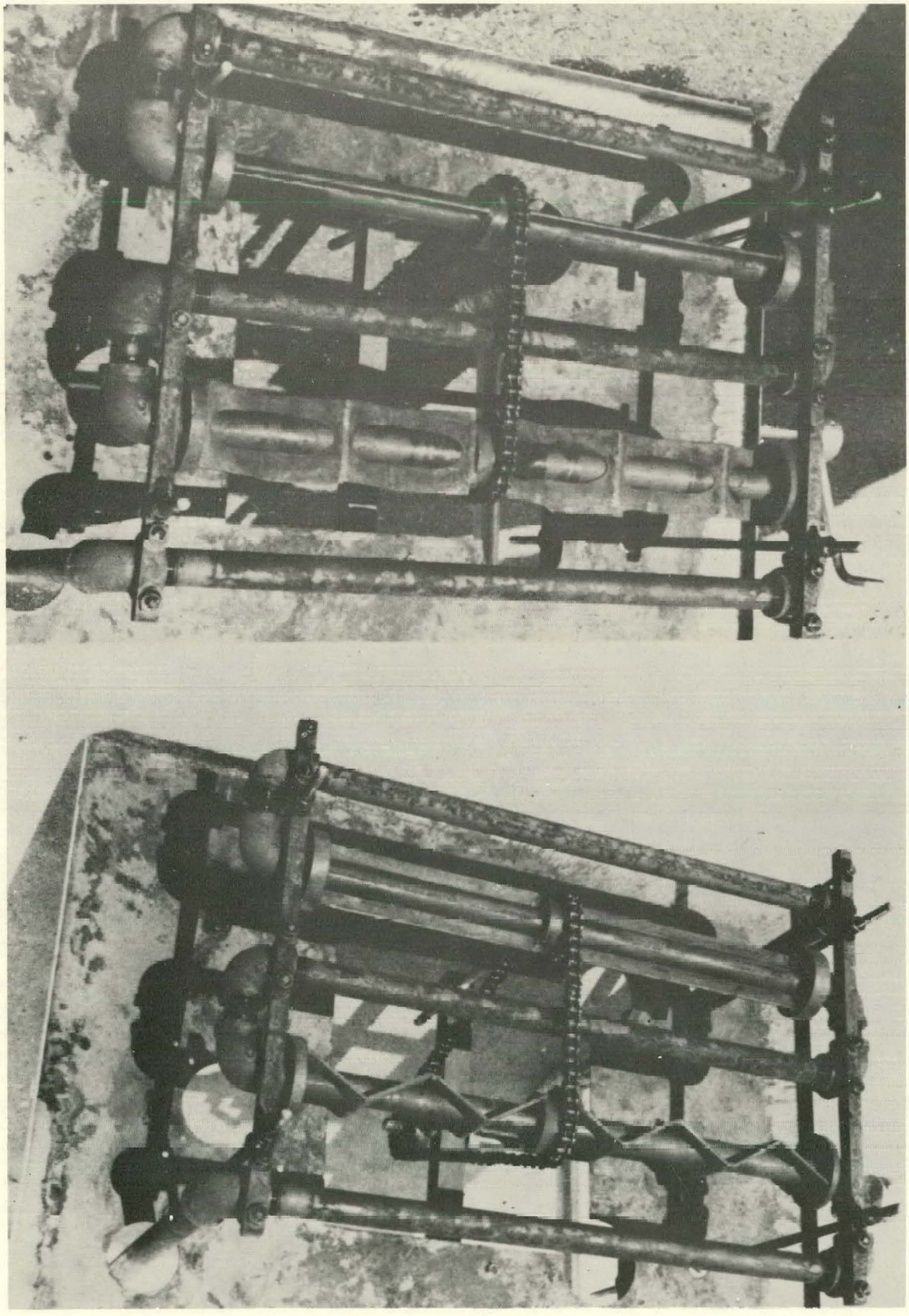

Figure C-5. Rotary Scraper Units on Serpentine Heat Transfer Tubing

The system was charged with 5 gallons of Mobiltherm 603, a hydrocarbon-type high-temperature oil.

Oil flow was measured with a Rotometer equipped with a Pyrex tube and special stainless-steel float.

After preliminary tests with the scrapers shown in Figure C-5, a full set of scrapers similar to the straight bar scraper was installed on the heat exchanger tubes.

These scrapers were rather loosely fitted to the tubes, having clearances about 1 mm (0.04 in.). Heat transfer coefficients were relatively low, and improved models were made by applying sharp cutting edges to the blading and decreasing clearances to approximately 0.25 mm. Experiments were then conducted on a near-eutectic composition of NaOH and $NaHO_2$ (83 percent $NaNO_3$ and 17 percent NaOH).

The 107-kg (411-lb) eutectic charge was then shifted to an "off" eutectic by the addition of 18.2 kg (50 lb) of NaNO. Further tests were made with the sharp-edged straight scrapers on this composition.

Problems with unscraped area salt buildup and drive chains and sprockets led to replacement of the five scrapers with a single, improved, zig-zag scraper. This scraper has very close clearances (approximately 0.12 mm (0.005 in.) and completely scraped the tube, leaving only a very thin film.

Tests were generally run after the salt was completely melted and raised above the eutectic freezing point of 247°C (476°F) by using immersion heaters. The cooling oil was then heated to the desired temperature, 232°C (450°F). Scrapers were activated and the cooling oil pumped through the system. Oil temperature rise, flow rates and salt temperature data were recorded at fixed intervals. Scraping was continued until the scrapers became frozen to the tubes.

The system was hand-scraped for periods up to 1 hour. Data on heat transfer were taken for further reduction. In all cases, the salt bath temperature fell slowly, and, eventually, the scrapers became firmly frozen to the tubes. Experiments with improved scrapers with sharper edge improved heat transfer but did not permit continued scraping.

The addition of mechanical drives improved operation but the same problem occurred. After a period of time, generally about 1 hour, the scrapers froze. Scrapers were closely examined but no mechanical damage was found.

The zig-zag-version single scraper worked at periods up to nearly 3 hours before freezing. An interesting feature of all these tests was that the salt bath temperature always kept dropping, never reaching a fixed temperature. In all freeze-ups, the temperature curve would become nearly flat just before the end.

It appears that the "off" eutectic compositions were rejecting the excess component until the true eutectic was reached. At that point, the eutectic, when cooled a short distance below the freezing point, becomes hard and strong, freezing the scrapers.

A special test fixture built to measure shear strength showed that the shearing strength of the NaOH - $NaHO_3$ eutectic was about 551 kPa (80 psi) about 0.25°C (0.5°F) below the melting point.

A series of photographs, Figures C-6 and C-7, taken after a run with the five element scrapers, indicates the effectivenss of the scrapers. The end-tubing connections are heavily encrusted with salt. The tubes have a small layer of salt clinging to the heat transfer surfaces. Later designs scraped better and maintained better heat transfer rates.

An improved scraper design was developed to permit easy installation and removal. Figure C-8 shows the three elements of the new inclined scraper drive installed on a three-element test heat exchanger. This scraper will be tried on $NaNO_3$, NaCl, and Na_2SO_4 eutectic and off-eutectic salt combinations.

Figure C-9 shows an additional high-temperature test facility that is being constructed for the salt thermal storage test program.

The test tanks presently are being heated by external electric range top-type heaters clamped tightly to the outside bottom of the tanks. High-temperature insulation around these heaters and tanks conserves energy and helps maintain the tanks at 316°C (600°F).

The oil loop is equipped with four 2400-watt immersion heaters installed in the oil sump. The oil may be heated above the temperatures needed for charging the tank. An extended surface heat exchanger consisting of three 45.7-cm (18-in.) finned heat transfer tubes is being constructed for installation at the bottom of the tank. This will permit a test program involving both charging and discharging of the salt storage system.

TEST ANALYSIS

Phase change heat transfer experiments were conducted on engineering models of the tube scraper concept. The test instrumentation is noted in Table C-1, and the experimental parameters in Table C-2. Major performance parameters of interest were heat transfer coefficients, scraping force, and percent heat recovery. Heat transfer coefficients of salt resistance were measured up to 5.67 kW/m^2-°C (1000 $Btu/hr-ft^2$-°F). Scraping force and heat recovery performance was impaired due to scraper freeze-up. Scraper freeze-up is apparently caused by the strength of the eutectic solid and solid buildup around portions of the scraper which are not cutting edges. Heat recoveries

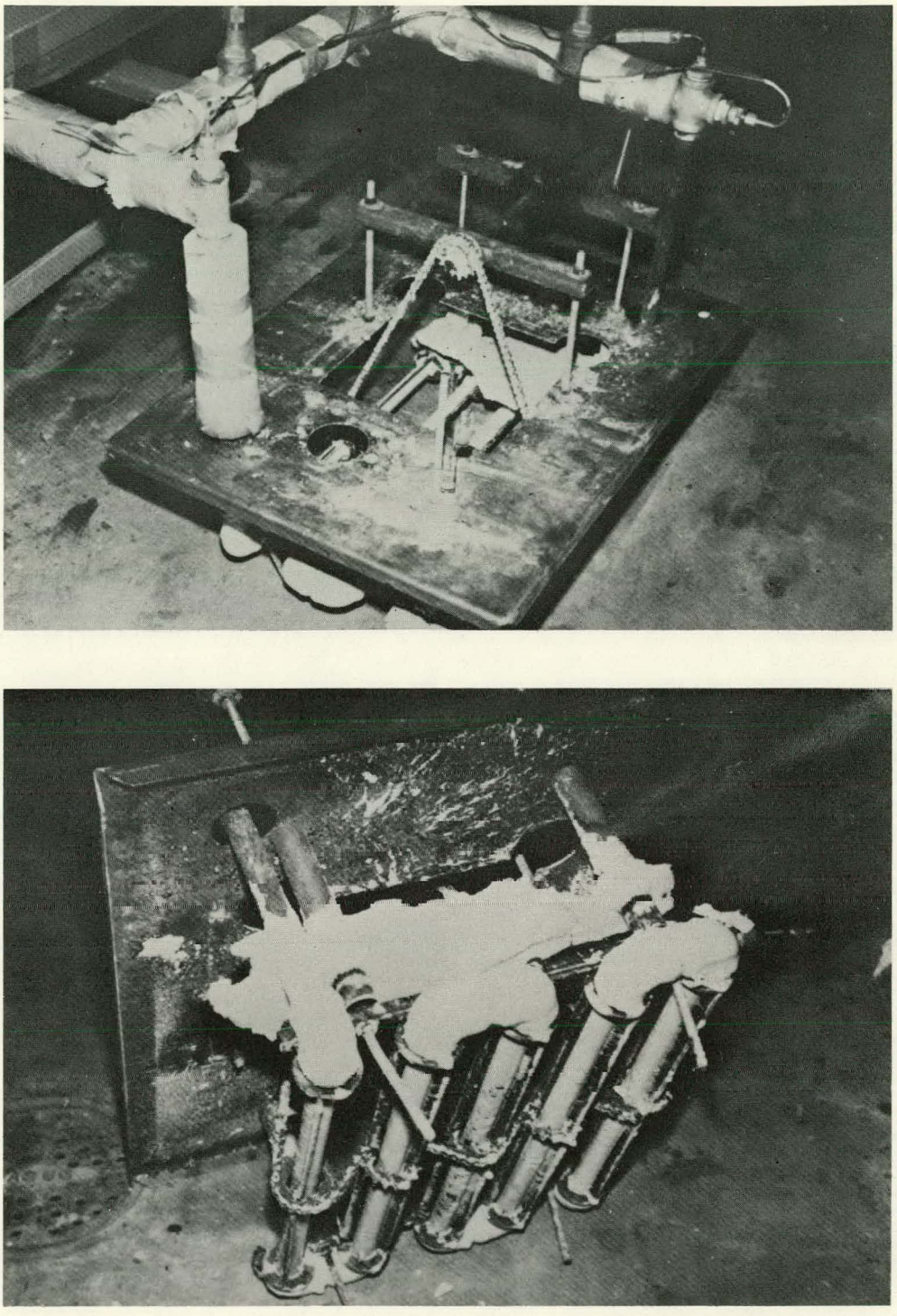

Figure C-6. Straight Bar Rotary Scrapers After Operation

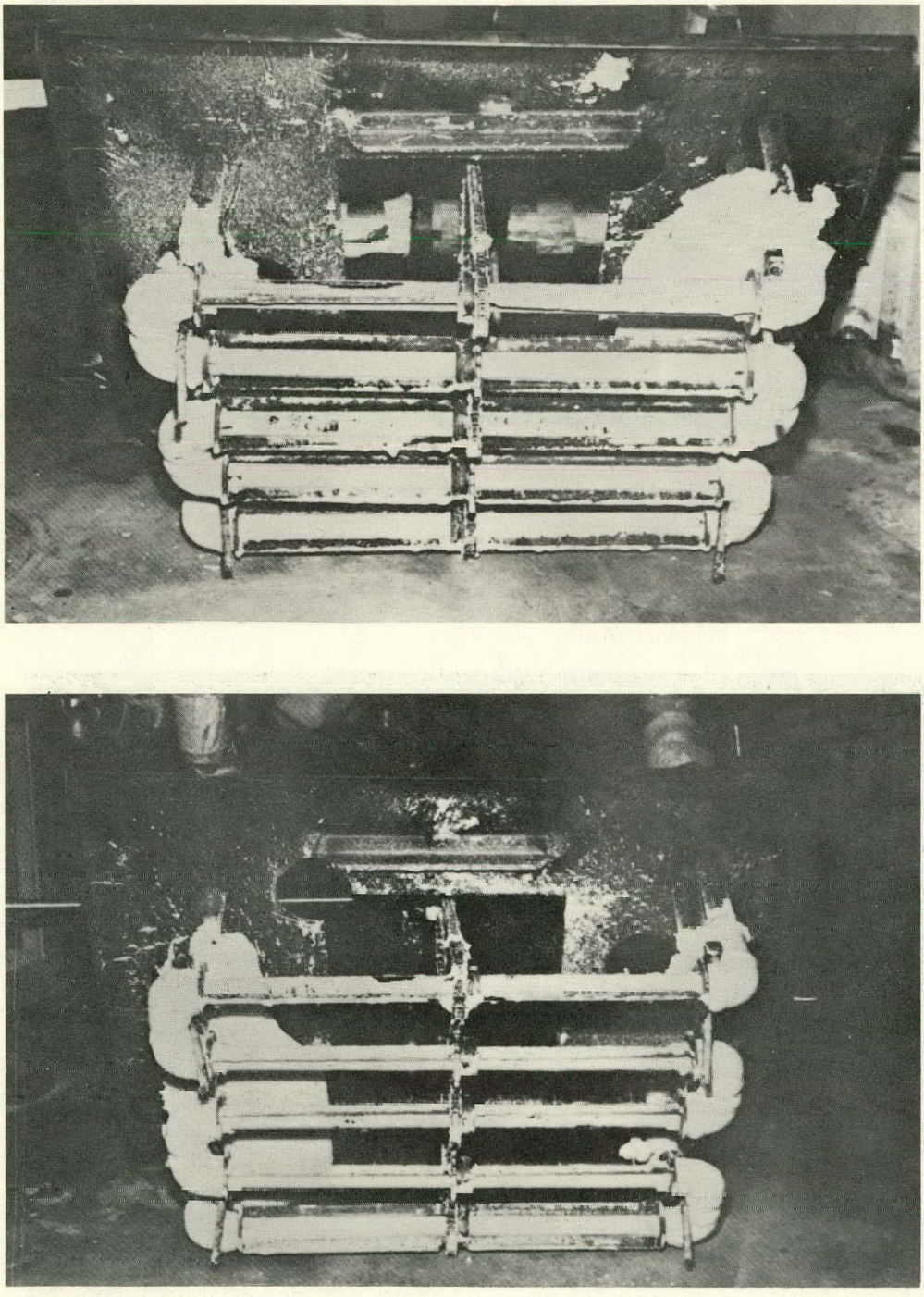

Figure C-7. Bottom View of Straight Bar Rotary Scrapers After Operation

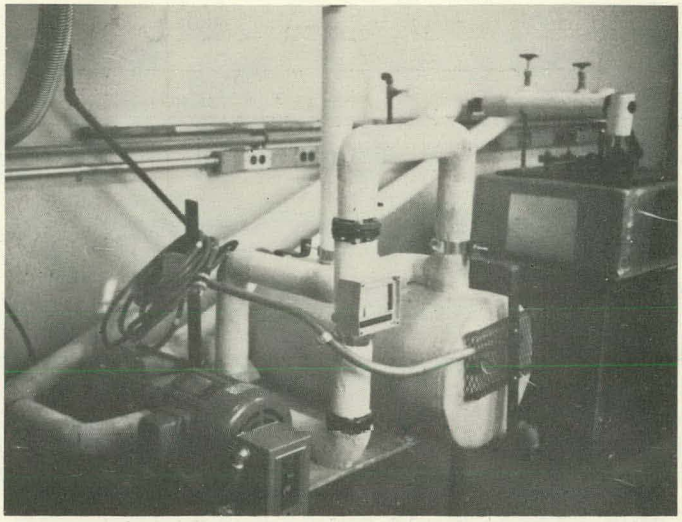

Figure C-8. Improved Scraper Design

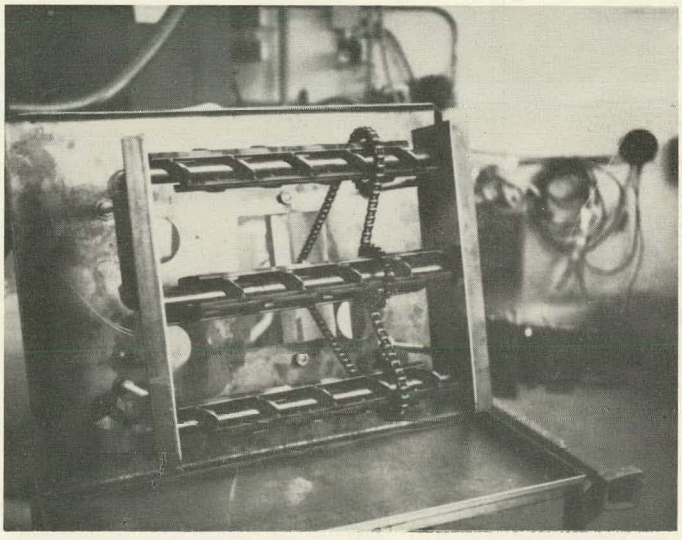

Figure C-9. High-Temperature Salt Storage Test Facility

Table C-1. Test Instrumentation

Instrument	Data Measured
Brown Rubicon potentiometer (2)	Thermopile output (μV)
Ircon digital thermocouple indicator	Thermocouple output (mV)
Brown recorder	Salt bath temperature
Brooks rotometer	Oil flow rate (gpm)

Table C-2. Experiment Parameters

Parameter	Requirement
Salt composition	$NaNO_3$-NaOH (83% - 17%)
Vaporizer configuration:	
Tube length	7.5 ft scraped (2.28×10^2 cm)
Tube size	0.622 ID/0.840 OD (1.58 cm ID/2.13 cm OD)
Material	Steel
Scraped Area	1.52 ft^2 (-0.412×10^3 cm^2)
Internal Heat Transfer Fluid:	Mobiltherm 603
Thermodynamic properties at 450°F:	(232°C)
Specific gravity	0.73
Kinematic viscosity	1.0 cps (1.0×10^{-3} N sec/m^2)
Specific heat	0.68 Btu/lb-°F[6.8×10^{-1} g cal/(g°C)]
Thermal conductivity	0.068 Btu/hr-ft-°F[2.82×10^{-4} cal/(sec-cm-°C)]
Oil flow rate	8.24 gpm (5.198×10^{-1} l/sec)
Internal heat transfer	474 Btu/hr-ft^2-°F(6.44×10^{-2} cal/sec-cm^2-°C)
Tank size	24 in. x 18 in. x 18 in. (60.96 cm x 45.72 cm x 45.72 cm)
Salt depth	14 in. (35.56 cm)
Salt weight	411 lb (eutectic)(1.8643×10^2 kg)
Thermal capacity ($NaNO_3$-NaOH)	9.4 kWhr(t)

of 30 percent with an oil temperature of 11.1C° (20F°) below eutectic were measured. This performance was achieved with a salt composition with 10-percent extra weight of the $NaNO_3$ from the eutectic mixture of $NaNO_3$-NaOH.

Heat Transfer Coefficients

The objective of these engineering model tests was to determine the heat transfer coefficients and heat recovery performance of tube scrapers. The first quantitative data taken demonstrated poor heat transfer coefficients, as seen in Figure C-10. This was caused by a large clearance of 1.016×10^{-1} cm (0.040 in.) between the scrapers and the tubes. The large variation in coefficients was caused by variations in solid-film thickness as salt froze under the scrapers. Note also in Figure C-10 the change in coefficient when the scrapers were turned on. The local turbulence caused by the scrapers is important for reducing thermal resistance in the liquid salt. Figures C-11 and C-12 show more precisely the same data as Figure C-10. The scrapers provide high coefficients when the tubes are bare, but the coefficients drop off as the solid builds up under the scraper.

During these tests, a slushy solid was being removed from the tubes due to the slightly off-eutectic salt mixture. The off-eutectic composition is evident by the continuous drop in the liquid temperatures. As the external resistance increased, the temperature gradient increased, causing the solid material to become colder and harder. This hard material slowly developed until it froze the scrapers.

Sharp liners were added to the scrapers to reduce the clearance and increase their ability to scrape hard material. A 75-percent increase in heat transfer to coefficients was achieved (see Figure C-13).

The next step taken was to move the salt composition farther from the eutectic by adding 22.68 kg (50 lb) of $NaNO_3$. As seen in Figure C-14, the high initial coefficients lasted longer in time, but the coefficient at freeze-up was about the same. The scrapers keep the tubes cleaner when the material is slushy, but after the extra nitrate freezes out of solution, the resultant eutectic material builds up.

The last step was to install a scraper with very close fit and sharp edges. A 300-percent increase in coefficient was achieved. As shown in Figure C-15, the total elapsed time was considerably greater. This was primarily due to the fact that only one of the five serpentine legs was being scraped. The heat transfer coefficient was calculated by measuring the heat flow through the unscraped tubes on a separate run and subtracting it from the scraping run. Note, however, that a considerable amount of eutectic material must have been formed, as 45.36 kg(100 lb) of solid was formed, although the bath never reached the eutectic temperature.

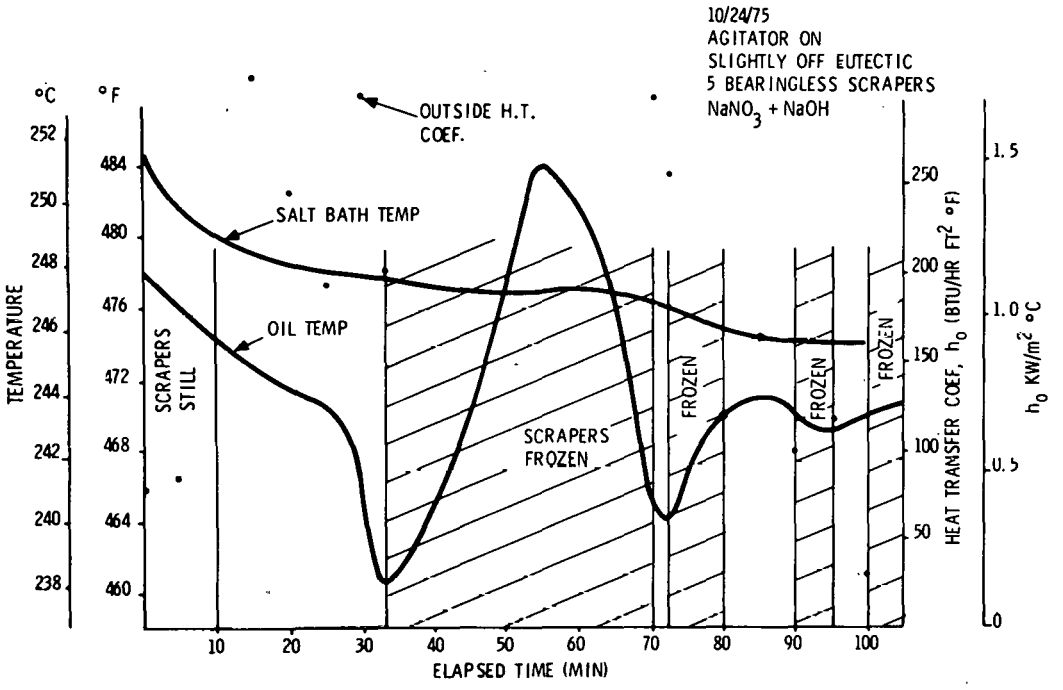

Figure C-10. Loose-Tolerance Scraper - Slightly Off Eutectic

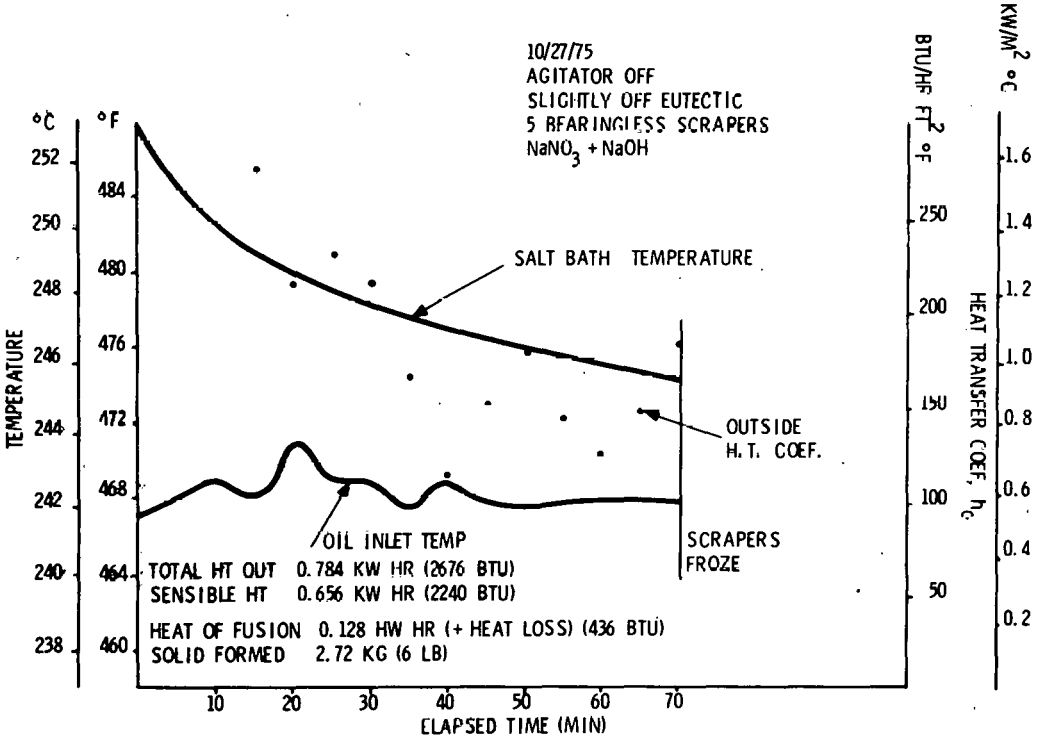

Figure C-11. Loose-Tolerance Scraper - Slightly Off Eutectic

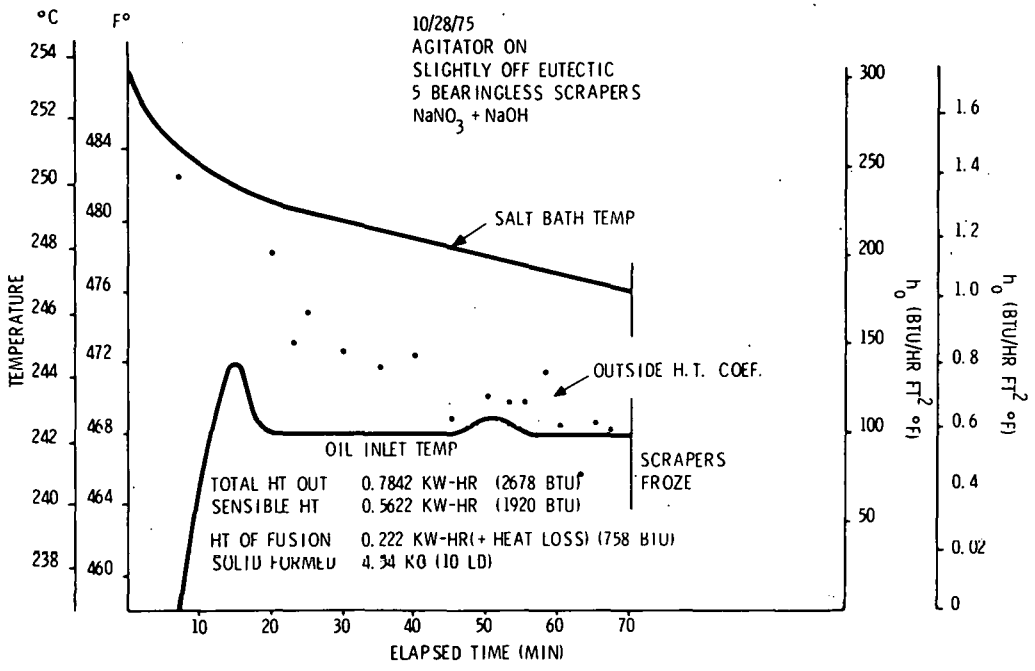

Figure C-12. Loose-Tolerance Scraper - Slightly Off Eutectic

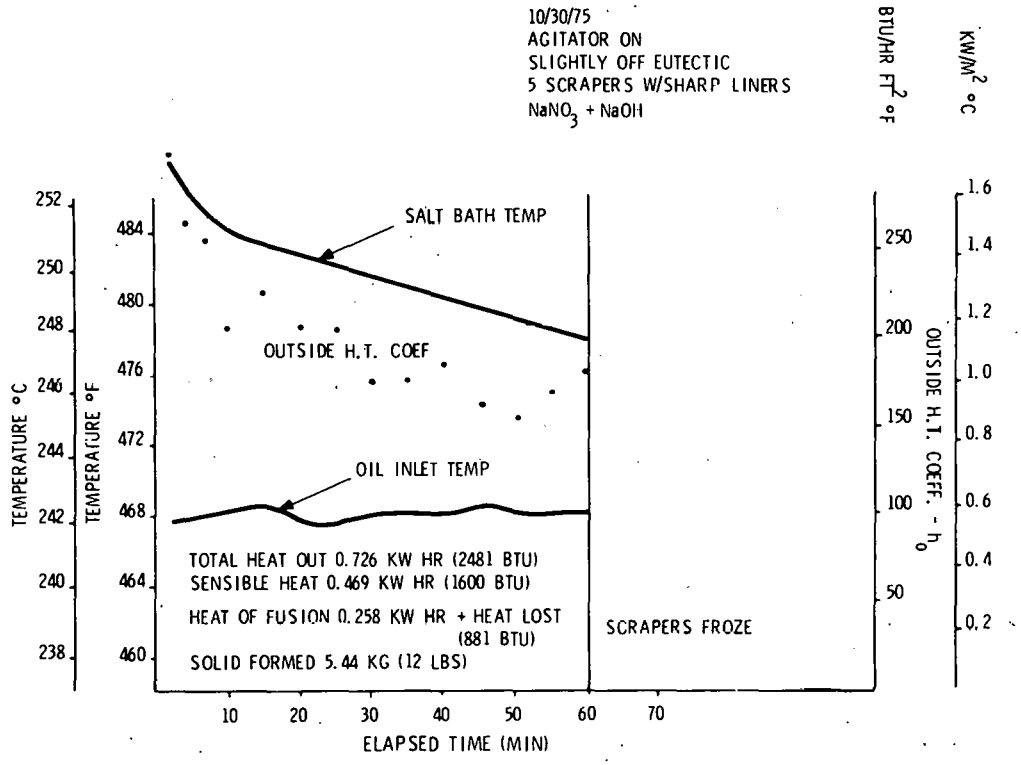

Figure C-13. Medium-Tolerance Scraper - Slightly Off Eutectic

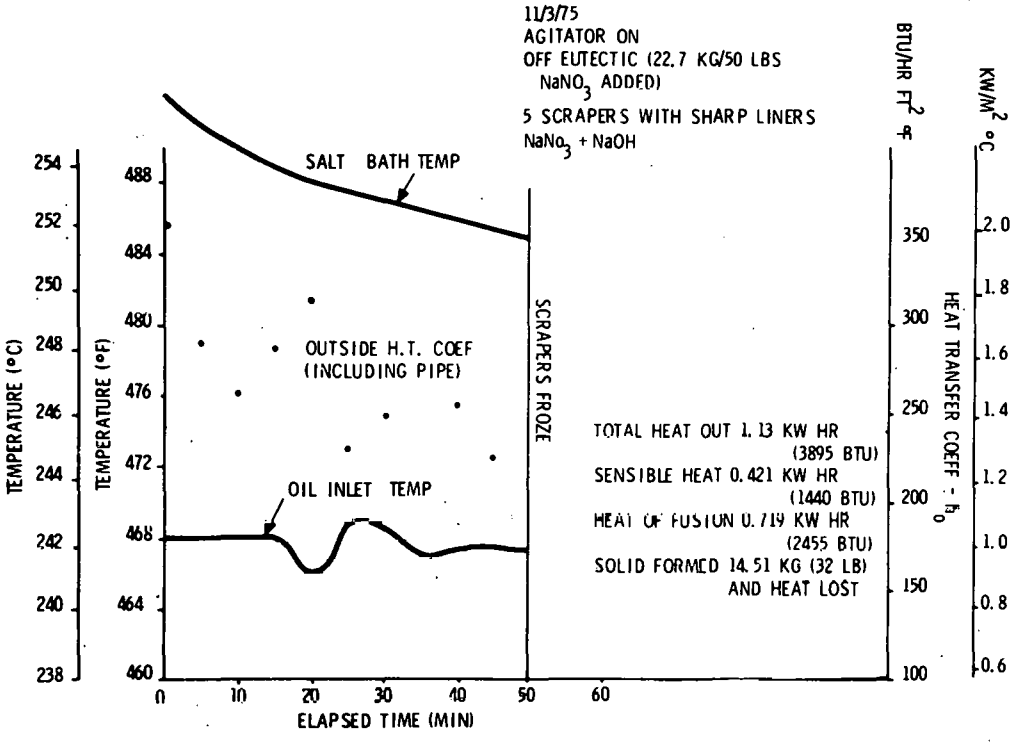

Figure C-14. Medium-Tolerance Scraper - Off Eutectic

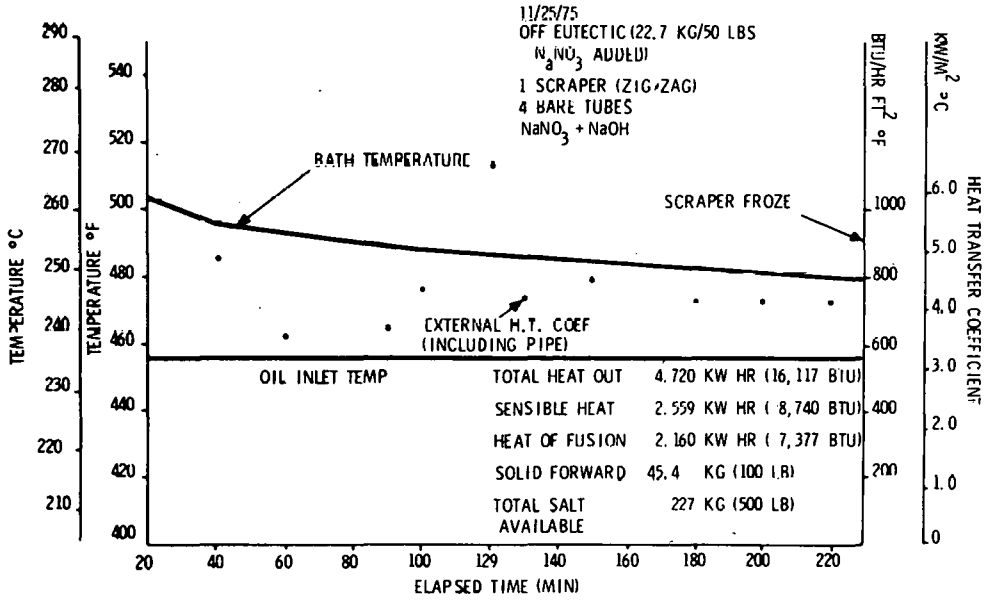

Figure C-15. Close-Tolerance Scraper - Off Eutectic

Scraper Freeze-Up

The most obvious factor revealed in the experimental data is that the scrapers freeze before the heat is recovered from the salt bath. The experimental parameters (Table C-3) affecting freeze-up are: salt composition, oil temperature, scraper clearance, and unscraped scraper boundaries. The first three of these factors cause eutectic solids to come in contact with the scrapers. This material apparently has strong mechanical properties.

Figure C-10 shows that the scrapers freeze very quickly with an oil temperature 5.5C° (10F°) below the eutectic temperature when the salt composition is near eutectic. Figures C-11 and C-12 show that about 2 percent of the salt was solidified with the oil temperature 4.4C° (8F°) below eutectic. Improving the scraper clearance in Figure C-13 did not improve heat recovery.

When the composition was moved off etuectic, the heat recovery was increased to about 6 percent, as shown in Figure C-14. Then a new scraper was installed with small clearance [0.01016 cm = 1.016×10^{-2} cm (0.004 in.)], sharp edges, and all boundaries scraped. The small clearance keeps the solid on the tubes near the bath temperature. The sharp edges allow cutting harder material. The scraped ends and self-scraping bearing surface prevent a solid buildup on boundaries which can prevent scraper motion. As shown in Figure C-15, this scraper was able to recover 30 percent of the tank heat with the oil temperature 11.1C° (20F°) below eutectic.

Computation of Heat Transfer Coefficient

Energy Balance Across the Tube Wall --

$$q = \dot{m} C_p (T_{out} - T_{in})_{oil} = U_o A_o (T_{salt} - T_{oil})$$

$$U_o = \frac{\dot{m} c_p \Delta T_1}{A_o \Delta T_2}$$

where

$$\Delta T_1 = (T_{out} - T_{in})_{oil}$$

$$\Delta T_2 = T_{salt} - T_{oil}$$

Separating the conductance of the internal fluid from the pipe and salt

$$h_o = \frac{1}{1/U_o - 1/h_i \, A_o/A_i}$$

Table C-3. Summary of Results

Date	Scraper Type	Salt Composition	$\Delta T_{oil} - T_{eu}$		Final Heat Transfer Coefficient	cal/sec-cm^2-°C	Total Heat Out		Solid Formed	
			F°	C°	(Btu/hr-ft^2-°F)		Btu	cal	lb	kg
(1) 11/25/75	Tight zig-zag	50 lb off eutectic	20	11.1	725	9.85×10^{-2}	16,000	4.03×10^6	100	45.36
(2) 11/03/75	Straight blades with liners	50 lb off eutectic	8	4.4	200	2.72×10^{-2}	4,000	1.008×10^6	32	14.52
(3) 10/30/75	Straight blades with liners	Near eutectic	8	4.4	175	2.38×10^{-2}	2,400	6.048×10^5	12	5.44
(4) 10/28/75	Straight blades	Near eutectic	8	4.4	100	1.36×10^{-2}	2,700	6.804×10^5	10	4.536
(5) 10/27/75	Straight blades	Near eutectic	8	4.4	150	2.04×10^{-2}	2,700	6.804×10^5	6	2.72
(6) 10/24/75	Straight blades	Near eutectic	5 to 15	15 to 8.3	---	---	---	---	---	

Ex. $\dot{m}$ = 2990 lb/hr (1.356×10^3 kg/hr) $\quad \Delta T_1$ = 4.2°F (-15.44°C) h_i = 500

e_p = 0.69 $\quad \Delta T_2$ = 32°F (0°C)

A_o = 1.52 ft^2 (1.412×10^3 cm^2) $\quad A_o/A_i$ = 1.38

$$U_o = 178$$

$$h_o = \frac{1}{1/178 - 1.38/500} = 350$$

Internal Oil Heat Transfer Coefficient -- The Dittus-Boelter equation is:

$$h_i = 0.023\,(k/d)\,(Vd/\nu)^{0.8}\,(c_p\mu/k)^{0.4}$$

where

k = 0.068 Btu/hr-ft-°F (2.82×10^{-4} cal/sec-cm-°C)

d = 0.622 in. (1.58 cm) = 0.052 ft (158 cm)

V = 8.73 ft/sec (2.66×10^2 cm/sec) = $3.14\,(10)^4$ ft/hr (2.659 cm/sec)

ν = 1.0 Hz (1.0×10^{-3} N-sec/m^2) = 0.386 ft^2/hr (9.96×10^{-3} cm^2/sec)

c_p = 0.68 Btu/lb-°F [6.8×10^{-1} g-cal/(g-°C)]

μ = 0.73 cs = 1.76 lb/ft-hr (2.619 kg-s/m-hr)

$h_i = (0.023)(1.31)(42,300)^{0.8}\,(17.6)^{0.4}$

= 474 Btu/hr-ft^2-°F (6.44×10^{-2} cal/sec-cm^2°C)